Experimental investigation of the characteristic features of bremsstrahlung from high-energy electrons in thin amorphous targets

V. A. Verzilov, I. E. Vnukov, V. V. Zarubin, B. N. Kalinin, G. A. Naumenko, and A. P. Potylitsyn
Institute of Nuclear Physics, 634050 Tomsk, Russia

(Submitted 5 February 1997)
Pis'ma Zh. Éksp. Teor. Fiz. **65**, No. 5, 369–373 (10 March 1997)

Radiation from 0–900 MeV electrons in thin amorphous films is investigated experimentally in the photon energy range 20–700 keV. The Landau–Pomeranchuk–Migdal suppression of the soft part of the bremsstrahlung spectrum and the Ter-Mikaélyan density effect are detected. Coherent bremsstrahlung on macroscopic inhomogeneities in the target material is observed. © *1997 American Institute of Physics.* [S0021-3640(97)00105-9]

PACS numbers: 78.70.Ck

Despite the fact that bremsstrahlung from electrons with energy of the order of 1 GeV in amorphous targets has been investigated for a long time now, the region of the bremsstrahlung spectrum from several keV to 1 MeV has been little studied experimentally. Interesting effects such as the density effect,[1] Landau–Pomeranchuk–Migdal suppression,[2] and coherent bremsstrahlung on inhomogeneities in the target material[3] can occur in this in this region of the spectrum. The first two effects have been investigated for accelerated electron energies from 8 to 20 GeV[4] and the third effect has not been investigated. A theoretical analysis of this question was made in Ref. 5. We have performed in this connection an experimental investigation of the bremsstrahlung spectra in this energy range in thick ($\sim$1 mm) and thin ($\sim$10 μm) aluminum and molybdenum targets.

The investigations were performed on the ''Sirius'' synchrotron in Tomsk at accelerated electron energies up 900 MeV. The working accelerated-electron current was 10–20 mA with the electrons directed onto the target for 20 ms with an acceleration cycle of 200 ms. Bremsstrahlung from electrons with energy up to 900 MeV in targets consisting of different materials and different thickness was investigated in the spectral range from 20 to 800 keV. The collimation of the bremsstrahlung was equal to 0.6 mrad. The energy range up to 1 MeV is accessible for measurements with a NaI(Tl) detector.

The experimental arrangement is displayed in Fig. 1. A 64×64 mm NaI(Tl) detector was placed in the direct bremsstrahlung beam. In this arrangement the accelerated-electron current was lowered by 5 to 6 orders of magnitude from the nominal value so as not to overload the detector. The detector load was equal to 20–40 events per 20 ms. Furthermore, the load on the spectrometric channel was checked by recording the spectrum with random triggering of a charge-to-digit converter. To remove the Compton

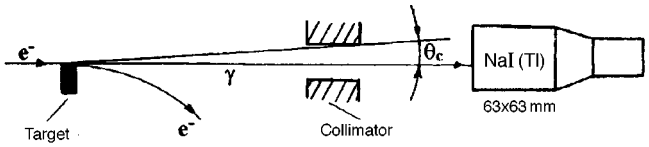

FIG. 1. Experimental arrangement.

component appearing in the response function of the detector due to hard γ rays, in addition to the main spectral measurements we took the spectra with an absorber, consisting of a lead plate 0.5 mm thick and a copper plate 1 mm thick, inserted into the bremsstrahlung beam. This information was then used in analyzing the spectra in order to remove the Compton component.

We investigated the radiation in targets consisting of 1.4 mm and 4 μm aluminum, 0.3 mm and 12 μm thick molybdenum, and 5 μm thick Mylar at accelerated electron energies of 600 and 900 MeV. The accelerated-electron current and the total energy of the radiation from a target were recorded in order to normalize the spectra.

The radiation spectra from thin and thick molybdenum targets with accelerated-electron energies of 600 and 900 MeV are presented in Fig. 2. For convenience, the critical energies for the density effect and for coherent bremsstrahlung in thin targets are also indicated here. The critical energy for the density effect is $\gamma\omega_p$, where γ is the

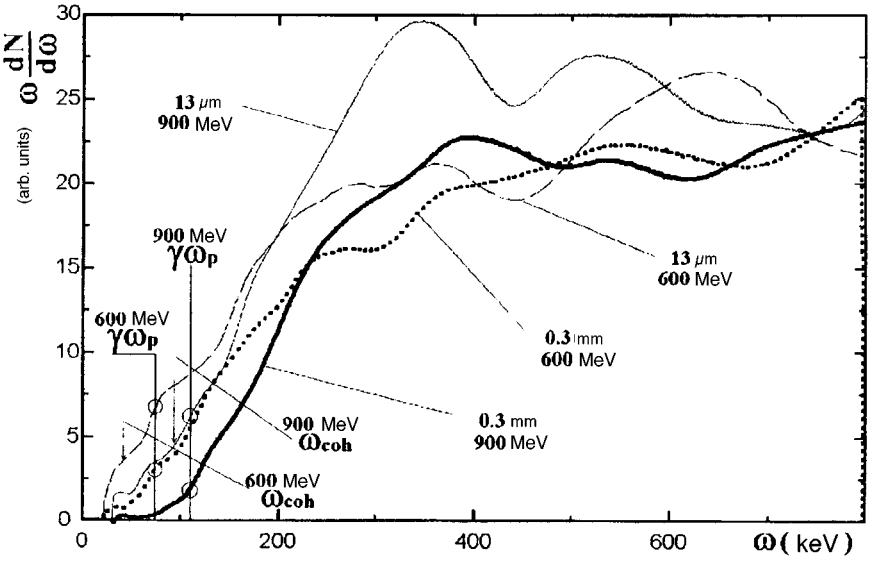

FIG. 2. Spectra of the intensity of radiation from 600 and 900 MeV electrons in 13 μm and 0.3 mm thick molybdenum targets; $\omega_{\rm coh}=2\gamma^2/l$, where l is the target thickness, γ is the Lorentz factor, and ω_p is the plasma frequency.

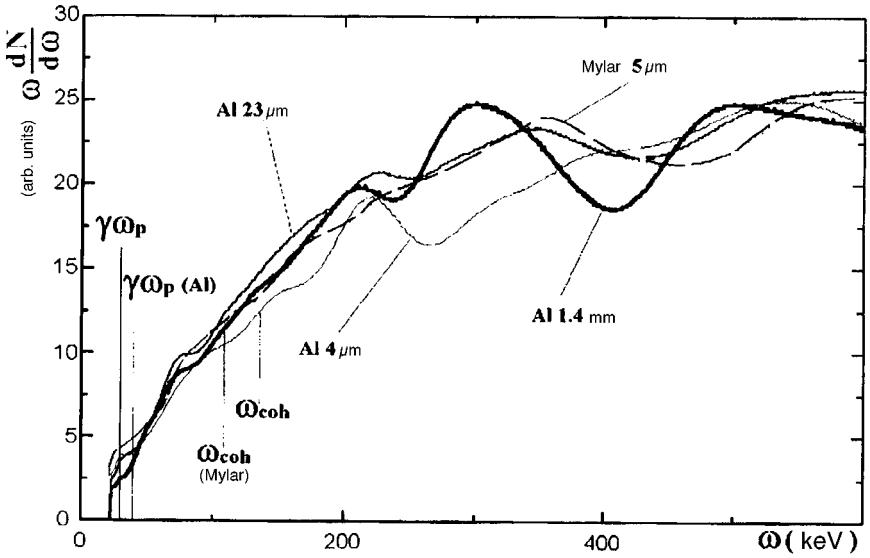

FIG. 3. Spectra of the intensity of radiation from 600 MeV electrons in aluminum and Mylar targets of different thickness, $\omega_{\rm coh}=2\gamma^2/l$.

Lorentz factor and ω_p is the plasmon energy. The critical energy for coherent bremsstrahlung is $2\gamma^2/l$, where l is the thickness of the target.

The radiation spectra from 600-MeV accelerated electrons in 1.4 mm, 25 μm, and 4 μm thick aluminum targets and in a 5 μm thick Mylar target are displayed in Fig. 3. The critical energies for the density effect and for coherent bremsstrahlung are also indicated in the figure.

Figure 4 shows the radiation spectra in the same targets as in Fig. 3 but at an accelerated electron energy of 900 MeV. The thickness of the targets and hence also the radiation intensity in different targets differ very strongly, and for this reason, for convenience in making comparisons, the spectra are normalized to the intensity of the radiation near 700 keV.

We can see that suppression of radiation in the soft part of the spectrum as compared with the classical Bethe–Heitler distribution is observed in all thick targets. The dependence of this suppression on the energy of the accelerated electrons corresponds to the analogous dependence of the density effect on the electron energy. However, the characteristic suppression energy in the experiment is higher than the theoretical value. This could be due to the presence of a Landau–Pomeranchuk–Migdal type effect in the observed spectra. According to Ref. 4, the suppression of the radiation intensity in the bremsstrahlung spectrum appears if

$$\omega<k_{\rm LPM}=E^2/E_{\rm LPM}, \tag{1}$$

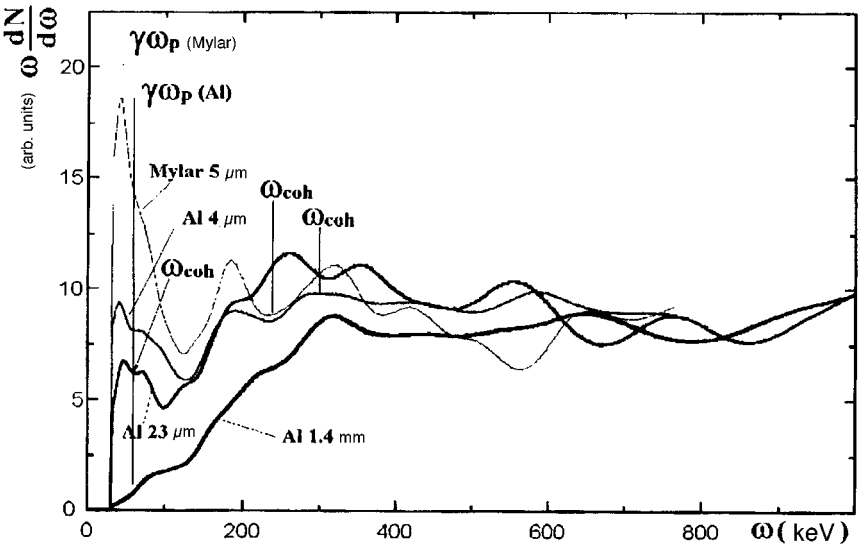

FIG. 4. Spectra of the intensity of radiation from 900 MeV electrons in aluminum and Mylar targets of different thickness, $\omega_{coh}=2\gamma^2/l$.

where ω is the energy of the emitted photon, E is the electron energy, $E_{LPM}=m^2c^4X_0\alpha/8\pi\hbar c$, m is the electron mass, X_0 is the radiation length, and α is the fine-structure constant.

For our conditions ($E=900$ MeV, aluminum target) $k_{LPM}=20$ keV. However, an approximate calculation of the spectrum taking account of the distribution of the electrons over the path length up to the exit within the limits of the angle $\theta_\gamma=1/\gamma$ shows that under our conditions a Landau–Pomeranchuk–Migdal contribution can exist in the spectral region 50–400 keV. The shape of the spectrum in this energy range also indicates this.

One can see that in Fig. 3 there is a dependence of the suppression effect on the target thickness. Analysis of this fact shows that this dependence is due to the large multiple-scattering angles of the electrons in molybdenum. This is why there is a large contribution from radiation to the collimator at large angles to the direction of motion of the electron, when its Lorentz factor no longer influences much the characteristics of the radiation. Allowing for multiple scattering in the density effect confirms the appearance of this dependence on the thickness. That is, there is no new effect here. This is also confirmed by the fact that there is no such dependence for light targets (Fig. 3).

At an accelerated electron energy of 600 MeV (Fig. 3) we see only suppression of radiation in the soft part of the spectrum, but for 900 MeV electrons (Fig. 4) the shape of the spectrum in thin targets is qualitatively different. As the target thickness decreases, the radiation intensity in the energy range up to 100 keV increases substantially. We note that for this energy range the target thickness (4 μm) is much smaller than the radiation formation length (>30 μm). Under these conditions the transition radiation is sup-

pressed. To be certain that the increase in the radiation intensity in the energy range up to 100 keV is not due to transition radiation, we measured the radiation spectrum in a 4 μm thick aluminum target with an electron energy of 900 MeV under conditions of strict collimation (0.2 mrad) of the bremsstrahlung. In this case, the ratio of the transition radiation intensity to the bremsstrahlung intensity should be several times lower. However, the shape of the experimental spectra with collimations of 0.6 and 0.2 mrad turned out to be the same. We note that the radiation intensity in the soft part of the spectrum from a 5 μm thick Mylar target is much higher than the radiation intensity of 700–800 keV photons. This can happen only if we are observing some kind of coherent radiation. In addition, this effect appears only in thin targets, when the target thickness is equal to or less than the radiation formation length. We assume that under these conditions there are no other coherent processes besides coherent radiation on macroscopic (of the order of several hundreds of angstroms) inhomogeneities in the target material. The intensity of this radiation depends very strongly on the character and size of the inhomogeneities, and for this reason it is still impossible to calculate it. Our estimates showed a qualitative correspondence between the forms of the theoretical and experimental spectra of the coherent radiation and the dependence of this radiation on the energy of the accelerated electrons.

Our investigations with accelerated electron energies less than 1 GeV confirmed the density effect, predicted by Ter-Mikaélyan, in bremsstrahlung from electrons in amorphous targets. It was shown that the suppression of the soft component of the radiation in thin amorphous targets (when the thickness of the target is less than the radiation formation length) is different from the suppression calculated neglecting the target thickness. The shape of the measured spectra suggests that the Landau–Pomeranchuk–Migdal effect makes a substantial contribution under these conditions. Coherent bremsstrahlung on macroscopic inhomogeneities in the material of thin amorphous targets was observed experimentally.

[1] M. L. Ter-Mikaélyan, *Higher-Energy Electromagnetic Processes in Condensed Media*, Wiley-Interscience, New York, 1972 [Russian original, Erevan, 1969].
[2] L. D. Landau and Ya. Pomeranchuk, Dokl. Akad. Nauk SSSR **92**, 735 (1953).
[3] K. Yu. Platonov, I. P. Toptygin, and G. D. Fleĭshman, Usp. Fiz. Nauk **160**(4), 59 (1990) [Sov. Phys. Usp. **33**, 289 (1990)].
[4] P. L. Anthony, R. Becker *et al.*, Phys. Rev. Lett. **75**, 1949 (1995).
[5] N. N. Nasonov, Ukr. Fiz. Zh. **37**(2), 210 (1992).

Translated by M. E. Alferieff

On ''Hodge'' topological strings at genus zero

A. Losev[a)]

Institute of Theoretical and Experimental Physics, 117259 Moscow, Russia; Department of Physics, Yale University, New Haven, CT 06520

(Submitted 9 January 1997; resubmitted 13 February 1997)
Pis'ma Zh. Éksp. Teor. Fiz. **65**, No. 5, 374–379 (10 March 1997)

A ''Hodge strings'' construction of solutions to associativity equations based on the t-part of $t-t^*$ equations is proposed. This construction formalizes and generalizes the ''integration over the position of the marked point'' procedure for computation of amplitudes in topological conformal theories coupled to topological gravity. © *1997 American Institute of Physics.* [S0021-3640(97)00205-3]

PACS numbers: 11.25.−w

1. TOPOLOGICAL STRINGS AND ASSOCIATIVITY EQUATION

The ''topological string theory''[1–6] studies genus-q ''generalized amplitudes'' $\underline{GA}_q$ which take on values in cohomologies of the Deligne–Mamford compactification $\underline{M}_{q,n}$ of the moduli space of complex structures of genus-q Riemann surfaces with n marked points. The pairing between GA_q and the cycle $C \in \underline{M}_{q,n}$ is given by[1,2,5] the functional integral:

$$(GA_q, C)(V_1, \ldots, V_n) = \int_{C \in \underline{M}_{q,n}} \int \mathcal{D}\phi V_1(\phi(z_1)) \ldots V_n(\phi(z_n)) \exp(S_{TS}(\phi)), \tag{1}$$

where the fields $V_i(\phi(z))$ are called vertex operators and the ordinary amplitudes $A_q(V_1, \ldots, V_n)$ correspond to $C = \overline{M}_{q,n}$.

The Deligne–Mamford compactification $\overline{M}_{0,n}$ is a union of $M_{0,n}$ (set of n noncoincident points on CP_1 moduli $SL(2,C)$ action) and a compactification divisor *Comp*. The divisor *Comp* is a union of components $C(S)$, where S is a partition of n marked points into two groups consisting of $n_1(S)$ and $n_2(S)$ points, $n_i > 1$. A surface corresponding to a general point in $C(S)$ is a union of two spheres having one common point with $n_1(S)$ marked points on the first sphere and $n_2(S)$ on the second. The set of general points in $C(S)$ form a space $M_{0,n_1+1} \otimes M_{0,n_2+1}$.

It is expected[1] that the functional integral for surfaces corresponding to points in $C(S)$ factorizes, and

$$(GA_0, C(S))(V_{i_1}, \ldots, V_{i_n}) = \eta^{jk} A_0(V_{i_1}, \ldots, V_{i_{n_1}}, V_j) A_0(V_{i_{l+1}}, \ldots, V_{i_{n_2}}, V_k), \tag{2}$$

where η is a matrix of symmetric bilinear nondegenerate products of vertex operators.

Keel found that the homology ring H_* of $\overline{M}_{0,k}$ is generated by cycles $C(S)$. He described relations between these cycles in homologies leading (by virtue of (2)) to constraints on GA_0.

An elegant way of formulation of these constraints uses the generating function for the amplitudes. Introducing formal parameters T_i we define

$$F(T)=\sum_{k=3}^{\infty}\frac{1}{k!}A_0(T_{i_1}V_{i_1},\ldots,T_{i_k}V_{i_k})\,. \tag{3}$$

Then

$$\frac{\partial^3F(T)}{\partial T_i\partial T_j\partial T_k}\,\eta^{kl}\,\frac{\partial^3F(T)}{\partial T_l\partial T_p\partial T_q}=\frac{\partial^3F(T)}{\partial T_i\partial T_p\partial T_k}\,\eta^{kl}\,\frac{\partial^3F(T)}{\partial T_l\partial T_j\partial T_q}. \tag{4}$$

Using the factorization property and Keel's decription of homologies of the moduli space, one can reconstruct GA_0 from A_0 (Ref. 5; see also 4).

2. AMPLITUDES IN TOPOLOGICAL CONFORMAL THEORY COUPLED TO TOPOLOGICAL GRAVITY

The Hodge string construction generalizes the ''integration over the position of the marked point'' procedure[1–4] of computation of amplitudes in the ''conformal topological theory coupled to topological gravity.''

The general covariant action S_m of the topological field theory is a sum of a topological (metric-independent) Q-closed term $S_{\rm top}$ and a Q-exact term for a fermionic scalar symmetry Q:

$$S_m=S_{\rm top}(\phi)+Q(R(\phi),g),$$

where g denotes the metric on the Riemann surface. The energy–momentum tensor T is Q-exact:

$$T=Q\left(\frac{\delta R}{\delta g}\right)=Q(G)\,. \tag{5}$$

We call a topological field theory conformal if R is conformal invariant, i.e., if G is traceless.

We introduce fermionic two-tensor fields ψ, such that functions of g, ψ are forms on the space of metrics and external differential on these forms: $Q_g=\psi(\delta/\delta g)$.

The action for topological theory coupled to topological gravity is

$$S_{TS}=S_m+\psi G=S_{\rm top}+(Q+Q_g)(R).$$

The functional integral $Z(g,\psi)$ over the set of fields ϕ with the action S_{TS} is a closed form on the space of metrics. Since G is traceless, Z is a horizontal[4,8] form[b)] with respect to conformal transformations of the metric and diffeomorphisms of the Riemann surface, and thus it defines a closed form on the moduli space of conformal (=complex) structures on the genus-q Riemann surface.

To construct generalized amplitudes, at marked points on the Riemann surface we insert fields(zero-observables or ''vertex operators'') V_i such that

$$Q(V_i)=0, \quad G_{0,-}(V_i)=0. \tag{6}$$

Here $G_{0,-}$ is the superpartner of the component of the energy–momentum tensor $T_{0,-}$ that corresponds to the rotation, with the constant phase $z\to e^{i\theta}z$, of the local coordinate at the marked point. The first condition in (6) is needed to construct a closed form on the space of metrics, while the second provides horizontality of the corresponding form with respect to diffeomorphisms that leave the marked points fixed but rotate the local coordinate.[4,8,10,11]

3. INTEGRATION OVER POSITIONS OF THE MARKED POINTS

The ''integration over marked points'' procedure reduces all genus-zero amplitudes to the three-point amplitude:

$$F_{ijk}=A_0(V_i,V_j,V_k),$$

which can be computed from the topological matter theory.

In conformal topological theory we associate to a zero-observable V_i a two-observable $V_i^{(2)}=G_{L,-1}G_{R,-1}V_i$. Thus we deform a topological theory to a family of theories parametrized by t, with the action $S_m(t)=S_m+t_iV_i^{(2)}$, and so the zero-observables V form a tangent bundle to this space of theories[4].

If in the functional integral that computes the measure on $M_{0,n}$ we first integrate over the position of the marked point and only then take the functional integral, the n-point amplitude becomes the derivative in t of the $n-1$ point amplitude.

In the process of integration we should take the special care about the region where the moving point tends to hit a fixed point, since the geometry there is not a ''naive'' one. The contribution from this region (contact terms[3,6,8,9]) leads to a specific contact term connection on the bundle of zero-observables over the space of theories and thus on the tangent space to the space of theories.

Repeating this procedure again and again, we can recover the amplitudes from $F_{ijk}(t)$. The amplitudes should be symmetric and independent of the order of integration over the positions of the marked points.

In other words, the generating parameters T from (3) should become so-called special coordinates on the space of theories, the derivatives with respect to special coordinates should become covariantly constant sections of the contact term connection, and the symmetric tensor F_{ijk} (in the special coordinate frame) should be a third derivative of $F(T)$. Moreover, $F(T)$ has to satisfy the WDVV equations (4).

This implies that the contact term connection is quite a special one!

To gain a better understanding of this connection we will study the space of states in 2D theory associated to the boundary of the Riemann surface — to the circle. Moreover, we will restrict ourselves to the subspace H of these states that are invariant under the constant rotations of the circle.

The fermionic symmetry Q of the theory and $G_{0,-}$ reduce to odd anticommuting operators Q and G_- on H.

Zero-observables V_i, when inserted at the middle of the punctured disc, generate states h_i that are Q- and G_--closed:

$$Qh_i = G_- h_i = 0; \tag{7}$$

the zero-observable 1 generates the distinguished state h_0. The operation of stitching two discs together corresponds to the bilinear pairing $\langle , \rangle$. Integrals of zero-observables along the boundary give operators $\Phi_i = \int_{S_1} V_i d\sigma$.

One can show that they have the following properties:

$$Q^2 = G_-^2 = QG_- + G_- Q = 0, \quad [Q, \Phi_i] = 0, \quad [\Phi_i, \Phi_j] = 0, \tag{8}$$

$$Q^T = \epsilon Q, \quad G^T = -\epsilon G, \quad \Phi^T = \Phi . \tag{9}$$

Here the transpose ''T'' is taken with respect to the pairing $\langle , \rangle$, and the operator ϵ commutes with Φ and anticommutes with Q and G_-.

In the deformed theory one has $Q(t) = Q + [G_-, t_i \Phi_i]$ at first order in t. To ensure it globally we will take for simplicity[c)]

$$[[G_-, \Phi_i], \Phi_j] = 0. \tag{10}$$

The contribution from the region near the place where the ''moving'' ith point hits the marked jth point gives the ''cancelled propagator argument'' (CPA) constraint on states h_j over the space of theories:[3,8,9]

$$\delta_i^{(\mathrm{CPA})} h_j = G_- \int_0^\infty d\tau G_{0,+} \exp(-\tau T_{0,+}) \Phi_i h_j , \tag{11}$$

so $\delta^{(\mathrm{CPA})} h$ is G_--exact. Here $T_{0,+}$ is the Hamiltonian acting on the space H, and $G_{0,+}$ is its superpartner: $T_{0,+} = Q(G_{0,+})$.

Covariantly constant sections[d)] of the CPA connection will be denoted as $h_i(t)$. This connection induces the connection on the space of zero-observables: covariantly constant sections of contact term connections $V_i(t) = u_i^j(t) V_j$ are such that, when inserted in the middle of the disc in the t-deformed theory, they produce covariantly constant sections $h_i(t)$:

$$h_i(t) = \lim_{r \to 0} r^{T_{0,+}} \Phi_j h_0(t) u_i^j(t). \tag{12}$$

Let us denote by $C_i(t)$ the matrix of operations of Φ_i in $Q(t)$-cohomologies. Then relation (12) reads:

$$[h_i(t)]_{Q(t)} = u_i^j(t) C_j(t) [h_0(t)]_{Q(t)} \tag{13}$$

here and below $[h]_Q$ stands for a class of a Q-closed element h in Q-cohomologies.

From the functional integral we get:

$$F_{ijk}(t) = \langle h_i(t), \Phi_l h_k(t) \rangle u_j^l(t) . \tag{14}$$

While the string origin of the above procedure is quite natural, its consistency is far from being obvious.

In the next section we will show how to construct solutions to the associativity equations (and thus all GA_0) from the Hodge data $(H,Q,G_-,\Phi_i,\langle\rangle)$ if we assume the Hodge property and the primitive element property. In particular, this would demonstrate the consistency of the ''integration over the positions of the marked point'' procedure if the Hodge data were obtained from some topological conformal theory.

Hodge property: There is a set of Q- and G_--closed vectors h_i such that classes $[h_i]_Q$ and $[h_i]_{G_-}$ form bases in Q- and G_--cohomologies.

Primitive element property: There is a class $[h_0]_Q$ in Q-cohomologies such that the matrix $D_{ia}=C^b_{i,a}h_{0,b}$ is square and nondegenerate. Here the indices a label some basis in Q-cohomologies, $C^b_{i,a}$ is a matrix representing the operation of Φ_i in these cohomologies, and $h_{0,b}$ are components of the class $[h_0]_Q$.

4. ''HODGE STRING'' CONSTRUCTION

The Hodge string construction gives the solution to the associativity equations starting from the following data: Z_2 -graded vector space H, odd operators Q and G_-, even operators Φ_i, and a bilinear pairing $\langle,\rangle$, having properties satisfying Eqs. (8), (9), and (10), the Hodge property,[e)] and the primitive element property.

The construction goes in two steps. In the first step we construct a flat connection with the spectral parameter from the Hodge data. In physical terms it is a constraint on the space of states. The primitive element property is not used in the first step. In the second step, with the help of the primitive element property we induce flat constraint on the tangent bundle to the deformation space from the constraint constructed in the first step (i.e., we induce connection on the space of zero-observables from the connection on the space of states, like in (13)). Then we will integrate covariantly constant vector fields of this constraint to special coordinates T on the deformation space and finally construct $F(T)$.

Step 1. From the Hodge data one canonically constructs the connection (first constructed by Saito[12] in a slightly different context)

$$\frac{\partial}{\partial t_i}\delta_{ab}+z^{-1}C_{i,ab}(t) \tag{15}$$

such that this connection is flat for all z and $C_{i,ab}=C_{i,ba}$. This connection is known as the t-part of $t-t^*$ equations[7].

Idea of the proof: The Hodge property leads to the Hodge property for $Q(t)$ and G_- for all t close enough to zero (with the preferred vectors $h_i(t)$, such that $\partial_t h_i(t)$ is G_- exact — they generalize covariantly constant sections of the CPA connection (11)). Consider $Q(t,z)=Q(t)+zG_-$ cohomologies in $H\otimes C[z,z^{-1}]$. Classes of $[P_i(z,z^{-1}h_i(t)]_{Q(t,z)}$ (for P_i being t-independent polynomials) form a Hodge basis in $Q(t,z)$ cohomologies. Next, we construct the Gauss–Manin (in the Saito[12] sense) flat connection in $Q(t,z)$-cohomologies through its covariantly constant sections

$$\left[\exp\left(\frac{-t_i\Phi_i}{z}\right)\right]_{Q(t,z)}.$$

The Gauss–Manin constraint written in the Hodge basis takes the form (15). Since bilinear pairing descends to G_- cohomologies it is t independent in the Hodge basis and can be taken to be equal to δ_{ab}. This leads to the symmetry of matrix C_i.

Step 2. From Step 1 we conclude that there exists a symmetric matrix τ_{ab}, such that

$$C_{i,ab}=\frac{\partial}{\partial t_i}\tau_{ab}.$$

Let us define special coordinates T_a on the deformation space with the help of the primitive element

$$T_a(t)=\tau_{ab}(t)h_{0,b}. \tag{16}$$

Statement: There exists a function $F(T)$ defined by

$$\frac{\partial}{\partial T_a\partial T_b}F(T)=\tau_{ab}(t(T)) \tag{17}$$

such that it satisfies the associativity equations with $\eta^{ab}=\delta^{ab}$.

Proof: Explicit check.

Then we define a new set of coordinates[f)] T_i as linear combinations of T_a by:

$$T_a=C_{i,ab}(0)h_{0,b}. \tag{18}$$

A function $F(T_a(T_i))$ is the desired function that solves associativity equations with η^{ij} such that its inverse is given by:

$$(\eta^{-1})_{ij}=\langle h_0,C_iC_jh_0\rangle=h_{0,a}(C_iC_j)_{ab}h_{0,b}.$$

Below we present some explicit formulas. Define

$$C_{i,ab}(t)=\sum C_{ij_1\ldots j_n,ab}\frac{t_{j_1}\ldots t_{j_n}}{n!},\quad F(T_i)=\sum F_{j_1\ldots j_n}\frac{T_{j_1}\ldots T_{j_n}}{n!}. \tag{19}$$

Then

$$F_{ijk}=\langle h_0,C_iC_jC_kh_0\rangle,\quad F_{ijkl}=\langle h_0,C_i[C_j,C_{kl}]h_0\rangle, \tag{20}$$

$$F_{ijklm}=\langle h_0,C_i[C_{jkl},C_m]h_0\rangle+\langle h_0[C_{im},C_j]C_{kl}h_0\rangle+\langle h_0[C_{im},C_l]C_{jk}h_0\rangle$$
$$+\langle h_0[C_{im},C_k]C_{lj}h_0\rangle.$$

I would like to thank R. Dijkgraaf, A. Gerasimov, G. Moore, N. Nekrasov, I. Polyubin, A. Rosly, and S. Shatashvili for helpful discussions.

This work was supported by Grant 96-02-18046 from the Russian Fund for Fundament Research.

[a)]e-mail: lossev@vitep3.itep.ru, losev@genesis5.physics.yale.edu
[b)]A differential form on the principal bundle is called horizontal if its contraction with the vertical (tangent to the fiber) vector is zero. Closed horizontal forms on the total space correspond to closed forms on the base of the bundle.
[c)]In the general case one has to make arguments of the Kodaira–Spencer type, see Ref. 6.
[d)]Flatness of the CPA connection is nessesary for consistency of the procedure.
[e)]The Hodge property is possessed, for example, if Q and G_- are two supersymmetries in $N=2$ supersymmetric quantum mechanics with a discrete spectrum of the Hamiltonian.
[f)]The coordinates T_i integrate the vector fields u_i introduced in Eqs. (12) and (13).

---

[1] E. Witten, Nucl. Phys. B **340**, 281 (1990).
[2] R. Dijkgraaf and E. Witten, Nucl. Phys. B **342**, 486 (1990).
[3] E. Verlinde and H. Verlinde, Nucl. Phys. B **348**, 457 (1991).
[4] R. Dijkgraaf, E. Verlinde, and H. Verlinde, *Proc. of the Trieste Spring School 1990*, Eds. M. Green *et al.*, World Scientific, 1991.
[5] M. Kontsevich, Yu. Manin, Commun. Math. Phys. **164**(3), 525 (1994); S. Keel, Trans. AMS **330**, 545 (1992).
[6] M. Bershadsky, S. Cecotti, H. Ooguri, and C. Vafa, Commun. Math. Phys. **165**, 311 (1994).
[7] S. Cecotti, Nucl. Phys. B **335**, 755 (1991); S. Cecotti and C. Vafa, Nucl. Phys. B **367**, 359 (1991).
[8] R. Dijkgraaf, ''Infinite dimensional analysis,'' talk at RIMS Conf., July, 1993.
[9] A. Losev, Theor. Math. Phys. **95**, 595 (1993); A. Losev and I. Polyubin, Int. J. Mod. Phys. A **10**, 4161 (1995); A. Losev, *Proceedings, Integrable Models and Strings*, Helsinki, 1993; publ. 1995, p. 172.
[10] L. Alvarez-Gaume *et al.*, Nucl. Phys. B **303**, 455 (1988); J. Distler and P. Nelson, Commun. Math. Phys. **138**, 273 (1991).
[11] T. Eguchi *et al.*, Phys. Lett. B **305**, 235 (1993).
[12] K. Saito, Publ. RIMS, Kyoto Univ. **19**, 1231 (1983).

Published in English in the original Russian journal. Edited by Steve Torstveit.

Non-envelope formulation for femtosecond optical pulses in semiconductors

I.V. Mel'nikov[a)]
Institut für Festkörpertheorie und Theoretische Optik, F. Schiller–Universität Jena, D-07743 Jena, Germany

D. Mihalache
Department of Theoretical Physics, Institute of Atomic Physics, P.O. Box MG-6, Bucharest, Romania

F. Moldoveanu
Department of Physics, University of Maryland, College Park, MD 20781, USA

N.-C. Panoiu
Department of Physics, New York University, New York, NY 10003, USA

(Submitted 26 December 1996)
Pis'ma Zh. Éksp. Teor. Fiz. **65**, No. 5, 380–384 (10 March 1997)

We analyze the response of an ensemble of 1*s*-excitons driven by a femtosecond optical pulse, beyond traditional ''slowly varying amplitudes'' approach. For optical pulses of a given duration it is shown that the off-resonance optical field can evolve into a stable soliton with nonzero asymptotic behavior. © *1997 American Institute of Physics.* [S0021-3640(97)00305-8]

PACS numbers: 02.30.Jr, 42.50.Md, 42.65.Tg, 71.36.+c

Over the past few years, optical pulse durations as short as 6–10 femtoseconds have been demonstrated for wavelengths ranging from the blue-green to the near-infrared. These have been widely exploited to generate a unipolar single-cycle electromagnetic pulse in a variety of nonlinear media[1] and have prompted a flurry of activity in theoretical studies in order to answer the question of whether it is possible to obtain correct knowledge relevant to the dynamics of such pulses within the traditional framework of the slowly varying envelope approximation (SVEA) operating with a quasi-monochromatic field. From this point of view there is much importance in the recent observation, *apropos* Kerr self-focusing, that the SVEA loses its justification long before the pulse duration approaches an optical cycle.[2]

The problem encountered by the SVEA in a femtosecond domain is that both the wide spectrum of the pulse and its intense field increase the number of harmonics that have to be included in the series expansion of the polarization in powers of the field and whose phase-matching conditions must be adjusted for all harmonics simultaneously. This violates the basic assumptions of the SVEA as to the presence of a weakly nonlinear and highly dispersive medium; superposition does not hold, preventing one from limiting consideration to a finite number of interacting waves. And, what is more, quantum-mechanical effects may come into play at the subwavelength scale.

The purpose of this letter is to go beyond the SVEA to show the advantages of a self-consistent description based on the semiconductor Maxwell–Bloch equations (SMBEs) and to impose proper relationships among nonlinearity, dispersion, dissipation (or amplification), and backscattering effects. We derive an asymptotic analytic solution for the induced polarization of excitons at low density. It gives rise to new features in the quasiadiabatic following which are absent in the standard SVEA model; known results[3] are also recovered.

Consider the response of a semiconductor to a femtosecond electromagnetic field. It is described by the total macroscopic polarization $\mathcal{P}$ obtained by summing over all wave vectors $\mathbf{k}$, i.e., $\mathcal{P}=2\Sigma_{\mathbf{k}} d_{vc} P_{\mathbf{k}}$, where d_{vc} is the interband dipole matrix element; in the summation, the factor of 2 takes the spin degeneracy into account. The time dependence of $P_{\mathbf{k}}$ is given in the Hartree–Fock limit by the semiconductor Bloch equations written in the notation of Ref. 4:

$$i\hbar\ \partial_t\ P_{\mathbf{k}}=(\epsilon_{c,\mathbf{k}}-\epsilon_{v,\mathbf{k}}+\epsilon_g^0)P_{\mathbf{k}} + (n_{e,\mathbf{k}}+n_{h,\mathbf{k}}-1)d_{cv}E-\sum_{\mathbf{q}}\ V_{|\mathbf{k}-\mathbf{q}|}P_{\mathbf{q}}, \tag{1}$$

$$i\hbar\ \partial_t\ n_{e,\mathbf{k}}=d_{vc}EP_{\mathbf{k}}-d_{cv}EP_{\mathbf{k}}^*, \tag{2}$$

here the subscript t indicates the corresponding derivative. The sum in the right-hand side of Eq. (1) is conventionally termed a Coulomb hole and is given by the departure of the screened Coulomb potential $V_{\mathbf{k}}$ from its unscreened value. For simplicity the collision terms in Eqs. (1) and (2) are neglected; this places an upper limit of 60 fs on the pulse width τ_p which can give rise to a quasiadiabatic following.[5] Since we are interested in low carrier densities, the contribution dominated by changes in the chemical potential (i.e., phase-space filling), conventionally called screened exchange, can be neglected, and the sums $\Sigma_{\mathbf{q}} V_{k-q} P_q n_q$, $\Sigma_{\mathbf{q}} V_{k-q} n_q P_q$, and $\Sigma_{\mathbf{q}} V_{k-q} P_q P_k^*$, can be also omitted in Eqs. (1) and (2).

Following the steps used to calculate the macroscopic polarization $\mathcal{P}$ we subsequently Fourier transform Eqs. (1) and (2) and scale the transformed polarization P_λ and excitation density n_λ with the Wannier function ψ_λ defined at the lattice site. In this way, one can formally write out $\tilde{P}_\lambda$ as

$$\tilde{P}_\lambda(z,t)=id_{cv}\hbar^{-1}\int_{-\infty}^{t}[1-2\tilde{n}_\lambda(z,\tau)]E(z,\tau)\exp[-i\omega_\lambda(t-\tau)]d\tau, \tag{3}$$

where λ labels the discrete exciton energy states. In turn, the macroscopic polarization $\mathcal{P}$ may be written as $\mathcal{P}(t)=2d_{cv}\Sigma_\lambda|\psi_\lambda(R=0)|^2\tilde{P}_\lambda+\text{c.c.}$

These equations show that if one knows a functional relation $\tilde{P}_\lambda=\tilde{P}_\lambda(\tilde{n}_\lambda,E)$ among the induced polarization, excitation density, and the pulse field, then $\tilde{n}_\lambda(E)$ may be determined. Furthermore, if both $\tilde{n}_\lambda(E)$ and $\tilde{P}_\lambda(\tilde{n}_\lambda,E)$ are known, then one can derive, at least formally (by resolving the SBEs), the functional relation $\mathcal{P}=\mathcal{P}(E)$. This turns the wave equation into a nonlinear partial differential equation for $E(z,t)$ alone. Pursuing this program, we replace the integral (3) by

$$\int_{-\infty}^{t}\cdots d\tau \rightarrow \frac{1}{i\omega_\lambda}\sum_{0}^{m}\frac{(-1)^k}{(i\omega_\lambda)^k}\frac{\partial^k}{\partial t^k}[(1-2\tilde{n}_\lambda)E], \tag{4}$$

which presumes that the dependence $n(E)$ is a power series in E and $\partial_t E$. In principle, the series (4) generates an infinite hierarchy of coupled equations. Thus the best one can hope to do is to truncate this expansion, i.e., to find an expansion parameter which makes such a truncation meaningful. In general, this means long pulses, i.e., $\omega_\lambda \tau_p \gg 1$, which is essentially the approach first introduced by Crisp,[6] whose expansion parameter was $s=1/(\omega_g-\omega_p)\tau_p \ll 1$.

From Eqs. (3) and (4) one can derive the relation

$$\mathcal{P}(z,t)=\frac{4\epsilon_{\rm exc} r_0}{\pi\epsilon_\lambda}\left(E-\frac{\hbar^2}{\epsilon_\lambda^2}\frac{\partial^2 E}{\partial t^2}-\frac{1}{2}E\frac{E^2}{E_0^2}\right), \tag{5}$$

where $r_0=[1-2\tilde{n}_\lambda(t=-\infty)]$, $E_0=\epsilon_\lambda/2d_{cv}$, and $\epsilon_{\rm exc}$ is the exciton binding energy. Note that we dropped all terms of the order higher than two in the expansion (4), and that both amplifying and absorbing semiconductors are described by Eq. (5). It is also of particular importance for the analysis below that the nonlinearity and dispersion contribute to the polarization (5) with the same sign. In the plane-wave approximation, its substitution into the classical wave equation leads to

$$\partial_{zz}E=c^{-2}\partial_{tt}[1+16r_0(\epsilon_{\rm exc}/\epsilon_\lambda)(1-(\hbar/\epsilon_\lambda)^2\partial_{tt})-8r_0(\epsilon_{\rm exc}/\epsilon_\lambda)(E/E_0)^2]E. \tag{6}$$

This can be further simplified under the assumption that $E_t+cE_z \approx E_t$, which physically means that we consider a femtosecond pulse propagating in the positive z direction and stipulates that the backscattered wave is taken into account on a spatial scale larger than the pulse length. Under these circumstances, Eq. (6) becomes

$$E_z+v_g^{-1}E_t+c_1E^2E_t+c_2E_{ttt}=0, \tag{7}$$

where the following set of parameters is used:

$$v_g=c[1+4\pi r_0\chi_l(0)]^{-1/2}, \quad c_1=\frac{6\pi v_g}{c^2}r_0\chi_{nl}(0),$$

$$c_2=r_0\frac{\pi v_g}{c^2}\left[\frac{\partial^2\chi_l}{\partial\omega^2}\right]_{\omega=0}, \text{ and } \chi_{nl}(0)=\frac{1}{4\pi}\frac{\hbar\omega_{LT}}{\epsilon_\lambda}\frac{1}{E_0^2},$$

where $\chi_l(\omega)$ is the linear susceptibility of excitons, $\omega_{LT}=8\pi s d_{cv}^2\hbar^{-1}$, and s is the Sommerfeld factor; $\chi_{nl}(0)$ is related to the traditional cubic susceptibility of the semiconductor as follows:

$$\chi_{nl}(0)=\frac{4}{3}\chi^{(3)}(3\omega,\omega,\omega,\omega)\big|_{\omega=0}=4\chi^{(3)}(\omega,\omega,\omega,-\omega)\big|_{\omega=0}.$$

Equation (7) is the modified Korteweg–de Vries equation (mKdV) which belongs to the class of partial differential equations integrable by the inverse scattering transform.[7] The general solutions of Eq. (7) are governed by the relative sign between the nonlinear

and dispersion terms, the asymptotic values of the field (the boundary condition), and by the pulse width. In the notation $E(z=\pm\infty)=E_\infty$, the general single-soliton solution takes the form

$$E(z,t)=E_\infty\left[1-\frac{4e^{-\beta}(1-E_d/E_0)}{(1-E_d/E_0-2\delta^2e^{-\beta})^2+2\delta^2e^{-2\beta}}\right]. \tag{8}$$

Here

$$\beta=(t-z/v)/\tau_p+\beta_0, \quad E_d^2=2E_\infty^2+E_0^2, \quad \delta=E_\infty/E_0,$$

$$v^{-1}=v_g^{-1}[1+2\pi r_0\chi_{nl}(0)(3E_\infty^2+E_0^2)], \text{ and } \tau_p=\sqrt{\frac{[\partial^2\chi_l/\partial\omega^2]_{\omega=0}}{2E_0^2\chi_{nl}(0)}},$$

where E_0 labels the maximum amplitude of the bright soliton, and its displacement from E_∞ is given by E_d, which is to be found for a given set of boundary conditions. It turns out that the solutions $E(z,t)$ lie in the range $E_\infty\leqslant E\leqslant E_\infty+4\delta E_0^2$. They describe either a bright soliton superimposed on a continuous-wave background, i.e., a unbound soliton, or a hyperbolic-secant solitary pulse; the behavior depends on the value of E_∞. The transition between bound and unbound solitons occurs at $E_\infty>0$, which may be brought about by biasing the semiconductor with a dc electric field. It is under this condition that the unbound soliton (8) is excited and will propagate through the medium of excitons.

In the limiting case $E_\infty=0$ one can expect that the general solution (8) converges to the hyperbolic-secant form

$$E(z,t)=\frac{1}{\tau_p}\sqrt{\frac{[\partial^2\chi_l/\partial\omega^2]_{\omega=0}}{\chi_{nl}(0)}}\,\mathrm{sech}\left(\frac{t-z/v}{\tau_p}\right), \tag{9}$$

which is determined exclusively by the given pulse width τ_p; its velocity is

$$v^{-1}=v_g^{-1}\left(1+\frac{\pi r_0}{\tau_p^2}\left[\frac{\partial^2\chi_l}{\partial\omega^2}\right]_{\omega=0}\right). \tag{10}$$

This leads to the expected result that the soliton (9) has a lower velocity than that of a low-frequency electromagnetic wave in the inverted medium ($r_0=1$), and a greater velocity than that of a low-frequency electromagnetic wave in the absorbing medium ($r_0=-1$).

In the general case of the nonzero boundary condition, the unbound soliton (8) occurs, and its behavior is considerably more complicated. In Fig. 1 we plot the intensity of single bright solitons with nonzero boundary conditions for a variety of different ratios δ. There is a typical spreading out of the hump amplitudes for values of $\delta\geqslant 1$. Notice also the appearance of asymmetry for $\delta>0.5$. This is due to the line broadening by the dc field E_∞, which shifts the dispersion contour and thus makes the whole pulse profile asymmetric.

Let us return to Eq. (5). As we mentioned, the relative contributions to the polarization of excitons from nonlinearity and dispersion effects are of the same sign and this dictates our choice of the solution with nonzero asymptotic behavior of the form (8) and rules out the following dark soliton solution:

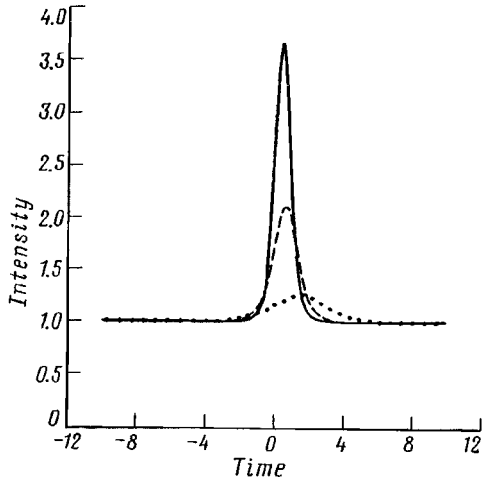

FIG. 1. Normalized intensity versus normalized time for single bright solitons with nonzero boundary conditions; $\delta=0.75$ — (solid), 1.0 — (dashes), and 2.0 — (dots). Note the asymmetry of the soliton acquired with the growth of δ.

$$E(z,t)=E_\infty\left[1-\frac{4e^{-\beta}}{(1+2\delta^2e^{-\beta})^2-2\delta^2e^{-2\beta}}\right], \tag{11}$$

where

$$\beta=(t-z/v)/\tau_p+\beta_0, \text{ and } v^{-1}=v_g^{-1}[1+2\pi r_0\chi_{nl}(0)(3E_\infty^2-E_0^2)].$$

This solution is depicted in Fig. 2 and describes the bifurcation of the dark-grey soliton state into the coupled state of two dark-black solitons of equal width, with $\delta\to\sqrt{2}/2$ as a

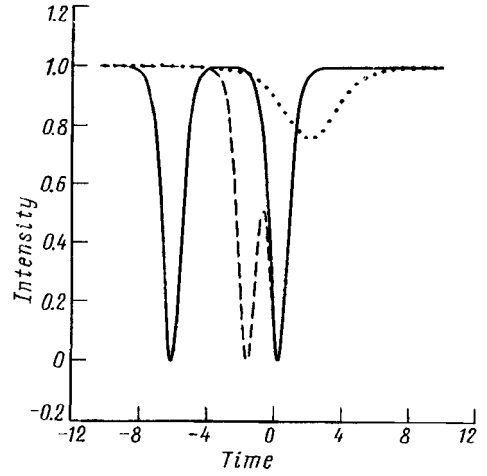

FIG. 2. Dark-grey to dark-black soliton bifurcation; $\delta=\sqrt{2}/2$ — (solid), 0.72 — (dashes), and 2 — (dots). Note the asymmetry as in Fig. 1.

point of bifurcation. Although this topology of the femtosecond field should be regarded as only illustrative, it is noteworthy that it refutes the misconception of Hayata and Koshiba[3] that a prerequisite of its existence is the presence of a quadratic nonlinearity in the system.

It would be of interest to verify our results experimentally for, say, a GaAs/AlGaAs guiding structure, in which Harten *et al.* observed the escape of a subpicosecond pulse from a quasiadiabatic following.[8] This was identified with carrier density oscillations in the semiconductor. It is anticipated in our study that the effects of phase-space filling and exciton screening may be quasiadiabatically ruled out, and thus the line broadening must be lifted. On the other hand, the quasiadiabatic following regime requires that the pulse contains several optical cycles, and hence sets a window for the pulse width used in experiments. In addition, one must have a structure as long as several soliton interaction lengths in order to ensure soliton formation. The first step is thus to do shape measurements to see if the pulse reaches the steady-state shape corresponding to the given pulse width and the material parameters. If the soliton is observable, its shape can be changed by a dc seed field, and this provides a further test of the theoretical predictions. Therefore, 1-cm long GaAs/AlGaAs guiding structure at room temperature may yield the predicted behavior upon a 10 GW/cm^2 excitation by a Ti:sapphire laser generating 20–60 fs pulses at $\lambda = 850 - 940$ nm. Such an experiment may dramatically change the picture of quasiadiabatic following in semiconductors obtained so far within the SVEA.

We thank S. A. Darmanyan, F. Lederer, A. Miller, and S. G. Tikhodeev for helpful suggestions and comments. The work performed in Jena was supported by Deutsche Forschungsgemeinschaft (DFG).

[a)]e-mail: ivm@gpi.ac.ru. Permanent address: General Physics Institute, Russian Academy of Sciences, ul. Vavilova 38, 117942 Moscow, Russian Federation

---

[1] D. H. Auston and M. C. Nuss, IEEE J. Quantum Electron. **QE-24**, 255 (1988); D. You, R. R. Jones, P. H. Bucksbaum, and D. R. Dykaar, Opt. Lett. **18**, 290 (1993); R. R. Jones, D. You, and P. H. Bucksbaum, Phys. Rev. Lett. **70**, 1236 (1993); C. O. Reinhold, M. Melles, H. Shao, and J. Burgdörfer, J. Phys. B **26**, L659 (1993); M. R. X. de Barros, R. S. Miranda, T. M. Jedju, and P. C. Becker, Opt. Lett. **20**, 480 (1995); A. Bonvalet, M. Joffre, J. L. Martin, and A. Migus, Appl. Phys. Lett. **67**, 2907 (1995).
[2] J. E. Rothenberg, Opt. Lett. **17**, 1340 (1992).
[3] K. Hayata and M. Koshiba, J. Opt. Soc. Am. B **11**, 2581 (1994).
[4] W. W. Chow, S. W. Koch, and M. Sargent III, *Semiconductor-Laser Physics* (Springer-Verlag, Berlin, 1994).
[5] R. Binder, D. Scott, A. Paul *et al.*, Phys. Rev. B **45**, 1107 (1992).
[6] M. D. Crisp, Phys. Rev. A **1**, 1604 (1970).
[7] See, e.g., G. L. Lamb Jr., *Elements of Soliton Theory* (Wiley, New York, 1980) and references therein.
[8] P. A. Harten, A. Knorr, J. P. Sokoloff *et al.*, Phys. Rev. Lett. **69**, 852 (1992).

Published in English in the original Russian journal. Edited by Steve Torstveit.

Observation of oriented 2^3S_1 helium atoms in a sodium–helium plasma irradiated by polarization-modulated laser radiation

S. P. Dmitriev, N. A. Dovator, R. A. Zhitnikov, V. A. Kartoshkin, and V. D. Mel'nikov

A. F. Ioffe Physicotechnical Institute, Russian Academy of Sciences, 194021 St. Petersburg, Russia

(Submitted 5 January 1997)
Pis'ma Zh. Éksp. Teor. Fiz. **65**, No. 5, 385–387 (10 March 1997)

An experiment on the observation of spin polarization of metastable helium atoms interacting with optically oriented sodium atoms under continuous rf discharge conditions is described. Laser radiation with alternating-sign circular polarization, tuned to the resonance excitation of the $3^2S_{1/2}$–$3^2P_{1/2}$ transition in Na atoms, is used as the source for optical pumping of ground-state sodium atoms. © *1997 American Institute of Physics.* [S0021-3640(97)00405-2]

PACS numbers: 67.65.+z, 52.80.Pi, 32.80.Bx

Spin orientation of atoms can be obtained not only as a result of their interaction with optical resonance radiation but also as a result of spin-orientation transfer from atoms of one kind (preoriented) to atoms of a different kind (initially unoriented). For example, orientation of metastable triplet helium atoms can occur as a result of the interaction of the atoms with optically oriented alkali atoms in a pulsed rf discharge plasma. Orientation of 2^3S_1 helium atoms in Cs–He,[1] Rb–He,[2,3] and K–He[4] plasmas has been obtained by this method. The characteristic experimental features of these works were the use of a pulsed rf discharge (which produced the alkali–helium plasma), the use of electrode-free spectral lamps as light sources for optical pumping of the alkali-metal atoms, and detection of the orientation of the helium atoms according to the change in the absorption of the pump light accompanying the excitation of magnetic resonance in the $2^3S_{1/2}$ state of the helium atoms.

In the present work we observed the transfer of spin orientation from sodium atoms oriented by laser radiation to 2^3S_1 metastable helium atoms excited in the Na–He plasma of a continuous rf discharge. The use of polarization-modulated laser pump radiation in this experiment made it possible to detect spin orientation of the helium atoms according to a change in the absorption of the resonant helium light without using the magnetic-resonance technique.

The experimental arrangement is displayed in Fig. 1. In this work, we used a ≈ 70 mW tunable continuous dye laser (rhodamine-6G), built in the laboratory, with a 4-watt argon pump laser tuned to the wavelength ($\Lambda = 589.6$ nm) of the $3^2S_{1/2}$–$3^2P_{1/2}$ transition in the sodium atoms. The essence of the experiment was as follows. An alternating-sign orientation of the sodium atoms is produced by the action of the pump laser radiation

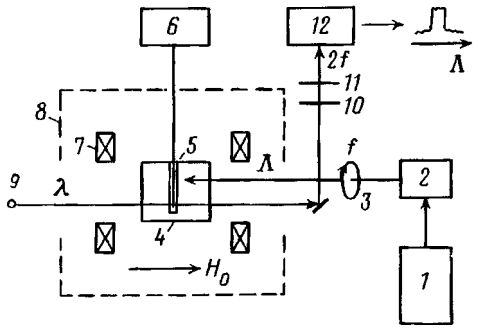

FIG. 1. Schematic diagram of the experimental apparatus: *1* — Argon laser, *2* — tunable laser, *3* — rotating $\Lambda/4$ plate, *4* — thermostatted gas-discharge chamber, *5* — enameled electrode, *6* — rf discharge generator, *7* — Helmholtz coil, *8* — ferromagnetic shield, *9* — helium spectral lamp, *10* — circular analyzer, *11* — interference filter (λ), *12* — photodetecting unit with a synchronous detector.

which is directed along a constant magnetic field $H_0 = 40$ mOe and passes through a mica quarter-wave ($\Lambda/4$) plate rotating with frequency $f = 60$ Hz. The 2^3S_1 metastable helium atoms were aligned as a result of spin-dependent collisional processes[a)] occurring in a gas-discharge chamber, consisting of a glass cell with metallic sodium and helium-4 under a pressure of 1 torr. Unpolarized radiation from a helium lamp was passed through the plasma in the direction of the pump beam and was used to detect the spin orientation of the helium atoms that arises in atom–atom and electron–atom collisions. A circular analyzer and an optical filter ($\lambda = 1083$ nm, 2^3S_1–$2^3P_{0,1,2}$ transition in He atoms) were placed between the gas-discharge chamber and the photodetector. In this case the intensity of the light recorded by the photodetector depends on the direction and degree of orientation of the ensemble of 2^3S_1 helium atoms.[5] Since the sign of the circular polarization of the light pumping the Na atoms changes from σ^+ to σ^- twice during every revolution of the $\Lambda/4$ plate and the orientation of the helium atoms follows the change in the orientation of the Na atoms, the output signal of the photodetector consists of an alternating voltage with a frequency $2f = 120$ Hz.

Figure 2 displays the signal showing the variation in the intensity of the probe light from the helium lamp. The signal was obtained by synchronous detection at the frequency $2f$ while slowly varying the wavelength of the tunable laser near the resonance line of sodium (D_1 line, $\Lambda = 589.6$ nm). Detection of such a signal indicates unequivocally the appearance of spin-oriented helium atoms in a sodium–helium plasma. The width of the signal in Fig. 2 is determined by the spectral width of the tunable laser radiation and equals 0.007 nm. The relative amplitude of signal corresponds to $\delta I/\Delta I = 0.001$, where δI is the change occurring in the intensity of the probe light as the wavelength of the laser radiation is scanned and ΔI is the change in the intensity of the probe light due to absorption of the light in the chamber when the discharge is switched on. The ratio $\delta I/\Delta I$ can serve as an estimate of the degree of orientation of 2^3S_1 metastable He atoms.

In conclusion it should be noted that the comparatively low degree of orientation (0.1%) of the helium atoms which is obtained in the present experiment can be increased

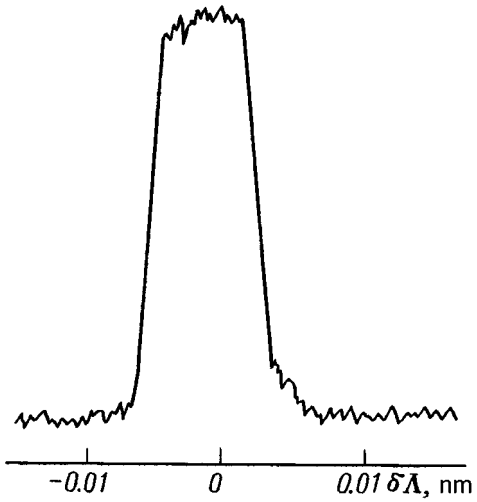

FIG. 2. Signal showing the variation in the intensity of the probe light as the wavelength of the radiation from a tunable laser is scanned in the region of the D_1 line of sodium ($\Lambda = 589.6$ nm). The signal was recorded at a gas-discharge temperature of ≈ 150 °C.

by decreasing the depolarization of the sodium atoms at the walls of the chamber (by increasing the pressure of the buffer gas (He)), optimizing the parameters of the gas discharge, and increasing the spectral power of the laser radiation. We plan to do this in future experiments.

[a)]Elementary processes of this kind in an alkali–helium plasma also include spin-dependent Penning ionization of $n^2S_{1/2}$ alkali-metal atoms interacting with 2^3S_1 helium atoms, interatomic spin exchange occurring in elastic collisions of these atoms, and also collisions of He atoms with electrons polarized in the process of spin exchange of free plasma electrons with optically oriented alkali-metal atoms.

[1] E. V. Blinov, R. A. Zhitnikov, and P. P. Kuleshov, Pis'ma Zh. Tekh. Fiz. **2**, 305 (1976) [Sov. Tech. Phys. Lett. **2**, 117 (1976)].
[2] G. M. Keiser, H. G. Robinson, and C. E. Jonson, Phys. Lett. A **51**, 5 (1975).
[3] E. V. Blinov, B. I. Ginzburg, and R. A. Zhitnikov, Zh. Tekh. Fiz. **54**, 287 (1984) [Sov. Phys. Tech. Phys. **29**, 168 (1984)].
[4] E. V. Blinov, B. I. Ginzburg, R. A. Zhitnikov, and P. P. Kuleshov, Zh. Tekh. Fiz. **54**, 2315 (1984) [Sov. Phys. Tech. Phys. **29**, 1362 (1984)].
[5] R. J. Knoze, Z. Wu, and W. Happer, Adv. At. Mol. Phys. **24**, 224 (1988).

Translated by M. E. Alferieff

Achromatic reconstruction of the wave front of femtosecond laser pulses

D. A. Dement'ev
N. N. Andreev Acoustics Institute, 117036 Moscow, Russia

A. L. Ivanov, O. B. Serov, A. G. Stepanov, and S. V. Chekalin[a)]
Institute of Spectroscopy, Russian Academy of Sciences, 142092 Troitsk, Moscow Region, Russia

A. M. Smolovich
Central Office of Design of Unique Instrumentation, Russian Academy of Sciences, 117342 Moscow, Russia

(Submitted 10 January 1997)
Pis'ma Zh. Éksp. Teor. Fiz. **65**, No. 5, 388–390 (10 March 1997)

Wave-front reconstruction by geometric-optical reflection of the reconstructing radiation from interference surfaces of a structure recorded in the bulk of a medium by counterpropagating laser pulses is observed. The recording is done with the aid of a sapphire titanate laser. Pulse durations of 30–40 fs are used. © *1997 American Institute of Physics.* [S0021-3640(97)00505-7]

PACS numbers: 42.40.Kw, 42.15.Dp, 42.40.Ht

This paper reports an experimental check of the following mechanism of wave-front reconstruction.[1] Let the interference pattern of the object $A_0(\mathbf{r})\exp[ikL_0(\mathbf{r})]$ and reference $A_R\exp[ikL_R(\mathbf{r})]$ waves, satisfying the scalar equations of geometric optics, be recorded in a bulk medium. Here $k=2\pi/\lambda$ is the wave number and λ is the wavelength of the radiation, $L_0(\mathbf{r})$ and $L_R(\mathbf{r})$ are the eikonals of the waves, $A_0(\mathbf{r})$ and A_R are the amplitudes of the waves, and $\mathbf{r}$ is the coordinate vector. Under the conditions of geometric-optical reflection of the reconstructing wave $A_C\exp[ik'L_R(\mathbf{r})]$ from the surface of constant phase difference of the object and reference waves

$$L_R(\mathbf{r})-L_0(\mathbf{r})=p, \tag{1}$$

where p is a constant for a given surface, the phase $k'L_{\text{refl}}(\mathbf{r})$ of the reflected wave on this surface equals the phase of the incident wave

$$k'L_{\text{refl}}(\mathbf{r})=k'L_R(\mathbf{r}). \tag{2}$$

It follows from Eqs. (1) and (2) that

$$L_{\text{refl}}(\mathbf{r})=L_0(\mathbf{r})+p, \tag{3}$$

i.e., to within an additive constant, the eikonal of the object wave is reconstructed for an arbitrary value of the wave vector k'. Hence follows achromatic reconstruction of the wave front — the surface $L_0(\mathbf{r})=$ const.

This wave-front reconstruction mechanism was proposed by Denisyuk[2] for three-dimensional holograms. However, in Ref. 1 it was noted that this mechanism is fundamentally different from the holographic mechanism of reconstruction because there is no diffraction of the reconstructing radiation by the periodic interference structure whose local period contains holographic information about the form of the wave front. At the same time, in Ref. 3 it was shown that the mechanism of geometric-optical reconstruction does not work in real volume holograms. This is because diffraction by a transverse (in the plane of the hologram) periodic structure dominates. This is indicated by the experimentally observed presence of dispersion on reconstruction. For example, in the simplest case of a plane-wave hologram the change in the wavelength of the reconstructing radiation results in a change in the direction of propagation of the reconstructed beam according to the formula of the grating, the period of the grating corresponding to the period of the transverse structure. Since the reconstructed beam can be observed only for the wavelength varying within the spectral selectivity band of the hologram, a large increase in the thickness of the hologram makes this observation impossible for waves which differ appreciably from the Bragg reconstruction. At the same time, in the case of Bragg reconstruction the diffraction and geometric-optical images are identical.[3] To observe achromatic wave-front reconstruction the number of surfaces of interference maxima recorded in the bulk medium must be decreased while the thickness is increased. This can be done by using ultrashort laser pulses for recording.[4,5]

The experiment was performed with the aid of a femtosecond-pulse generator based on sapphire titanate with an argon ion laser pump. Dispersion compensation, achieved by inserting a system of prisms in the cavity, made it possible to obtain consistently at the output of the generator pulses with a duration of 30–40 fs, measured by an autocorrelation method, and diffraction divergence. The radiation wavelength was varied in the range 780–830 nm and the pulse repetition frequency was equal to 80 MHz with average power exceeding 100 mW. The laser beam was divided with the aid of a half-transmitting interference mirror into two beams, which were directed toward one another. The recording plate was positioned so that its photosensitive layer was located in the region of overlapping of the oppositely propagating pulses. The method of Ref. 5 was used to equalize exactly the lengths of the optical paths. The normal to the plate made an angle of the order of 20° with the optic axis. Specially prepared photographic plates with a photosensitive layer of thickness from 110 to 280 μm were used. An IAÉ opposed-type photoemulsion, produced at the Kurchatov Institute Russian Science Center, was sensitized to a wavelength of 800 nm. The exposure was set experimentally and was of the order of a tenth of a Joule per square centimeter. Several fields with different exposure were irradiated on each photographic plate. As a control, some fields were exposed with continuous radiation in the same geometry as with the pulsed radiation. Use was made of the possibility of rapidly transferring the laser from the femtosecond-pulse lasing regime into a continuous lasing regime.

In processing the photographic plates, we encountered a number of problems connected with the large thickness of the photosensitive layer. These included the problem of ensuring that the development process occurs over the entire thickness of the photographic layer, separation of the photoemulsion during the processing and drying operations, and strong diffusion of light in the processed layer. These difficulties were over-

come mainly by optimizing the processing regime. Two basic processing methods were employed: physical development in GP-2 developer and development in phenidolmetol-hydriquinone developer, followed by bleaching. Development and washing were conducted in a refrigerator at a temperature of the order 4 °C. Drying was gradual, and initially it occurred in a closed volume with a little exchange of air. When the photographic plates were processed, the photographic layer shrank substantially, as a result of which the reconstruction band shifted to wavelengths of the order of 600 nm. In contrast to Ref. 5, in this range the brownish-black color, acquired by the exposed sections of the photosensitive layer as a result of processing in GP-2 developer, did not present an obstacle for penetration of the reconstructing radiation to a large depth.

An argon-laser pumped dye laser (rhodamine 6G solution in ethylene glycol) was used for reconstruction. A continuous lasing regime with wavelength tuning from 580 to 630 nm with the aid of a dispersing element was used. The constructed beam of light was observed in a reflective geometry on a diffuse screen placed about 4 m from the photographic plate. The spectral selectivity of the structure recorded with the pulsed radiation made it possible to observe the reconstructed beam with a smooth variation of the wavelength of the radiation from 585 to 607 nm. With this variation the spot produced on the screen by the reconstructed beam did not move, i.e., the direction of propagation of the reconstructed beam did not change. At the same time, for the structure recorded with the continuous radiation under the same conditions the spot on the screen moved by 6 cm. This proves that in the present case the geometric-optics mechanism of reconstruction and not the diffraction mechanism operates for structures recorded with femtosecond pulses.

In summary, achromatic restoration of a wave front by geometric-optical reflection of the reconstructing radiation from surfaces of constant phase difference between the object and reference waves has been realized experimentally.

We thank R. V. Ryabova for preparing the photographic materials. These investigations were made possible by a grant from the Russian Fund for Fundamental Research (95-02-05996) and a US CRDF grant (RP-2-154) for independent states of the former Soviet Union.

[a)]e-mail: yumatv@isan.msk.su

---

[1]I. N. Sisakyan and A. M. Smolovich, Pis'ma Zh. Tekh. Fiz. **17**(1), 41 (1991) [Sov. Tech. Phys. Lett. **17**, 16 (1991)].
[2]Yu. N. Denisyuk, Opt. Spektrosk. **15**, 522 (1963) [Opt. Spectrosc. **15**, 279 (1963)].
[3]I. N. Sisakyan and A. M. Smolovich, *Computer Optics* [in Russian], MTsNTI, Moscow, 1990, Vol. 7, p. 56.
[4]A. M. Tolmachev, Opt. Spektrosk. **76,** 645 (1994).
[5]D. A. Dement'ev, Yu. A. Matveets, O. B. Serov *et al.*, Kvantovaya Elektron. (Moscow) **23,** 293 (1996).

Translated by M. E. Alferieff

Contribution to the theory of Lorentzian ionization

B. M. Karnakov[a)] and V. D. Mur
Moscow State Engineering-Physics Institute (Technical University), 115409 Moscow, Russia

V. S. Popov
Institute of Theoretical and Experimental Physics, 117259 Moscow, Russia

(Submitted 21 January 1997)
Pis'ma Zh. Éksp. Teor. Fiz. **65**, No. 5, 391–396 (10 March 1997)

The probability w_L of Lorentzian ionization, which arises when an atom or ion moves in a constant magnetic field, is calculated in the quasiclassical approximation. The nonrelativistic ($v \lesssim e^2/\hbar = 1$, v is the velocity of the atom) and ultrarelativistic ($v \to c = 137$) cases are examined and the stabilization factor S, which takes account of the effect of the magnetic field on tunneling of an electron, is found. © *1997 American Institute of Physics.* [S0021-3640(97)00605-1]

PACS numbers: 03.30.+p, 79.70.+q

1. When an atom or ion enters a magnetic field, an electric field $\mathcal{E}_0$ giving rise to ionization of the atom appears in its rest system K_0 as a result of the Lorentz transformation. This process has been termed Lorentzian ionization. We shall examine the quasiclassical theory of the Lorentzian ionization and obtain formulas for the probability w_L which are asymptotically exact in weak fields ($\epsilon, h \ll 1$). We shall use, as a rule, the atomic units $\hbar = e = m_e = 1$ and the ''reduced'' intensities of the external fields:

$$\epsilon = \mathcal{E}_0 / \kappa^3 \mathcal{E}_a, \quad h = \mathcal{H}_0 / \kappa^2 \mathcal{H}_a,$$

where $\kappa = \sqrt{-2E_0}$ (E_0 is the energy of the atomic level), $\mathcal{E}_a = 5.14 \cdot 10^9$ V/cm, and $\mathcal{H}_a = 2.35 \cdot 10^9$ G. Here we confine our attention to the most important case of the ionization of an s level ($l = 0$).

2. If an atom moves with velocity v at an angle φ with respect to the direction of the magnetic field $\mathcal{H}$, then in the fields $\mathcal{E}_0$ and $\mathcal{H}_0$ ($\mathcal{E}_0 \perp \mathcal{H}_0$) given by

$$\mathcal{E}_0 = q\mathcal{H} = (\Gamma^2 - 1)^{1/2} \sin\varphi \cdot \mathcal{H},$$

$$\mathcal{H}_0 = (1 + q^2)^{1/2} \mathcal{H} = (\Gamma^2 \sin^2\varphi + \cos^2\varphi)^{1/2} \mathcal{H}, \tag{1}$$

where $q = p_\perp / mc$ and $p_\perp$ is the transverse (relative to the field $\mathcal{H}$) momentum of the particle and $\Gamma = (1 - v^2/c^2)^{-1/2}$ is the Lorentz factor, operate the rest system of the atom. An important physical parameter determining the subbarrier motion of an electron is $\gamma_L = \omega_c / \omega_t$,[b)] where $\omega_c = e\mathcal{H}_0 / m_e c$ is the Larmor or cyclotron frequency, $\omega_t = \mathcal{E}_0 / \kappa$ is the tunneling frequency in an electric field[3,4]

$$\gamma_L = \frac{\kappa \mathcal{H}_0}{c \mathcal{E}_0} = \frac{\kappa}{v} \left(1 + \frac{\cot^2 \varphi}{\Gamma^2} \right)^{1/2}, \tag{2}$$

where the velocity v is expressed in the atomic units $e^2/\hbar = 2.19 \cdot 10^8$ cm/s. For nonrelativistic particles $\mathcal{E}_0/\mathcal{H}_0 = v_\perp/c \ll 1$ and $\gamma_L = \kappa/v_\perp$ can assume arbitrary values. At the same time, in the case of ultrarelativistic ($\Gamma \gg 1$) particles $\mathcal{E}_0/\mathcal{H}_0 = 1-(2q^2)^{-1} \to 1$ and crossed fields appear in the system K_0, i.e., $\mathcal{E}_0 \perp \mathcal{H}_0$ and $\mathcal{E}_0 = \mathcal{H}_0$. Here $\mathcal{E}_0$ can be many times greater than the initial magnetic field $\mathcal{H}$, and the parameter

$$\gamma_L = \frac{\kappa}{137}[1+(2\Gamma^2 \sin^2\varphi)^{-1}] \ll 1.$$

Using the quasiclassical solution[3,4] obtained by the imaginary time method[5] for the problem of ionization of an atom in electric and magnetic fields we find for the probability of Lorentzian ionzation (in the laboratory system K)

$$w_L = \Gamma^{-1}\kappa^2 A_\kappa^2 \left(\frac{\epsilon}{2}\right)^{1-2\eta} P(\gamma_L)[Q(\gamma_L)]^\eta \exp\left\{-\frac{2}{3\epsilon}g(\gamma_L)\right\}. \tag{3}$$

Here A_κ is an asymptotic factor of the wave function in the free ($\mathcal{E}=\mathcal{H}=0$) atom at infinity (see Eq. (9) in Ref. 4), $\eta = Z/\kappa$ is the Sommerfeld parameter, Z is the charge of the atomic core,[c)]

$$\epsilon = \mathcal{E}_0/\kappa^3 = \Gamma \frac{v_\perp h}{137\kappa}, \tag{4}$$

$$g(\gamma) = \frac{3\tau_0}{2\gamma}\left[1-\frac{\sqrt{\tau_0^2-\gamma^2}}{\gamma^2}\right], \tag{5}$$

$$P(\gamma) = \frac{\gamma^2}{\tau_0}\left[\left(\frac{\sinh\tau_0}{\tau_0}+\frac{\tau_0}{\sinh\tau_0}\right)\cosh\tau_0 - 2\right]^{-1/2}, \tag{5a}$$

$$Q(\gamma) = \left(\frac{\tau_0}{2\gamma}\right)^2 \exp\left(2\int_0^{\tau_0} d\tau \left\{\frac{\gamma}{\tau_0}\left[\left(\frac{\cosh\tau_0-\cosh\tau}{\sinh\tau_0}\right)^2 - \left(\frac{\sinh\tau}{\sinh\tau_0}-\frac{\tau}{\tau_0}\right)^2\right]^{-1/2} - \frac{1}{\tau_0-\tau}\right\}\right), \tag{5b}$$

and, finally, $\tau_0 = \tau_0(\gamma)$ is determined from the equation

$$\tau_0^2 - (\tau_0 \coth \tau_0 - 1)^2 = \gamma^2 \tag{6}$$

(see Fig. 1). We note that τ_0 has a simple physical meaning $\tau_0 = -i\omega_c t_0$, where t_0 is the initial (purely imaginary) moment of subbarrier motion, which terminates at $t=0$ when the electron emerges from beneath the barrier. The factor Γ^{-1} in Eq. (3) takes account of the time dilation on transforming from the rest system K_0 to the system K.

The functions g, P, and Q calculated according to the formulas presented above are shown in Fig. 2. We note that the factor $(\epsilon/2)^{-2\eta}Q^\eta$ in Eq. (3) is due to the Coulomb interaction between the emerging electron and the atomic core (for negative ions of the type H^-, He^- and others it changes to one, since $Z=\eta=0$). As follows from Fig. 2, this (Coulomb) factor is much greater than the ionization probability w_L, especially in the case $\gamma_L \gg 1$. The pre-exponential factor $P(\gamma_L)$ arises as a result of summing the contributions to the tunneling probability from the pencil of subbarrier trajectories close to the

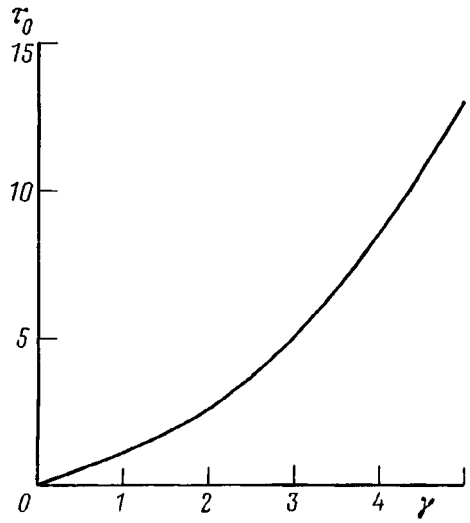

FIG. 1. τ_0 versus γ according to Eq. (6).

extremal trajectory (see Eq. (3) in Ref. 4), and it operates in the opposite direction. Although the functions $P(\gamma)$ and $Q(\gamma)$ vary more rapidly than $g(\gamma)$, the probability w_L is most sensitive to a change in $g(\gamma_L)$, since this function appears in Eq. (3) in the exponential with a large coefficient $2/3\epsilon$.

It is convenient to write the probability of Lorentzian ionization in the form

$$w_L = \Gamma^{-1} S w(\mathcal{E}_0), \tag{7}$$

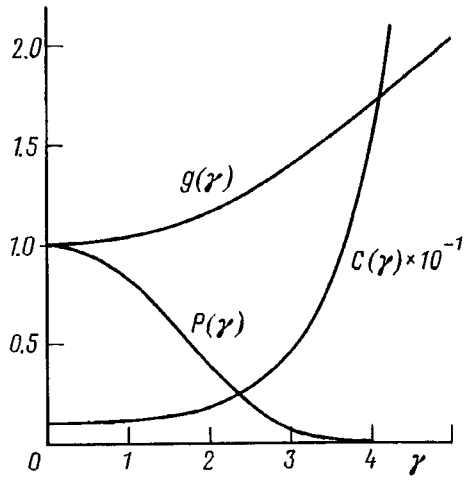

FIG. 2. Plots of the functions appearing in Eq. (3). $C(\gamma) \equiv \sqrt{Q(\gamma)}$.

where $w(\mathcal{E}_0)$ is the probability of ionization of an s level under the action of only the electric field $\mathcal{E}_0$ and S is a stabilization factor which takes account of the suppression of the decay of the ground state by the magnetic field:

$$S = P(\gamma_L)[Q(\gamma_L)]^{\eta}\exp\{-h^{-1}f(\gamma_L)\}, \tag{8}$$

where

$$f(\gamma) = \frac{2}{3}\gamma[g(\gamma)-1] = \begin{cases} \dfrac{\gamma^3}{45}\left(1+\dfrac{11}{252}\gamma^2+\ldots\right), & \gamma \ll 1 \\ \dfrac{\gamma^2}{4}\left(1-\dfrac{8}{3\gamma}+\dfrac{2}{\gamma^2}+\ldots\right), & \gamma \gg 1 \end{cases}, \tag{9}$$

$$PQ^{\eta} = \begin{cases} 1+\dfrac{2}{9}\left(\eta-\dfrac{3}{4}\right)\gamma^2+\ldots, & \gamma \ll 1 \\ 0.177\,\exp\left\{-\left[\dfrac{1}{2}\gamma^2-\pi\eta\gamma+(2\eta-1)(\ln\gamma+2.27)\right]\right\}, & \gamma \gg 1 \end{cases}. \tag{10}$$

For slow particles the stabilization factor is exponentially small:

$$S \approx \exp\left\{-\frac{1}{4h}\left(\frac{\kappa}{v_\perp}\right)^2\right\}, \quad v \ll \kappa \tag{11}$$

($\gamma \ll 1$). However, it increases rapidly with the velocity of the atom and approaches 1 for $v \gg 0.3\kappa h^{-1/3}$, when $\gamma \ll 3.5h^{1/3}$:

$$S = 1-\frac{1}{45h}\left(\frac{\kappa}{v_\perp}\right)^3(1+2h)+\ldots\ . \tag{12}$$

3. A numerical calculation gives for S the curves in Fig. 3, whence one can see that $S \ll 1$ in the case of quite ''weak'' magnetic fields as well as for $\gamma_L \gtrsim 1$. The effect of the Coulomb interaction on S becomes appreciable for $\gamma_L > 1.5$ (compare the solid and dashed curves in Fig. 3, referring to the same values of the parameter γ_L). The pre-exponential factor $P(\gamma_L)$ sharply decreases the ionization probability if $\gamma_L > 10$.

The static magnetic fields obtained under laboratory conditions do not exceed 1 MG. The method of magnetic cumulation (i.e., compression of an axial magnetic field with the aid of an explosion), proposed by Sakharov in 1951,[6] made it possible to reach record-high values $\mathcal{H} = 25$ MG in the USSR[6,7] and $\mathcal{H} = 15$ MG in the USA.[8] With further progress in this field it can be expected that fields of $3\cdot 10^7 - 10^8$ G will be reached.[9] On this basis, we calculated the stabilization factor S for a hydrogen atom (see Table I, where the magnetic field is expressed in MG, the velocity v in atomic units, $\varphi = \pi/2$, and $a(b) \equiv a\cdot 10^b$). It is evident from the table that for the range of values of $\mathcal{H}$ and v considered, a sharp transition occurs from exponential suppression (11) of the probability w_L to the case (12), when the effect of the magnetic field can be neglected. For fast ($v \gtrsim 10\kappa$ and especially for $\Gamma \gg 1$) particles $S \approx 1$, i.e., ionization of the atomic level occurs practically with the same rate as in the case of a purely electric field $\mathcal{E}_0$. This

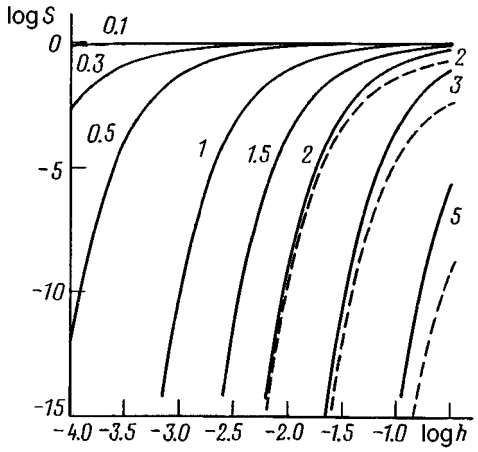

FIG. 3. Stabilization factor S: Solid lines — for the ground state of the hydrogen atom ($\kappa=\eta=1$), dashed curves — for a negative ion with $\kappa=1$, $\eta=0$. The numbers on the curves are the values of the parameter γ_L.

distinguishes Lorentzian ionization with $\Gamma \gg 1$ from the well-known problem of pair production from vacuum, whose probability in the case of crossed fields vanishes identically.[10]

We shall present some numerical estimates. For $\mathcal{H}<1$ MG an atom is essentially stable, since the electric field $\mathcal{E}_0$ is too weak ($\mathcal{E}_0<0.01$ for $\Gamma<25$). Lorentzian ionization can be observed in the region $\mathcal{H}>10$ MG if the velocity v is not too low. For example, for $\mathcal{H}=25$ MG we obtain $w_L \approx 10^{-9}$, $7\cdot 10^{-4}$; $1.5\cdot 10^{5}$; 10^{13} and $3\cdot 10^{15}$ s^{-1} for $v=1$; 1.25; 2; 5 and 10 a.u., respectively. Therefore in this range of velocities the situation changes from practically complete stability of an atom up to ionization of the atom over a time comparable to the atomic time.

4. In closing we shall make several remarks.

a) The theory examined above can be extended to the case with $l \neq 0$. The form of the exponential factor in Eq. (3) remains the same but the pre-exponential factor changes substantially.

b) Extending the imaginary time method to the relativistic case, it is possible to

TABLE I.

v / $\mathcal{H}$	1.0	1.25	2	10
1	2.2(−24)	1.2(−12)	1.38(−3)	0.950
10	4.53(−3)	6.63(−2)	0.524	0.995
25	0.119	0.345	0.779	0.9985
50	0.355	0.598	0.889	0.9995

study ionization of a level whose binding energy is comparable to $m_e c^2$. Taking account of corrections of order α^2, the ionization probability in the case of crossed fields $\mathcal{E}$ and $\mathcal{H}$ equals

$$w(\mathcal{E},\mathcal{H}) \propto \exp\left\{-\frac{2}{3\epsilon}(1-c_1\alpha^2\kappa^2)\right\} \tag{13}$$

(with exponential accuracy), where

$$c_1 = -\frac{1}{30}\left[\frac{9}{4}-\left(\frac{\mathcal{H}}{\mathcal{E}}\right)^2\right], \quad \alpha = \frac{e^2}{\hbar c} = \frac{1}{137}. \tag{13a}$$

Specifically, $c_1 = 3/40$ for a purely electric field and $c_1 = 1/24$ for crossed fields. In these cases the relativistic correction slightly increases the ionization probability.

We note that the leading term $(-2/3\epsilon)$ in the exponential (13) is determined only by the electric field and does not depend on $\mathcal{H}$. A different situation arises when the level approaches the limit of the lower continuum.[d)] We shall postpone this question to a more detailed paper.

c) For negative ions and the Rydberg states of atoms, the parameter $\kappa \ll 1$. For example, $\kappa = 0.236$ and 0.75 for H^- and He^- and $\kappa = 1/n$ for the excited states of the hydrogen atom with principal quantum number n. Weakly bound states with $\kappa \ll 1$ are also encountered in solid-state physics, for example, Wannier–Mott excitons in semiconductors ($\kappa \sim 0.01$ for a germanium crystal), and elsewhere. In these cases, substantially lower fields[e)] than those presented above for the hydrogen atom are required to ionize a level; this will undoubtedly make it easier to formulate an experiment.

We are grateful to Yu. N. Demkov for a helpful discussion in the course of this work and also to S. G. Pozdnyakov and A. V. Sergeev for assisting in the numerical calculations.

[a)]e-mail: karnak@theor.mephi.msk.su

[b)]We note that this parameter is analogous to the well-known Keldysh parameter[1,2] $\gamma = \omega/\omega_t$ in the theory of multiphoton ionization of atoms by laser light with frequency ω.

[c)]$Z = 1$, 0, and 2 for the neutral atom and singly-charged negative and positive ions. For the ground state of the hydrogen atom $\kappa = \eta = 1$ and $A_\kappa = \sqrt{2}$. We note that for the outer s electrons in neutral atoms the coefficient A_κ varies over quite narrow limits: from $A_\kappa = 1.31$ for the Cs atom to $A_\kappa = 1.72$ for Hg. Therefore the probability w_L is determined mainly by the binding energy of the level.

[d)]This can be realized[11,12] in superheavy ($Z \sim Z_{cr} = 173$) atoms or in a collision of two heavy nuclei ($Z_1 + Z_2 > Z_{cr}$).

[e)]The characteristic external field intensities $\sim \kappa^3 \mathcal{E}_a$ and $\kappa^2 \mathcal{H}_a$ for $\kappa \ll 1$ are much lower than atomic fields.

[1] L. V. Keldysh, Zh. Éksp. Teor. Fiz. **45**, 1945 (1964) [Sov. Phys. JETP **20**, 1307 (1965)].
[2] N. B. Delone and V. P. Kraĭnov, *Atoms in Strong Light Fields*, Springer-Verlag, New York, 1985 [Russian original, Énergoizdat, Moscow, 1984].
[3] L. P. Kotov, A. M. Perelomov, and V. S. Popov, Zh. Éksp. Teor. Fiz. **54**, 1151 (1968) [Sov. Phys. JETP **27**, 616 (1968)].
[4] V. S. Popov and A. V. Sergeev, JETP Lett. **63**, 417 (1996).
[5] A. M. Perelomov, V. S. Popov, and M. V. Terent'ev, Zh. Éksp. Teor. Fiz. **50**, 1393 (1966) [Sov. Phys. JETP **23**, 924 (1966)]; *ibid.* **51**, 309 (1966) [**24**, 207 (1967)].

[6] A. D. Sakharov, R. Z. Lyudaev, E. N. Smirnov *et al.*, Dokl. Akad. Nauk SSSR **165**, 65 (1965) [Sov. Phys. Dokl. **10**, 1045 (1966)].
[7] A. D. Sakharov, *Scientific Works* [in Russian], Tsentrkom, Moscow, 1995.
[8] D. Bitter, Sci. Amer. **213**, 65 (1965).
[9] A. I. Pavlovskiĭ in Ref. 7, p. 85.
[10] J. Schwinger, Phys. Rev. **82**, 664 (1951).
[11] Ya. B. Zel'dovich and V. S. Popov, Usp. Fiz. Nauk **105**, 403 (1971) [Sov. Phys. Usp. **14**, 673 (1972)].
[12] W. Greiner, B. Müller, and J. Rafelski, *Quantum Electrodynamics of Strong Fields*, Springer, Berlin, 1985.

Translated by M. E. Alferieff

Dissociation energy and ionization potentials of molecules and molecular ions in a collisional hydrogen plasma

S. I. Anisimov and Yu. V. Petrov
L. D. Landau Institute of Theoretical Physics, Russian Academy of Sciences, 142432 Chernogolovka, Moscow Region, Russia

(Submitted 30 January 1997)
Pis'ma Zh. Éksp. Teor. Fiz. **65**, No. 5, 397–401 (10 March 1997)

It is shown that the dissociation energies of a hydrogen molecule and a hydrogen molecular ion are virtually independent of the screening length of the Coulomb potential in plasma even at densities for which the decrease in the ionization potential of the molecule reaches 30%. For this reason, ionization of hydrogen in high-temperature shock-wave experiments should occur in a molecular phase with the formation of the molecular ion. © *1997 American Institute of Physics.* [S0021-3640(97)00705-6]

PACS numbers: 71.30.+h, 33.15.Fm, 33.15.Ry, 52.25.Mq

The metal–insulator phase transition in hydrogen under pressure is the subject of intense investigations both in low-temperature static experiments on compression in diamond anvils[1,2] and at high temperatures with shock compression in the liquid phase.[3–5]

Under normal conditions the molecular phase of hydrogen is an insulator. It is of interest to know what the high-temperature high-pressure phase is, whether remains molecular (in the form of hydrogen molecular ions[5]) or is atomic. Both possibilities have been discussed in the literature (see, for example, Refs. 6–9). The calculations showed that in both cases the dielectric gap closes at megabar pressures. However, the calculations were performed for crystalline phases and therefore they do not have any direct bearing on the dynamical experiments,[3–5] in which compressed hydrogen was in a liquid or plasma state.

A decrease of the dielectric gap is equivalent in plasma to a decrease in the ionization potential (which occurs in a nondegenerate plasma as a result of a decrease of the Debye screening radius λ under compression). Under sufficiently strong compression, this decrease is substantial and results in virtually complete ionization of the plasma. For a substance consisting of molecules, such as hydrogen, the question of the effect of the screening length λ on both the dissociation and ionization energies of the molecules is important.

In this letter we calculate the dissociation energy of molecular formations of hydrogen (the H_2 molecule and the molecular ion H_2^+), in which the interaction potential energy of the charged particles has the form of a screened Coulomb interaction

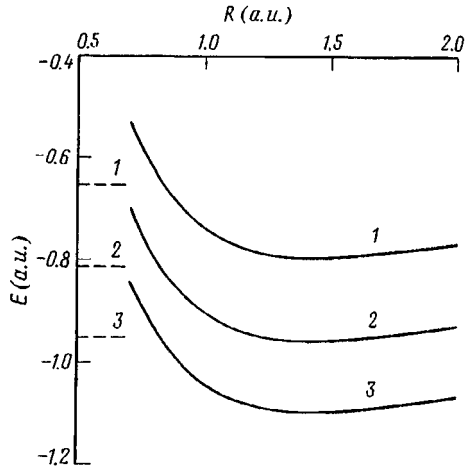

FIG. 1. Energy of the bound state of two hydrogen atoms, allowing for screening of the potential, as a function of the distance between the atoms: *1* — $\lambda = 5$; *2* — $\lambda = 10$; *3* — $\lambda = 40$.

$$v(r) = \frac{q_1 q_2}{r} e^{-r/\lambda}, \tag{1}$$

where q_1 and q_2 are the charges of the particles. The Hamiltonian of the molecule (neglecting the motion of the nuclei in the adiabatic approximation) has the form (in atomic units)

$$\hat{H} = -\frac{1}{2}(\Delta_1 + \Delta_2) + \frac{e^{-r_{12}/\lambda}}{r_{12}} - \frac{e^{-r_{1a}/\lambda}}{r_{1a}} - \frac{e^{r_{1b}/\lambda}}{r_{1b}} - \frac{e^{r_{2a}/\lambda}}{r_{2a}} - \frac{e^{-r_{2b}/\lambda}}{r_{2b}} + \frac{e^{-R/\lambda}}{R}. \tag{2}$$

Here r_{12} is the distance between the electrons 1 and 2, r_{1a} and r_{1b} are the distances between the electron 1 and the nuclei of the molecules a and b with the coordinates $\mathbf{R}_a$ and $\mathbf{R}_b$, respectively, and $R = |\mathbf{R}_a - \mathbf{R}_b|$ is the distance between the nuclei a and b.

TABLE I. Equilibrium interatomic distance R_0, the interatomic distance R_* at which the interatomic interaction energy vanishes, and the dissociation energy D of the H_2 molecule as a function of the screening length λ.

λ (a.u.)	R_0 (a.u.)	R_* (a.u.)	D (a.u.)
5	1.45561	0.83089	0.13340
10	1.43673	0.82086	0.13666
20	1.43367	0.81809	0.13760
40	1.43057	0.81737	0.13782
80	1.43152	0.81715	0.13791

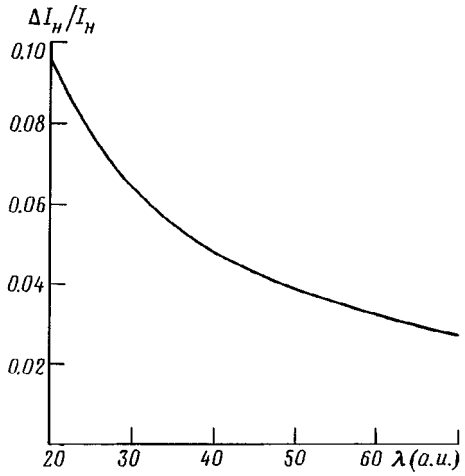

FIG. 2. Relative decrease of the ionization potential of a hydrogen atom as a function of the screening length.

We take the wave function of the electrons with a fixed distance R between the nuclei in the valence-bond approximation as a linear combination of the covalent Ψ_1 and ionic Ψ_2 and Ψ_3 basis functions:

$$\Psi_1=(a\overline{b})-(b\overline{a}), \tag{3}$$

$$\Psi_2=a\overline{a}, \tag{4}$$

$$\Psi_3=b\overline{b}. \tag{5}$$

Here

$$(a\overline{b})=\begin{vmatrix} a(1)\alpha(1) & a(2)\alpha(2) \\ b(1)\beta(1) & b(2)\beta(2) \end{vmatrix}, \tag{6}$$

$a(1)$ is the atomic orbital of electron 1 on nucleus a, $\alpha=\begin{pmatrix}1\\0\end{pmatrix}$ and $\beta=\begin{pmatrix}0\\1\end{pmatrix}$ are the spin states of the electrons in the atomic orbitals. We chose as atomic orbitals a linear combination of six Gaussian $1s$ orbitals

$$\varphi(r)=\sum_{i=1}^{6} c_i\varphi_g^i(r), \tag{7}$$

where

$$\varphi_g^i(r)=\left(\frac{2\alpha_i\xi^2}{\pi}\right)^{3/4} e^{-\alpha_i\xi^2 r^2}. \tag{8}$$

Here ξ is a variational parameter, and the coefficients c_i and α_i $(i=1, 2, \ldots, 6)$ are taken from Ref. 10. The function (7) is a good approximation to the $1s$ Slater atomic orbital.

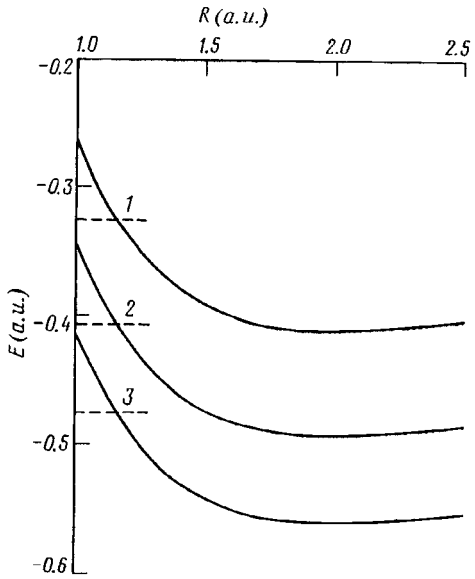

FIG. 3. Energy of the hydrogen molecular ion as a function of the internuclear distance with different screening lengths: *1* — $\lambda = 5$; *2* — $\lambda = 10$; *3* — $\lambda = 40$.

In finding the smallest eigenvalue of the Hamiltonian (2) in the basis functions (3)–(5), the following one- and two-electron matrix elements in a Gaussian basis arise:

1) the overlap integral

$$\langle a_g^i | b_g^j \rangle = \int \varphi_g^i(\mathbf{r}-\mathbf{R}_a)\varphi_g^j(\mathbf{r}-\mathbf{R}_b)d\mathbf{r}; \tag{9}$$

2) the matrix element of the kinetic energy:

$$\langle a_g^i | t | b_g^j \rangle = \int \varphi_g^i(\mathbf{r}-\mathbf{R}_a)\left(-\frac{1}{2}\Delta\right)\varphi_g^j(\mathbf{r}-\mathbf{R}_b)d\mathbf{r}; \tag{10}$$

3) one-electron electrostatic matrix elements:

$$\langle a_g^i | v_b | a_g^j \rangle = \int \varphi_g^i(\mathbf{r}-\mathbf{R}_a)v(\mathbf{r}-\mathbf{R}_b)\varphi_g^j(\mathbf{r}-\mathbf{R}_a)d\mathbf{r}; \tag{11}$$

$$\langle a_g^i | v_a | b_g^j \rangle = \int \varphi_g^i(\mathbf{r}-\mathbf{R}_a)v(\mathbf{r}-\mathbf{R}_a)\varphi_g^j(\mathbf{r}-\mathbf{R}_b)d\mathbf{r}; \tag{12}$$

4) two-electron electrostatic matrix elements:

$$\langle a_g^i a_g^j | b_g^k b_g^l \rangle = \int \varphi_g^i(\mathbf{r}_1-\mathbf{R}_a)\varphi_g^j(\mathbf{r}_1-\mathbf{R}_a)v(\mathbf{r}_{12})\varphi_g^k(\mathbf{r}_2-\mathbf{R}_b)\varphi_g^l(\mathbf{r}_2-\mathbf{R}_b)d\mathbf{r}_1 d\mathbf{r}_2, \tag{13}$$

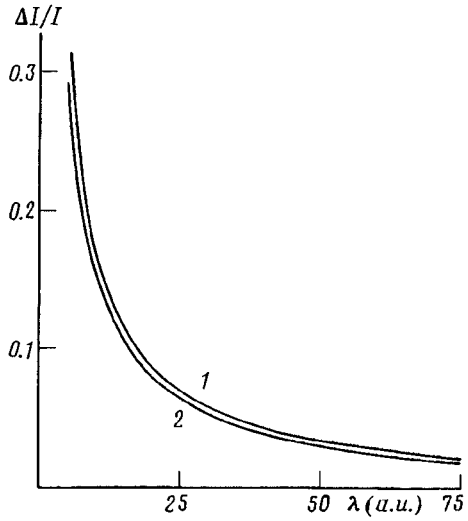

FIG. 4. Relative decrease of the ionization potentials as a function of the screening length: *1* — H_2, *2* — H_2^+.

$$\langle a_g^i a_g^j | a_g^k b_g^l \rangle = \int \varphi_g^i(\mathbf{r}_1 - \mathbf{R}_a)\varphi_g^j(\mathbf{r}_1 - \mathbf{R}_a)v(\mathbf{r}_{12})\varphi_g^k(\mathbf{r}_2 - \mathbf{R}_a)\varphi_g^l(\mathbf{r}_2 - \mathbf{R}_b)d\mathbf{r}_1 d\mathbf{r}_2, \tag{14}$$

$$\langle a_g^i b_g^j | a_g^k b_g^l \rangle = \int \varphi_g^i(\mathbf{r}_1 - \mathbf{R}_a)\varphi_g^j(\mathbf{r}_1 - \mathbf{R}_b)v(\mathbf{r}_{12})\varphi_g^k(\mathbf{r}_2 - \mathbf{R}_a)\varphi_g^l(\mathbf{r}_2 - \mathbf{r}_b)d\mathbf{r}_1 d\mathbf{r}_2. \tag{15}$$

The details of the calculation of these elements will be given in a detailed paper.

The computed energy $E(R,\lambda)$ of the H_2 molecule as a function of the internuclear distance R is presented in Fig. 1 for three values of the screening length λ: 5, 10, and 40. The dashed lines indicate the doubled values of the energy of a hydrogen atom for the same values of λ (i.e., the energy of the molecule in the limit $R \to \infty$). The equilibrium interatomic distance R_0 in this range of λ is virtually independent of the screening length (Table I). In exactly the same way, the depth of the potential well for the interaction of atoms in a hydrogen molecule $\epsilon = E(\infty,\lambda) - E(R_0,\lambda)$ is virtually independent of λ. We calculated the dissociation energy D of a molecule assuming that the interaction between the atoms in Fig. 1 is described by the Morse potential:

$$U(R) = E(R,\lambda) - E(\infty,\lambda) = \epsilon(e^{-2\beta x} - 2e^{-\beta x}), \tag{16}$$

where

$$x = (R - R_0)/R_0. \tag{17}$$

In this approximation the dissociation energy D of a H_2 molecule is

TABLE II. Equilibrium interatomic distance R_0, the interatomic distance R_* at which the interatomic interaction energy vanishes, and the dissociation energy D of the molecular ion H_2^+ as a function of the screening length λ.

λ (a.u.)	R_0 (a.u.)	R_* (a.u.)	D (a.u.)
5	2.02305	1.15250	0.080574
10	2.00652	1.14720	0.080990
20	2.00454	1.14586	0.081040
40	2.00362	1.14550	0.081039
80	2.00327	1.14540	0.081037

$$D=\epsilon-\frac{\ln 2}{R_0-R_*}\sqrt{\frac{\epsilon}{M}}, \tag{18}$$

where M is the mass of the hydrogen atom and R_* is the interatomic separation for which $U(R_*,\lambda)=0$. The corresponding values of R_* and D are presented in Table I. One can see that in the range of λ investigated the dissociation energy is virtually independent of the screening length. At the same time, as shown in Fig. 1, as λ decreases from 40 to 5, the ground-state energy of the hydrogen atom, i.e., its ionization potential, changes substantially. Its relative decrease for large values of λ is shown in Fig. 2.

The change in the ionization potential of the hydrogen molecule itself is also of interest. To find it, we calculated in the same approximation the energy of the molecular ion H_2^+. It is shown in Fig. 3 as a function of the distance between the nuclei for the same values of the screening length. The parameters of the molecular ion H_2^+ for different values of λ are presented in Table II. One can see that even for a molecular ion the dissociation energy is virtually independent of λ in the range of values investigated.

Now, knowing the ground-state energies $E(H_2)$ and $E(H_2^+)$ of the molecule and the molecular ion, respectively, for fixed λ, we can calculate the decrease in the ionization potentials of the molecule $I_1=E(H_2^+)-E(H_2)$ and its ion $I_2=-E(H_2^+)$ for this value of λ.

The relative decrease in the ionization potentials I_1 and I_2 (compared with the unscreened interaction $\lambda=\infty$) is shown in Fig. 4. Even for $\lambda=20$, it is of the order of 10%. Therefore a simultaneous increase in the free-electron density, resulting in a substantial decrease of the ionization potentials of the molecules, does not affect the dissociation energy. For this reason, it can be expected that at high temperatures appreciable ionization of hydrogen will be achieved in the molecular phase.

This work was supported by the Russian Fund for Fundamental Research (Grant 95-02-06381a) and INTAS-94-1105.

[1] H. K. Mao, R. J. Hemley, and M. Hanfland, Phys. Rev. Lett. **65**, 484 (1990).
[2] H. K. Mao and R. J. Hemley, Rev. Mod. Phys. **66**, 671 (1994).
[3] F. V. Grigor'ev, S. B. Kormer, O. L. Mikhaïlova *et al.*, JETP Lett. **16**, 201 (1972).
[4] W. J. Nellis, A. C. Mitchell, P. C. McCaudless *et al.*, Phys. Rev. Lett. **68**, 2937 (1992).
[5] S. T. Weir, A. C. Mitchell, and W. J. Nellis, Phys. Rev. Lett. **76**, 1860 (1996).

[6] D. Saumon and G. Chabrier, Phys. Rev. Lett. **62**, 2397 (1989).
[7] A. Garcia, T. W. Barbie III, M. Cohen *et al.*, Europhys. Lett. **13**, 355 (1990).
[8] H. Chacham and S. G. Louie, Phys. Rev. Lett. **66**, 64 (1991).
[9] D. Saumon and G. Chabrier, Phys. Rev. A **46**, 2084 (1992).
[10] G. Page and O. Ludwig, J. Chem. Phys. **56**, 5626 (1972).

Translated by M. E. Alferieff

New approach to the construction of flux coordinates in toroidal systems

V. D. Pustovitov[a)]
Kurchatov Institute Russian Science Center, 123182 Moscow, Russia

(Submitted 6 February 1997)
Pis'ma Zh. Éksp. Teor. Fiz. **65**, No. 5, 402–404 (10 March 1997)

A universal method for introducing flux coordinates in toroidal equilibrium plasma configurations is proposed. The characteristic features of this method are a prescription of two scalar functions, one of which determines the explicit form of the Jacobian, and a universal form of the equations for arbitrary flux coordinates. This makes the method simple, clear, and effective. © *1997 American Institute of Physics.* [S0021-3640(97)00805-0]

PACS numbers: 52.55.Hc

Magnetic surfaces and magnetic (or flux) coordinates are fundamental concepts without which a theory of toroidal systems for confinement of thermonuclear plasma is unthinkable. Magnetic surfaces are surfaces $a=\text{const}$ in which the lines of the magnetic field $\mathbf{B}$ lie. The position of a point on such a surface can be specified by two numbers (θ, ζ). Then (a, θ, ζ) are the flux coordinates.

Tying the coordinate system to magnetic surfaces greatly simplifies the description of the equilibrium configuration, since by definition $\mathbf{B}\cdot\nabla a=0$. Moreover, as follows from the equation of equilibrium

$$\nabla p=\mathbf{j}\cdot\mathbf{B}, \tag{1}$$

the lines of current $\mathbf{j}=\nabla\times\mathbf{B}$ also lie on these surfaces and the plasma pressure p is constant.

Evidently, the ''radial'' coordinate a and the angular coordinates θ and ζ are not of equal value. The first coordinate, being strictly related with the shape of the magnetic surfaces, is determined by the physics of the problem. But the construction of the coordinate grid (θ, ζ) on these surfaces is a formal mathematical procedure admitting great arbitrariness. This unavoidably raises the question of how best to make use of the freedom in choosing θ and ζ.

To answer this question one ordinarily turns to the general expression for the magnetic field in the flux coordinates[1,2]

$$2\pi\mathbf{B}=\nabla\psi\cdot\nabla\zeta+\nabla\Phi\cdot\nabla\theta+\nabla a\cdot\nabla\eta, \tag{2}$$

where $\psi(a)$ and $\Phi(a)$ are the poloidal and toroidal magnetic fluxes and η is some doubly periodic function that depends on the method for prescribing θ and ζ. It is considered obvious to expend one of the two degrees of freedom so as to make $\eta=0$. Then the field line will be straight in the (θ, ζ) plane. Accordingly, the variables $(a,$

θ, ζ) with $\eta=0$ are coordinates with straight field lines (SFLs). Other coordinates are very rarely used in plasma theory and only three variants from the one-parameter family of coordinates with SFLs have been widely recognized — coordinates with fixed ζ, Hamada coordinates,[3], and Boozer coordinates.[4] In constructing these coordinates, ordinarily, the equations in which the desired properties of the coordinates are taken into account at the outset are solved. In each of these three cases these equations have a different form. There exists a general theory[5,6] that explains the principles of the construction of systems with SFLs and for transforming from one to another. But for all its rigor and apparent completeness it does not contain any equations according to which all possible choices of θ and ζ and the advantages and disadvantages of different variants can be seen at a glance and the degree of similarity and difference of one set of coordinates from another can be assessed immediately. The objective of the present letter is to formulate such equations for the general case and not only for coordinates with SFLs.

Besides Eqs. (2), this requires only the simple expression

$$\frac{1}{\sqrt{g}}=\frac{4\pi^2}{V'}\frac{f}{\langle f\rangle} \tag{3}$$

for the Jacobian $\sqrt{g}=((\nabla a\cdot\nabla\theta)\cdot\nabla\zeta)^{-1}$. This is a trivial consequence of the definition of the averaging operation over a layer between close magnetic surfaces:

$$\langle X\rangle=\frac{d}{dV}\int_V X d^3\mathbf{r}=\frac{1}{V'}\int X\sqrt{g}\,d\theta d\zeta. \tag{4}$$

Here V is the volume of the torus $a=\text{const}$ and the prime denotes differentiation with respect to a.

After the equality (3) is written down, it appears obvious but uninformative or even useless — after all, f in Eq. (3) is unknown, just as is η in Eq. (2). But if, following to the end the logic of introducing coordinates with SFLs, both functions are assumed to be known (and it is by no means necessary that $\eta=0$), then with the aid this equality we arrive at a surprisingly simple and extremely clear method for constructing flux coordinates with the desired properties.

If f and η are given, then θ and ζ must be regarded as unknowns. From Eqs. (2) and (3) we obtain for θ

$$(2\pi\mathbf{B}-\nabla a\cdot\nabla\eta)\cdot\nabla\theta=-4\pi^2\frac{\psi'}{V'}\cdot\frac{f}{\langle f\rangle}. \tag{5}$$

An equation for ζ can be written in exactly the same manner, except that on the right-hand side $-\psi'$ must be replaced by Φ'. But even more elegant, when paired with Eq. (5), is

$$(2\pi\mathbf{B}-\nabla a\nabla\eta)\cdot\nabla(\zeta-q\theta)=0, \tag{6}$$

where $q=-\Phi'/\psi'$ is the stability excess. These two equations together with Eq. (3) are our goal. They show explicitly what the freedom in choosing θ and ζ which here transformed into the freedom of choosing η and f can give: The form of the operator on the

left-hand side of Eqs. (5) and (6) can be changed and the form of $\sqrt{g}$ can be changed independently. That is all. Evidently, no proofs besides Eqs. (3), (5), and (6) are not required.

The general equations (3), (5), and (6) make it possible to view all flux coordinate systems on the basis of a single approach and to switch easily from one system to another by changing η and f. For example, in the family of coordinates with SFLs ($\eta=0$, f arbitrary) we obtain the Hamada coordinates with $f=1$ and the Boozer coordinates with $f=\mathbf{B}^2$, and $f=\mathbf{B}\cdot\nabla\zeta$ corresponds to coordinates with SFLs with fixed ζ.

The Hamada and Boozer coordinates are introduced all the same: $\eta=0$ is assumed and the explicit form of $\sqrt{g}$ is prescribed. But in the ''old'' theory no small amount of work is required to establish the relation between these coordinates,[5–7] whereas our equation (5) solves this problem immediately. Moreover, the proposed method can be used for arbitrary coordinates.

For coordinates with prescribed ζ, however, the standard procedure is different: The conventional toroidal angle or the length of the geometric axis scaled to 2π is chosen for ζ and θ is sought under the condition $\eta=0$. Then the calculation of $\sqrt{g}$ becomes a separate problem.[5,8] In our case, however, everything is extremely simple — the explicit form of $\sqrt{g}$ is given. Here, it is true, there arises the question of whether or not it is possible, given only two degrees of freedom, to choose as the initial functions not two but three functions ζ, $\eta=0$, and $f=\mathbf{B}\cdot\nabla\zeta$. It turns out that it is possible because with $f=\mathbf{B}\cdot\nabla\zeta$ Eq. (6) becomes an identity after substituting $\mathbf{B}\cdot\nabla\theta$ from Eq. (5). The constraints on ζ are thereby removed and ζ can be arbitrary, including also the conventional toroidal angle.

The equations (3), (5), and (6) also make it possible to construct any other convenient system of coordinates. For example, for the same $\sqrt{g}$ as for the Hamada or Boozer coordinates but without SFLs a coordinate system with any other helpful property can be constructed. The equations (3), (5), and (6) make it extremely easy to invent new coordinates.

An equation of the type (5) could also be formulated without Eq. (3), but the previously unnoticed possibility of representing $1/\sqrt{g}$ in the form (3) makes it possible to ''materialize'' the freedom of choice in θ and ζ in the best manner. It should be noted that f can be regarded as a real ''free parameter'' only only because $1/\sqrt{g}$ can be expressed in this manner in terms of a different unknown function f and this is the main advantage of the proposed method. Indeed, if in Eq. (3) some function h appeared instead of $f/\langle f\rangle$, then the constraint $\langle h\rangle=1$ would follow from Eq. (4). The general theory[5,6] suggests that $h=1+\mathbf{B}\cdot\nabla\chi$. The new function χ appearing here is found as the operand of the operator $\mathbf{B}\cdot\nabla$, and moreover $\mathbf{B}\cdot\nabla\chi$ must be dimensionless so that the simplicity and clarity of the construction of the coordinates with χ prescribed are lost. But in our case neither the normalization nor the dimension of f are of any significance, since only $f/\langle f\rangle$ appears in Eqs. (3) and (5).

I thank Professor Y. H. Ichikawa (Chubu University, Japan; Committee for Promotion of Japan–FSU Science Collaboration) for support.

[a)]e-mail: pustovit@qq.nfi.kiae.su

[1] M. D. Kruskal and R. M. Kulsrud, Phys. Fluids **1**, 265 (1958).
[2] J. M. Greene and J. L. Johnson, Phys. Fluids **5**, 510 (1962).
[3] S. Hamada, Nucl. Fusion **2**, 23 (1962).
[4] A. H. Boozer, Phys. Fluids **24**, 1999 (1981).
[5] V. D. Pustovitov and V. D. Shafranov in *Problems of Plasma Theory* [in Russian], edited by B. B. Kadomtsev, Énergoatomizdat, Moscow, 1987, p. 146.
[6] W. D. D'haeseleer, W. N. G. Hitchon, J. D. Callen, and J. L. Shohet, *Flux Coordinates and Magnetic Field Structure. A Guide to a Fundamental Tool of Plasma Theory*, Springer-Verlag, New York, 1991.
[7] N. Nakajima, J. Todoroki, and M. Okamoto, Kakuyugo Kenkyu **68,** 395 (1992); see also NIFS report NIFS-173, Nagoya, 1992.
[8] A. B. Mikhaĭlovskiĭ, *Instability of Plasma in Magnetic Traps* [in Russian], Atomizdat, Moscow, 1978.

Translated by M. E. Alferieff

Stability limits, structure, and relaxation of a mixed state in superconducting films with an edge barrier

I. L. Maksimov and G. M. Maksimova[a)]
Nizhegorod State University, 603600 Nizhniĭ Novgorod, Russia

(Submitted 22 October 1996; resubmitted 6 February 1997)
Pis'ma Zh. Éksp. Teor. Fiz. **65**, No. 5, 405–410 (10 March 1997)

The interval of external magnetic fields where a mixed state can exist in a superconducting film with a fixed value of the flux is determined. The equilibrium and reversible magnetization curves of the sample are calculated, and the dynamics of the magnetic relaxation in the film is described. Nonuniform deformation of the Abrikosov lattice is predicted. © *1997 American Institute of Physics.*
[S0021-3640(97)00905-5]

PACS numbers: 74.76.Db, 74.60.Ec, 74.25.Ha, 65.50.+m

1. The structural features and the equilibrium and relaxational characteristics of a mixed state in low-dimensional superconductors (thin films, single crystals with a high demagnetizing factor, and others) have been comparatively little studied. At the same time, the fundamentally irremovable nonlocality of intervortex interaction as well as the possibility of the existence of an edge barrier for entry and/or exit of vortices can lead to the appearance of nontrivial structures of the magnetic flux[1,2] and, furthermore, they make possible a substantial overheating of the Meissner state. The latter condition is manifested as the existence of a continuum of metastable mixed states with finite trapped flux Φ. The corresponding situation in bulk superconductors has been described almost exhaustively in Refs. 3 and 4. For low-dimensional superconductors this question has almost not been discussed.[b)]

In the present letter the contribution ΔG_v of a test vortex to the Gibbs free energy of a superconducting film in a mixed state with a fixed magnetic flux Φ is calculated. Analysis of the conditions of vortex entry into and exit from the film made it possible to determine the range of external magnetic fields $H_{\max}(\Phi) \geqslant H \geqslant H_{\min}(\Phi)$ where a quasiequilibrium mixed state with a prescribed flux can exist. The thermodynamically equilibrium field $H_{\rm eq}(\Phi)$ is calculated, the complete magnetization curve of the sample (including equilibrium) is constructed, and the magnetic relaxation dynamics of the film is described. It is predicted that the Abrikosov lattice is subject to deformation as a result of the substantially different dependence of the parameter a_0 of the vortex lattice on the field intensity H.

2. Let us consider a thin-film strip of width $2W$ $(0 \leqslant |y| \leqslant W)$ and thickness d $(0 \leqslant z \leqslant d)$ placed in a magnetic field $H=(0, 0, H)$. In the absence of bulk pinning the vortex and current distributions in the film can be represented in the form

$$n(y) = \frac{H}{\Phi_0}\sqrt{\frac{b^2-y^2}{W^2-y^2}} \qquad |y| \leqslant b, \tag{1}$$

$$i(y)=\frac{cH}{2\pi}\sqrt{\frac{y^2-b^2}{W^2-y^2}}\ \mathrm{sign}(y),\quad b\leqslant|y|\leqslant W. \tag{2}$$

Here $n(y)$ characterizes the average density of vortices (per unit length of the film) and $i(y)=i_M(y)+i_V(y)$ is the total current density comprised of the Meissner (i_M) and vortex (i_V) components. Here and below we employ the current density per unit length (integrated over the thickness of the sample) $i(y)=\int_0^d j_x(y,z)dz$. Expression (1) and (2) are the solutions of the one-dimensional version of the Maxwell–London (ML) equations obtained (in the wide-film approximation $W\gg\Lambda$, where $\Lambda=2\lambda^2/d$ and λ is the London length) in the absence of bulk pinning.[1,2,5] We note that expression (2) holds sufficiently faraway from the film edges ($W-\Lambda>|y|\geqslant b$). In a narrow region near the edges ($|y|>W-\Lambda$) the expression for the current density can be approximated by a constant $i(y)=i_{\max}$ determined by matching expression (2) with the exact solution of the ML equations. The trapped flux Φ, per unit length, corresponding to this distribution of vortices is

$$\Phi=\Phi_0\int_{-W}^{W}n(y)dy=2HWF(\kappa), \tag{3}$$

where $\kappa=b/W$ is a dimensionless parameter characterizing the width of the region occupied by the flux and $F(\kappa)=E(\kappa)-[1-\kappa^2]K(\kappa)$ is expressed in terms of complete elliptic integrals of the first (E) and second (K) kinds, respectively.

To determine the characteristics of the vortex entry and exit barriers it is necessary to calculate the part ΔG_v of the total Gibbs energy G_v of a film in a field as a function of the position of a test vortex with coordinates $(0,y)$. In so doing, the renormalization of the screening currents which arises in the presence of vortices (1) penetrating the film must be taken into account. A nontrivial calculation, performed according to a scheme similar to that in Ref. 6, yields ΔG_v in the form

$$\Delta G_v=\frac{1}{2c}\int(\mathbf{i}_1\cdot\mathbf{F}_1)dS+\frac{1}{c}\int(\mathbf{i}\cdot\mathbf{F}_1)dS, \tag{4}$$

where $\mathbf{i}_1$ and $\mathbf{F}_1$ are the current density and vector potential referring to the test vortex and found taking account of the corresponding boundary conditions.[6] The first term in Eq. (4) describes the self-energy of a vortex in the film (taking account of the image of the vortex); the second term describes the interaction of the vortex with the total current $i=i_M+i_V$ given by Eq. (2). After integrating along the longitudinal coordinate x, the expression for ΔG_v acquires the form

$$\Delta G_v(y,\Phi)=E_0(y)-\frac{\Phi_0}{c}\int_y^W i(y')dy', \tag{5}$$

where the self-energy $E_0(y)$ is

$$E_0(y)=\frac{\Phi_0^2}{(8\pi^2\Lambda)}\cdot\begin{cases}\ln(\Lambda/\xi), & |y|\leqslant W-\Lambda\\ \ln\left[\dfrac{|W-|y||}{\xi}\right], & W-\Lambda\leqslant|y|\leqslant W-\xi.\end{cases} \tag{6}$$

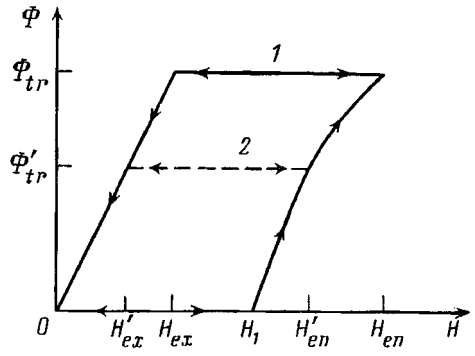

FIG. 1. Diagram of mixed states with trapped flux: *1* — $\Phi=\Phi_{tr}$; *2* — $\Phi=\Phi'_{tr}<\Phi_{tr}$; *3* — $H=H_{\rm eq}(\Phi)$.

We note that ΔG_v depends (via i_V) on the magnitude of the flux Φ entering the film. It is easy to see that in the absence of trapped vortices ($\Phi=0$) expression (5) becomes the well-known expression[6] describing the case of the interaction of a test vortex with the Meissner current.

3. From the condition[7]

$$H_{en}(\Phi)$$

$$\left.\frac{\partial \Delta G_v(y,\Phi)}{\partial y}\right|_{y=W-\xi}=0, \tag{7}$$

we find an equation for the barrier-suppressing field $H_{en}(\Phi)$ corresponding to the entry of the next vortex into the film:

$$\Phi=2H_{en}WF([1-(H_1/H_{en})^2]^{1/2}). \tag{8}$$

Here $H_1=\Phi_0/[2\pi\xi\sqrt{2\Lambda W}]$ is the entry field for the first vortex entering the film. The field H_{en} essentially determines the maximum possible magnetic field $H_{\max}$ in which a mixed state with a prescribed flux can still exist:[3] $H_{en}(\Phi)\equiv H_{\max}(\Phi)$. For small fluxes $\Phi\ll 2H_1W$ the behavior of $H_{en}(\Phi)$ (see Fig. 1) is characterized by the linear relation

$$H_{en}(\Phi)\simeq H_1+\Phi/(\pi W),$$

which is fundamentally different from the quadratic behavior ($H_{en}(\Phi)-H_1\sim\Phi^2$) occurring in bulk superconductors.[3,4] A uniform flux distribution is observed in the opposite case ($\Phi\gg 2H_1W$):

$$H_{en}(\Phi)\simeq\Phi/2W.$$

As follows from the explicit form given in Eq. (5) (substituting Eq. (2)) $\Delta G_v(y)$ increases with $|y|$ for $b\leqslant|y|\leqslant W-\Lambda$; this produces a potential well for confining vortices in the film. As the external field decreases, the limit $b(H)$ as well as the corresponding maximum of the function $\Delta G_v(y)$ shift to the edges of the strip. For this reason, the vortex exit field $H_{ex}(\Phi)$ is found from the condition $b(H_{ex})\simeq W-\Lambda$ corresponding (in our model) to the condition for vanishing of the exit barrier. This gives

$$H_{ex}(\Phi)\simeq\frac{\Phi}{2W}[1+\epsilon\ \ln(4/\epsilon)], \tag{9}$$

where $\epsilon=\Lambda/2W$. The expression (9) determines the minimum external magnetic field $H_{ex}(\Phi)\equiv H_{\min}(\Phi)$ for which a mixed state with a fixed flux Φ can still exist. As the field decreases further, the vortices start to leave the film, as a result of which the flux $\Phi_{\rm rem}$ remaining in the film for $H<H_{ex}(\Phi)$ is determined by the external field

$$\Phi_{\rm rem}=2WH.$$

The test-vortex method proposed in this letter also makes it possible to calculate the thermodynamically equilibrium field $H_{\rm eq}(\Phi)$ determined from the energy condition

$$\Delta G_v(y=0,\Phi)=\Delta G_v(y=W-\xi,\Phi) \tag{10}$$

together with Eq. (3). Using the explicit expression for ΔG_v, we obtain the condition of equilibrium in the general form

$$[\alpha(1-\kappa_{\rm eq}^2)]^{1/2}+J(\alpha,1-\kappa_{\rm eq}^2)=2H_{c1}/H, \tag{11}$$

where $H_{c1}=H_{c1}(d)$ is the first critical field of the film:

$$H_{c1}(d)=\frac{\Phi_0}{(2\pi W\Lambda)}\cdot\ln(\Lambda/\xi),$$

$\alpha=4\epsilon\ll 1$, $\kappa_{\rm eq}$ corresponds to the equilibrium width of the vortex region, and

$$J(\alpha,\beta)=\int_0^\beta\frac{du}{\sqrt{1-u}}\sqrt{\frac{\beta-u}{\alpha+u}}.$$

In the limit $\alpha\to 0$ $J(0,\beta)=2F(\sqrt{\beta})$, which together with Eq. (3) makes it possible to find an explicit expression for $H_{\rm eq}(\Phi)$ (see Fig. 1, curve *3*). For low values of the flux $\Phi\ll\pi H_{c1}W$ the function $H_{\rm eq}(\Phi)$ is strongly nonlinear

$$H_{\rm eq}(\Phi)\simeq H_{c1}+\frac{\Phi}{4\pi W}\ln\left[\frac{16\pi WH_{c1}}{\Phi}\right],$$

and for $\Phi\gg\pi H_{c1}W$ it is replaced by a function of the form (9). Note the singular behavior $dH_{\rm eq}/d\Phi\sim\ln[1/\Phi]\to\infty$ as $\Phi\to 0$, contrasting sharply with the smooth behavior of the function $H_{\rm eq}(B)$ in bulk superconductors $dH_{\rm eq}/dB|_{B\to 0}\sim\exp[-H_{c1}/B]\to 0$. This difference is due to the long-range character of the intervortex repulsion in films, which makes it difficult for vortices to enter the sample when $H>H_{c1}$.

4. The field dependence of the magnetization of the film

$$M=-\frac{1}{2c}\int_{-W}^{W}i(y)y\ dy \tag{12}$$

in the region $H_{\max}(\Phi)\geqslant H\geqslant H_{\min}(\Phi)$ is determined by the equation

$$\Phi=2HWF([1-M\ H_1/M_1\ H]^{1/2}), \tag{13}$$

where $M_1=M_m(H_1)=-H_1W^2/8$ and the function $F(z)$ is determined in Eq. (3). The function $M(H)$ displayed in Fig. 2 is characterized by the smooth behavior of the mag-

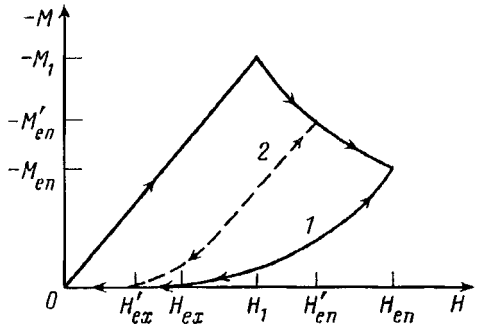

FIG. 2. Field dependence of the magnetization $M(H)$ of a film: *1* — $\Phi=\Phi_{tr}$; *2* — $\Phi=\Phi'_{tr}<\Phi_{tr}$; *3* — $M=M_{\rm eq}(H)$.

netization for $H-H_{ex}(\Phi)\ll H_{ex}(\Phi)$: $dM/dH\sim\ln^{-1}[H_{ex}/(H-H_{ex})]\to 0$, but it has a sharp kink in the derivative in the limit $H\to H_{en}(\Phi)$ (see Fig. 2). We call attention to the reversible (nondissipative) behavior of the magnetization in the range of fields $H_{\max}(\Phi)\geqslant H\geqslant H_{\min}(\Phi)$.

The equilibrium magnetization curve $M_{\rm eq}(H)$ (see Fig. 2, curve *3*) is described by Eqs. (10)–(13). Near H_{c1} the function $M_{\rm eq}(H)$ has the form

$$M_{\rm eq}(H)=M_{c1}\left\{1+\frac{H-H_{c1}}{H_{c1}}\left[1-4/\ln\left[\frac{8H_{c1}}{(H-H_{c1})}\right]\right]\right\}$$

(here $M_{c1}=M_m(H_{c1})$) and is characterized by anomalous behavior of the magnetic susceptibility $dM_{\rm eq}(H)/dH|_{H\to H_{c1}+0}<0$ arising as a result of comparatively slow penetration of the flux near H_{c1}. In strong fields $H>H_1$ the equilibrium magnetization becomes constant $M_{\rm eq}/M_1\simeq 4H_{c1}/\pi H_1\ll 1$.

5. The relations (5) and (13) make it possible to find the vortex entry (exit) activation energy U_a of the film and describe quantitatively the relaxation of the magnetization M to its equilibrium value $M_{\rm eq}$. Specifically, for vortex entry with $H\geqslant H_1$ the dependence of U_a^{en} on the local (in time) magnetization $M(t)$ has the form

$$U_a^{en}=U_0[\ln\sqrt{M_{en}/M}-1+\sqrt{M/M_{en}}], \tag{14}$$

where $U_0=\Phi_0^2/8\pi^2\Lambda$ is the characteristic electromagnetic energy of a solitary Peierls–Abrikosov vortex,[6] and $M_{en}=M_{en}(H)$. Assuming that the relaxation is of a thermal activation character, Eq. (14) implies the exotic dependence $|M_{en}-M(t)|\sim\sqrt{\ln t}$, describing the initial stage of relaxation $|M_{en}-M(t)|\leqslant|M_{en}|$. The next stage of relaxation at entry $|M_{en}|>|M(t)|\geqslant|M_{\rm eq}|$at finite temperature T is characterized by the power-law function

$$|M(t)-M_{\rm eq}|\sim t^{-1/s}$$

with exponent $s=U_0/T\gg 1$. Therefore the relaxation at flux entry through a barrier, strictly speaking, is not logarithmic in the entire time range. It can be shown that the relaxation at flux ''exit'' in the indicated range of fields is, conversely, practically always described by a logarithmic law.

We note that the characteristic activation energy in the films $\sim U_0$ contains a small parameter $d/\lambda\ll 1$ compared to its analog in bulk samples. Indeed, an estimate of the Arrhenius exponent $s=U_0/T$ in sufficiently thin high-T_c superconducting films $d\simeq 300$ Å in the temperature range $(T_c-T)/T_c\simeq 0.1$ gives, for typical values of the parameters, $s\simeq 10$, which is much less than in the case of surface relaxation.[8] Therefore the rate of edge relaxation in thin films can be much higher than the analogous quantity in bulk superconductors.

6. The situation discussed in the present letter can be realized by rapidly cooling a film in an external field H_0. It is obvious that at $H=H_0$, which on account of Eq. (9) is the vortex exit field $H_{ex}(\Phi_{tr})\simeq H_0$, the distribution of the trapped flux $\Phi_{tr}=2H_0W$ will be uniform over the entire film, and a triangular vortex lattice with period $a_0\simeq(\Phi_0/H_0)^{1/2}$ is established inside the film.[9] As the field H increases, additional magnetic flux starts to penetrate the sample for $H\geqslant H_{en}(\Phi_{tr})$, satisfying Eq. (7). In the region of fields $H_0\leqslant H\leqslant H_{en}(\Phi_{tr})$, however, the distribution of vortices will be compressed in the transverse (relative to the current) direction. This will destroy long-range order in the ensemble of fluxoids, i.e., it will ultimately destroy the Abrikosov vortex lattice.

Indeed, assuming that locally $a_0(B)\sim B^{-1/2}$, where $B=B(y)$ is the local induction produced in the film by vortices concentrated inside a strip of width Δy ($W\gg\Delta y\gg l_v$, where l_v is the average distance between the vortex rows), it is easy to obtain (in the limit $H_0\ll H\leqslant H_{en}$): $b(H)\simeq 2W\sqrt{H_0/2\pi}$. The local induction $B(y)\simeq n(y)\Phi_0$ (i.e., the flux density per unit length of the film) varies appreciably from the value $B=B_{\min}\simeq\Phi_0/\lambda^2$ (in the limit $y\to b$) to the value $B=B_{\max}\simeq 2(HH_0/\pi)^{1/2}$ (at $y\simeq 0$). Correspondingly, the local value of the lattice parameter will vary from $a=a_{\max}\simeq\lambda$ near the boundary of the region occupied by the flux to $a=a_{\min}<a_0(H_0)$ (since $a_{\min}/a_0(H_0)\simeq(0.25\pi H_0/H)^{1/4}<1$) at the center of the film.

Moreover, the uniaxial (along the y axis) compression of the lattice due to the effect of the Meissner currents will destroy the symmetry of the lattice, as a result of which the hexagonal structure of the lattice will be replaced by an orthorhombic structure. We underscore that such distortions of the vortex lattice can be observed only in low-dimensional superconducting samples (which sharply contrasts with the situation in bulk superconductors[3]). Therefore it can be concluded that a lattice of Peierls–Abrikosov vortices in low-dimensional superconductors is more easily deformed than its analog in macroscopic samples.

The predicted deformation of the vortex lattice can be observed in experiments on magnetic decoration of thin films (or single crystals with the corresponding geometry) or neutron scattering by a vortex structure. In the first case, a direct visualization of vortex bunching at the center of the sample should be expected. In the second case, the breakdown of the symmetry of the vortex structure should be accompanied by a smearing and even vanishing of the Bragg neutron-scattering peaks.

In real samples the presence of bulk pinning can appreciably distort the picture

being discussed. The structure, the limits of stability, and the relaxation characteristics of a mixed (critical) state in superconductors with bulk pinning will be analyzed separately.

As this paper was being prepared, we learned of the content of Ref. 10 where similar expressions were obtained for the vortex entry/exit field in the case of an edge geometric barrier on the basis of a qualitative analysis of its characteristics.

We are grateful to A. A. Andronov and V. Ya. Dmikhovskiĭ for valuable discussions and A. A. Elistratov for assisting in this work. I. L. M. thanks E. Kh. Brandt for many discussions, L. Ya. Vinnikov and G. P. Gordeev for a discussion of the experimental situation, and J. Clem for his interest in this work. This work was partially supported by the Ministry of Science of the Russia Federation (High-T_c Superconductors Project 95-057), the State Commission on Institutions of Higher Learning of the Russian Federation (Grant 95-0-7.3-178), and the government of the Russian Federation together with the International Science Foundation (Grant R8J300).

[a)]e-mail: ilmaks@phys.unn.runnet.ru

[b)]A preliminary report of some results of this work was made at the 21st Conference on Low-Temperature Physics (LT-21, Prague, 1996).

---

[1] E. Zeldov, A. Larkin, V. Geshkenbein *et al.*, Phys. Rev. Lett. **73**, 1428 (1994).
[2] I. L. Maksimov and A. A. Elistratov, JETP Lett. **61**, 208 (1995).
[3] F. F. Ternovskiĭ and L. N. Shekhata, Zh. Éksp. Teor. Fiz. **62**, 2297 (1972) [Sov. Phys. JETP **35**, 1202 (1972)].
[4] J. R. Clem, in *Proceedings of the 13th Conference on Low Temperature Physics (LT–13)* (1974), Vol. 3, p. 102.
[5] M. Yu. Kupriyanov and K. K. Likharev, Fiz. Tverd. Tela (Leningrad) **16**, 2829 (1974) [Sov. Phys. Solid State **16**, 1835 (1974)].
[6] K. K. Likharev, Radiofiz. **14**, 909 (1971).
[7] P.-G. de Gennes, *Superconductivity of Metals and Alloys*, W. A. Benjamin, New York, 1966 [Russin translation, Mir, Moscow, 1968].
[8] L. Burlachkov, Phys. Rev. B **47**, 8056 (1993).
[9] K. B. Efetov, Fiz. Tverd. Tela (Leningrad) **15**, 647 (1973) [Sov. Phys. Solid State **15**, 459 (1973)].
[10] M. Benkrauoda and J. R. Clem, Phys. Rev. B **53**, 5716 (1996).

Translated by M. E. Alferieff

Anisotropy of the hypersonic grating and spectra of four-photon Rayleigh-line-wing spectroscopy in water

N. P. Andreeva
A. Navoi Samarkand State University, 703061 Samarkand, Uzbekistan

(Submitted 9 January 1997)
Pis'ma Zh. Éksp. Teor. Fiz. **65**, No. 5, 411–413 (10 March 1997)

A model describing the Rayleigh-line-wing spectra obtained in water by four-photon polarized spectroscopy is proposed. © *1997 American Institute of Physics.* [S0021-3640(97)01005-0]

PACS numbers: 78.35.+c, 42.65.Es, 42.65.Hw, 77.65.Dq, 43.35.Cg

The study of the Rayleigh-line-wing spectra obtained in water by four-photon polarized spectroscopy (FPRLWS) showed that peaks shifted relative to one another by the Brillouin frequency Ω in the region of frequency detunings of up to 2 cm^{-1} on both sides of the Rayleigh frequency are observed in these spectra (Fig. 1).

As is well known,[1] the spontaneous Brillouin scattering is an isotropic process. However, in the present experiment a property of Brillouin scattering (shift of the frequency Ω) which requires explanation appears in the depolarized component. One likely mechanism for the appearance of the observed peaks is anisotropy of the hypersonic grating which appears as a result of the development of stimulated Brillouin scattering (SBS) accompanying the interaction of the pump radiation ω_1 with the experimental medium.[2]

In the general case electrostriction is not isotropic. For sufficiently strong electric fields, electrostriction produces anisotropy in the medium even in isotropic dielectrics.[3] The nonlinear susceptibility of the electrostriction-induced anisotropy is defined as follows:[4]

$$\Delta X^{AB}(\omega)=\frac{1}{4\pi}\frac{\partial\epsilon}{\partial\rho}\Delta\rho, \quad \Delta\rho=(\gamma/2\pi v^2)|E|^2, \quad \gamma=\left(\rho\frac{\partial\epsilon}{\partial\rho}\right), \tag{1}$$

where v is the hypersound velocity and E is the electric field intensity of the radiation giving rise to electrostriction. Therefore the electrostriction-induced hypersonic grating is not only a grating of density fluctuations but also a grating of anisotropy fluctuations.

It is well known[5] that the resonance behavior of the nonlinear susceptibility will be observed only if $(\omega_1-\omega_2)=\Omega$. Then we can write for the FPRLWS intensity

$$I_s\sim\left|\frac{X^{AB}}{i\pm(\omega_1-\omega_2\mp\Omega)/\delta\nu_{AB}}\right|^2 I_1^2 I_2 l, \tag{2}$$

where I_1 is the intensity of the pump radiation ω_1, I_2 is the intensity of the probe-beam radiation ω_2, l is the nonlinear interaction length, $\delta\nu_{AB}=10$ cm^{-1} is the half-width of the

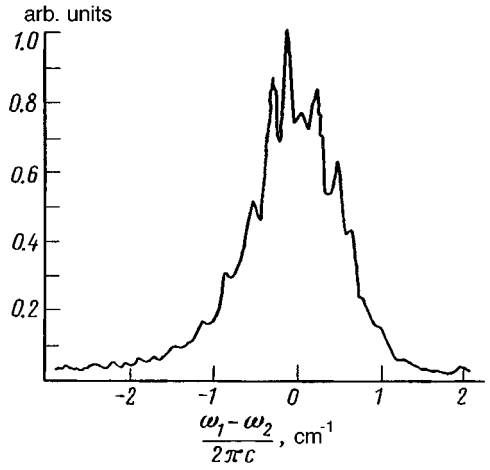

FIG. 1. FPRLWS spectrum in water at 34 °C.

Rayleigh-line wing at water temperature 34 °C.[6] Then the anisotropic-scattering spectrum should have the form displayed in Fig. 2, where the experimentally observed peaks are absent.

In the course of the experiments[5,6] the absence of the SBS radiation accompanying the interaction of the pump radiation ω_1 with the experimental medium was strictly controlled, i.e., the investigations were performed below threshold. However, it can be asserted that in this case a hypersonic grating does exist in the medium, though the SBS radiation is not recorded by the instruments.

It is known[7] that the exponential dependence of the SBS intensity I_B on the pump intensity I_1 decreases I_B by a factor of 400, i.e., I_B completely vanishes when the inten-

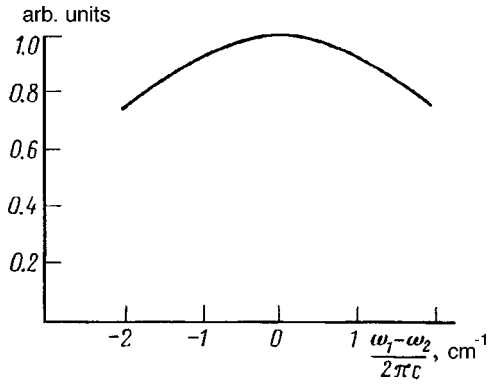

FIG. 2. Theoretically computed FPRLWS spectrum in water neglecting hypersonic grating anisotropy.

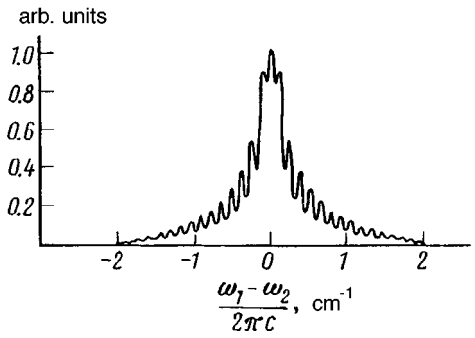

FIG. 3. Theoretically computed FPRLWS spectrum in water allowing for hypersonic grating anisotropy.

sity decreases by a factor of 1.2 below the threshold value. The intensity of the hypersonic grating is directly proportional to I_1 and I_B:[1]

$$P=\left[\frac{GI_1}{2\alpha}\right]\left[\frac{\Omega}{\omega_1}I_B\right], \tag{3}$$

where G is the SBS gain and α is the hypersound absorption coefficient. A decrease of I_1 by a factor of 400 and I_B by a factor of 1.2 gives a overall decrease of P by a factor of 500. The intensity of the signal I_B is 10^3 times higher than that of the FPRLWS signal, which ordinarily is 10^3-10^6 times weaker than the SBS signal, which says something about the intensity of the hypersonic grating formed as a result of the interaction of ω_1 with the medium. Therefore the anisotropy of the hypersonic grating associated with the interaction of the pump ω_1 with the medium must be taken into account in describing the FPRLWS spectra obtained in this series of experiments.

Tuning the difference frequency $\omega_1-\omega_2$ gives the greatest intensification of the hypersonic grating existing in the medium in the case when $\omega_1-\omega_2=\Omega_n$, where $n=0,\ 1,\ 2,\ \ldots$. The intensification is determined by the ratio of the detuning (in cm^{-1}) to the displacement and it shows that for a given value only each nth peak of the hypersonic grating is amplified. In this case expression (2) can be replaced by the expression

$$I_s\sim\left|\frac{X_{AB}}{i\pm(\omega_1-\omega_2+n\Omega)\,\delta\nu_{AB}}\right|, \tag{4}$$

where $\Omega=0.13$ cm^{-1} and $\delta\nu_{AB}$ was adjusted in the calculations and was found to be equal to 0.075 cm^{-1}. As one can see, even taking account of the interaction of the hypersonic grating with the tunable frequency $\omega_1-\omega_2$ in such an elementary manner gives dependences of the anisotropic scattering intensity which are close to those observed experimentally. On this basis, it can be asserted that in the present experimental arrangement the Rayleigh-line wing in the near region is formed mainly by the anisotropic scattering associated with the hypersonic grating formed as a result of the interaction of the pump wave ω_1 with the experimental medium. Of course, to obtain a better

description of this process it is necessary to perform calculations taking account of the dependence of X_{AB} on the intensity of the electric field according to expression (1), but this is a subject for a future work.

In conclusion, I wish to thank A. F. Bunkin and A. A. Nurmatov for providing the data for discussion.

[1] I. L. Fabelinskiĭ, *Molecular Scattering of Light*, Plenum Press, New York, 1968 [Russian original, Nauka, Moscow, 1965].
[2] A. F. Bunkin, D. V. Mal'tsev, and K. O. Surskiĭ, JETP Lett. **47**, 657 (1988).
[3] St. Kielich, *Molecular Nonlinear Optics*, Panstwowe wydawnictwo naukowe, Warsaw, 1981 [Russian translation, Nauka, Moscow, 1981].
[4] Y. R. Shen, *The Principles of Nonlinear Optics*, Wiley, New York, 1984 [Russian translation, Nauka, Moscow, 1989].
[5] S. A. Akhmanov and N. I. Koroteev, *Methods of Nolinear Optics in Scattered-Light Spectroscopy* [in Russian], Nauka, Moscow, 1981.
[6] C. I. Montrose, J. A. Bucaro, J. Marshall-Coakley, and T. A. Litovitz, J. Chem. Phys. **60**, 5025 (1974).
[7] B. Ya. Zel'dovich, N. F. Pilipetskiĭ, and V. V. Shkunov, *Principles of Phase Conjugation*, Springer-Verlag, New York, 1985 [Russian original, Nauka, Moscow, 1985].

Translated by M. E. Alferieff

Growth and structure of epitaxial diamond films grown on Si(111) single crystals

S. N. Polyakov, A. T. Rakhimov, N. V. Suetin, M. A. Timofeev, and A. A. Pilevskiĭ

Institute of Nuclear Physics, M. V. Lomonosov Moscow State University, 119899 Moscow, Russia

(Submitted 14 January 1997)
Pis'ma Zh. Éksp. Teor. Fiz. **65**, No. 5, 414–418 (10 March 1997)

Experiments on growing single-crystal diamond films on silicon crystals with (111) surface orientation have been performed. Results attesting to the possibility of obtaining thin heteroepitaxial films are presented. © *1997 American Institute of Physics.*
[S0021-3640(97)01105-5]

PACS numbers: 68.55.Jk, 68.55.Ln, 68.55.Nq, 85.40.Vx

The prospects for using diamond as a semiconductor material for the elemental base of a powerful, radiation-resistant, fast electronics have stimulated a search for methods for growing diamond films epitaxially on different substrates. At present there are no reliable technologies for heteroepitaxial growth of structurally perfect single-crystal diamond films on readily available and inexpensive substrates with a surface area that is adequate for mass production of electronic products. This is the main reason why diamond films have not yet found wide applications in solid-state electronics. We note that different methods for depositing polycrystalline and textured diamond films on a wide class of substrates have now been demonstrated but grain boundaries, interphase boundaries, and inclusions of other phases together with lattice defects strongly influence the electrophysical properties of such films, limiting their possible applications.

Epitaxial growth of diamond films is now possible only in the case when natural diamond crystals, usually with (100), (110), and (111) orientation of the faces, are used as substrates.[1,2] At the same time, new substrate materials for epitaxial growth of diamond films are being actively sought. Today, cubic boron nitride is still the best material from the standpoint of good coupling of the crystal lattices of the film and substrate as well as the values of the surface energy.[3–5] Unfortunately, substrates with a boron nitride buffer layer grown epitaxially on them are considered to be ''exotic,'' since the process of growing single-crystal c-BN films with a low density of structural defects is in itself a difficult technological problem. For this reason, preference is given to traditional substrates, specifically, silicon with no buffer layers. Moreover, silicon is one of the most perfect crystals with respect to the density of structural defects and impurity content, as a result of which it is the material most widely used for substrates.

As a result of attempts to use silicon substrates with a chemically-mechanically polished surface for epitaxial growth of diamond films, the films grew either with an axial texture or a faceted texture with misorientation angles of the (a, b) axes of the film in the substrate plane of $\approx 10° - 20°$.[6–8] The best results were demonstrated in Refs. 9, where

the authors were able to grow *c*-oriented films on Si(001) substrates with (*a, b)* misorientation angles $\approx 3.8°$. In all of these works, the now conventional gas-phase synthesis technology in which the gas medium is activated with a microwave discharge in a mixture of hydrogen and methane was used to deposit the diamond films, but a special procedure for depositing a thin carbon layer by applying an additional voltage to the substrate was used at the initial stage of growth in order to increase the density of nucleation centers. This stage is necessary, since the heterogeneous formation of nucleation centers of the diamond phase on the surface of silicon crystals is a very low-probability process.

Despite the substantial progress made in the technology of growing diamond films, including textured films, we know of no works where epitaxy was achieved.

This letter reports the growth of thin epitaxial diamond films by gas-phase deposition using an unconventional mixture activated with a DC discharge. In contrast to previous works, where methane was used as the source of carbon, we employed alcohol vapors and the films were deposited on silicon substrates not with (001) but rather (111) surface orientation. In addition, the surface of the silicon plate is slightly ($\approx 3°$) misoriented relative to the (111) crystallographic plane, which presupposes the presence of atomic steps on the silicon surface that are heterogeneous-nucleation centers. The effect of the misorientation angles of the silicon crystal surfaces relative to the (111) crystallographic planes on the growth rate of diamond films on them was investigated in Ref. 10.

The substrate was subjected to special treatment prior to deposition. The deposition process lasted for 1–2 h. Analysis of the obtained patterns with the aid of a scanning electron microscope showed (the data are not presented in this letter) that the films grown have a high resistivity and their surface is smooth and uniform with no extraneous protuberances over the entire area of the substrate (15×15 mm).

The modern methods of x-ray diffractometry and scanning electron microscopy were used to study the structure of the grown films. Attention was focused on the crystallinity of the films (i.e., whether or not the films are single- or polycrystalline, the texture of the film, and so on) and the relative orientation of the film and substrate lattices.

Before discussing the results obtained, we shall briefly consider the existing approaches to solving the question of the coupling of the crystalline lattices, one of the main questions in solving epitaxy problems. Of the large number of different approaches to solving this problem, two main approaches stand out. The first one involves the idea of pseudomorphism, i.e., a change in the lattice periods which produces epitaxy of the crystals before they completely match at the interface.[11] According to the second criterion of commensurateness of crystal lattices at an interface, it is thought that the natural lattice periods are preserved in epitaxy and the difference of the periods is compensated by misfit dislocations.[12] In most cases of epitaxy, however, matching of two undistorted lattices without pseudomorphism is most likely. In this case, the orienting action of the substrate is characterized according to a structural-geometric indicator: Oriented nucleation centers arise on account of the fine atomic topography of the surface, i.e., on account of the presence of rows of potential wells on the substrate along which it is advantageous for the atoms of the deposited substance to arrange themselves. This idea is

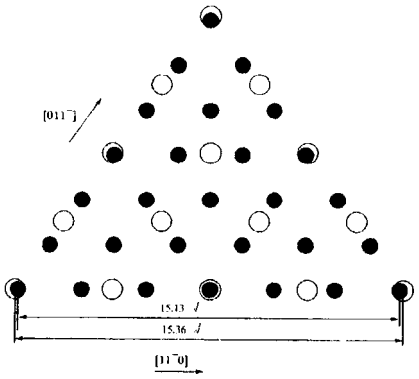

FIG. 1. Arrangement of atoms in diamond (fill dots) and silicon (open dots) lattices in the (111) planes.

the basis of a criterion that makes it possible to predict the relative orientations of the lattices of the grown epitaxial film and substrate. It is postulated that in epitaxy the relative orientations of the lattices are such that the directions with the maximum packing density of atoms of the same kind in the two lattices are parallel with respect to one another. We employed this very simple criterion for the special case of determining the relative orientations of lattices in epitaxial growth of diamond films on silicon single crystals with (111) surface orientation.

To perform such a crystal-geometric analysis it is convenient to use a scheme in which the atoms are arranged in the diamond and silicon lattices in (111) planes. The pattern of such a relative arrangement of atoms on the (111) crystallographic planes of diamond and Si lattices is reproduced in Fig. 1. It is evident from Fig. 1 that the best matching in the intergrowing planes is obtained when the following epitaxial relation is satisfied:

$$(111)[111]C_{\text{diamond}}//(111)[111]\text{Si}.$$

Calculation shows that the mismatch of the lattice periods (3 by 2) in the intergrowing planes equals 0.7% (for diamond and Si lattice parameters equal to 3.567 and 5.431 nm, respectively, at $T=300$ K). We note that for the (100) surface orientation this mismatch equals 1.5%. In Ref. 13 the conclusion that epitaxial growth of diamond films on silicon crystals is possible with (111) surface orientation was drawn in on the basis of calculations using a cluster model.

It is well known that in the case of silicon substrates with this orientation the surface tilted by a small angle (2–5°) with respect to the (111) crystallographic plane in the [110] direction has a stepped relief, which should increase the rate of nucleation, since it is easier for nucleation centers to form at the corners of the steps.[12] This circumstance was also used as a basis for choosing substrates with (111) surface orientation to obtain epitaxial growth of diamond films.

X-ray diffraction investigations of the grown films were performed on a Rigaku D-max/RC diffractometer (12 kW source, Cu$K\alpha$ radiation, graphite crystal analyzer). Only (111) reflections were observed in the $\theta/2\theta$-scan diffraction patterns. This means

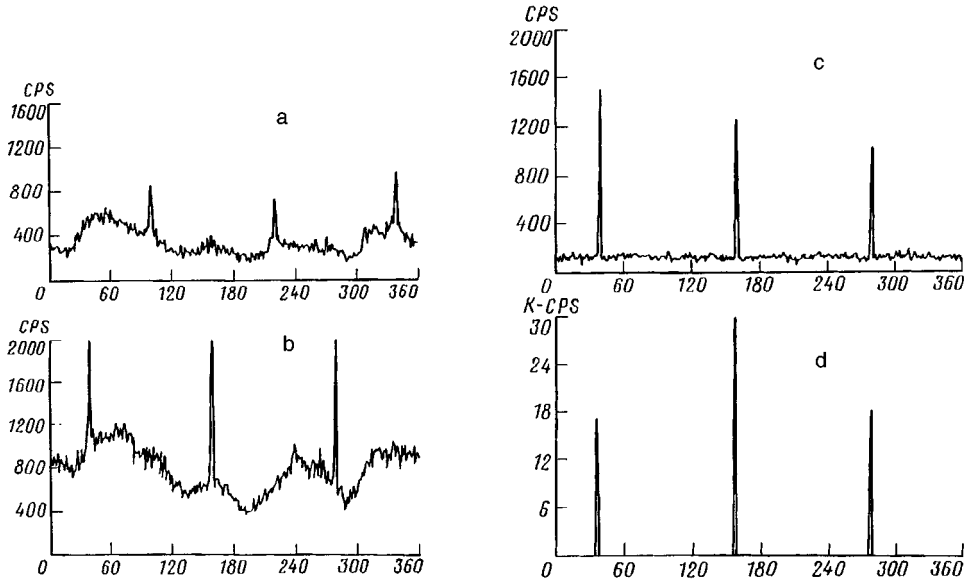

FIG. 2. Φ-scan diffraction patterns of the (311), (220), and (111) reflections of a diamond film (a, b, c) and (220) reflections of the silicon substrate (d).

that the orientation of the surface of the grown films corresponds to (111) atomic planes. To within the limits of sensitivity of the method, no other phases, such as β-SiC, graphite, and others, were found. The half-widths of the θ-scan diffraction-reflection curves for the (111) reflections do not exceed 0.4°, which attests to the very small variance in the misorientation of the [111] axis of the film relative to the substrate surface. The average values of the crystal lattice parameter of the films, determined from the $\theta/2\theta$-scan diffraction patterns, are equal to $3.590 \pm 0.001E$.

The Φ-scanning technique in a noncoplanar Bragg diffraction scheme was used to determine the relative orientation of the crystal lattices of the film and silicon substrate. To this end, the (220), (113), and (111) reflections of the film and the (220) reflections of the substrate were used. The Φ-scan diffraction patterns of the corresponding reflections are presented in Fig. 2. The presence of asymmetric (220), (113), and (111) reflections indicates unequivocally that the films grown are single-crystalline. It is evident from the diffraction pictures presented that the diamond films grow in the manner conjectured above (see Fig. 1).

It should be noted that our method makes it possible to achieve epitaxial growth only in thin $\leqslant$500 E layers. For large thicknesses misorientation of the [111] axis occurs as a result of the formation of blocks and appearance of regions with orientations different from (111).

Analysis of these investigations makes it possible to draw the following conclusions.

1. It was demonstrated experimentally that it is possible to grow thin single-crystal diamond films on silicon substrates with (111) surface orientation.

2. Epitaxial growth of diamond films without the deposition of buffer layers is achieved by using an unconventional mixture in the working chamber.

3. The films grown have a high resistivity and they are smooth and uniform over the entire area of the substrate.

[1] S. N. Polyakov, A. S. Savichev, E. K. Kov'ev *et al.*, in *Abst. Book of Second Intern. Symp. on Diamond Films*, 2–3 May, Minsk, Belarus, 1994, p. 84.
[2] L. L. Builov, A. E. Aleksenko, A. A. Botev, and B. V. Spitsin [*sic*], Dokl. Akad. Nauk USSR **287**, 888 (1986).
[3] L. Wang, P. Pirouz, A. Argoitia *et al.*, Appl. Phys. Lett. **63**, 1336 (1993).
[4] T. Suzuki, M. Yagi, and K. Shibuki, Appl. Phys. Lett. **64**, 557 (1994).
[5] B. R. Stoner, S. R. Sahaida, J. P. Bade *et al.*, J. Mater. Res. **8**, 1334 (1993).
[6] X. Jiang and C. L. Jia, Appl. Phys. Lett. **67**, 9 (1995).
[7] K. Helming, S. Geier, M. Schreck *et al.*, J. Appl. Phys. **7**, 4764 (1995).
[8] M. W. Geis, Appl. Phys. Lett. **55**, 550 (1989).
[9] M. Schreck and B. Stritzker, Phys. Stat. Sol. **154**, 197 (1996).
[10] T. Tsuno, H. Shiomi, Y. Kumazawa *et al.*, Jpn. J. Appl. Phys. **35**, 4724 (1996).
[11] L. Royer, Bull. Soc. Franc. Mineral. **51**, 7 (1928).
[12] J. H. Van der Merwe, J. Appl. Phys. **34**, 117 (1963); *ibid.* **34**, 123 (1963).
[13] R. Q. Zhang, W. L. Wang, J. Estev, and E. Bertran, Appl. Phys. Lett. **69**, 1086 (1996).

Translated by M. E. Alferieff

Superconductivity in impurity bands

A. I. Agafonov and E. A. Manykin
Kurchatov Institute Russian Research Center, 123182 Moscow, Russia

(Submitted 15 January 1997)
Pis'ma Zh. Éksp. Teor. Fiz. **65**, No. 5, 419–424 (10 March 1997)

We present a theory of superconductivity in doped insulators. In the magnetic metal state of the compound we obtain the self-consistency equations for the superconducting state in the spin-dependent impurity bands of both extended and localized states in the initial insulator gap. A BCS-type triplet pairing field is considered. We show that the superconducting gap in which single-electron extended states do not exist is overlapped by the distribution of the localized states. The formation of a latent superconducting gap is discussed in connection with the unusual properties of high-T_c compounds. © *1997 American Institute of Physics.* [S0021-3640(97)01205-X]

PACS numbers: 71.27.+a, 71.30.+h, 74.20.Mn, 74.72.−h

A surprising feature of high-T_c materials is the strong doping dependence of the density of electronic states (DOS). It has been established from experimental studies of the optical properties of these materials is that doping diminishes the DOS above the initial insulator gap and gives rise to new features deep in the gap.[1–5]

The formation of the substitution-induced gap states is inherent to the doped compounds.[6] The parent compounds have an antiferromagnetic insulating state. The magnetic phase disappears with small doping, and the material goes to a poor-metallic phase with a large T_c.

An adequate model for describing high-T_c superconductors must be consistent with the position of the Fermi level with doping. The most commonly used approach is to relate the superconductivity to processes occurring in structure elements of the parent compound, e.g., in the CuO_2 planes of the cuprates.[6–11] Then one would expect the Fermi level to lie outside the initial insulator gap in both the metal and superconducting states.[6,12] However, there are reliable experimental data which indicate that the Fermi level lies inside the gap, among the doping-induced gap states (see Ref. 6 and references cited therein). Moreover, the Fermi level appears to depend weakly on impurity concentrations.

From our point of view, the combined effect of disorder caused by impurity atoms and electron correlations in the doped system is a central issue in high-T_c superconductivity.

Upon substitutional doping, in $La_{2-x}Sr_xCuO_4$, for example, La^{3+} is randomly replaced by Sr^{2+}. Both valence electrons of Sr go to satisfy the bonding requirements, and a singly occupied acceptor level arises in the initial gap. Doping with nominal Ce^{4+} for Nd^{3+} in $Nd_{2-x}Ce_xCuO_4$ gives a singly occupied donor level in the gap. Hy-

bridization between the impurity levels and the initial band states of the insulator can significantly change the DOS.

The DOS modification caused by the hybridization and potential scattering of band electrons by impurity atoms randomly distributed in the host lattice has been studied in Ref. 13. With the use of multiple-scattering theory, the configuration-averaged Green's functions over the impurity ensemble were calculated by the Matsubara method. It was shown that doping sharply decreases the DOS above the gap near the band edge and gives rise to impurity bands of both extended and localized states in the gap region. The formation of the narrow, high-density band of extended states is caused by hybridization, which induces virtual electronic transitions over the impurity ensemble: an initial impurity site $\rightarrow$ a band state $\rightarrow$ another site $\rightarrow$ a band state, etc. It is important that the main high-concentration peak of the localized states lies within this band.

The Anderson model with strong on-site electron correlations for the impurity levels and the hybridization has been used to study magnetic ordering and insulator $\rightarrow$ metal phase transitions in the impurity bands in the self-consistent Hartree–Fock approximation.[14] The narrow, high-density bands of extended states (which are spin-degenerate only in the case of a paramagnetic metal) within the insulator gap have the same origin as in Ref. 13. Although the impurity band structure depends strongly on the impurity concentration (as a matter of fact, it causes the transitions in the system), the Fermi level depends only weakly on the doping. For the singly occupied donor levels a magnetic insulator state with a finite magnetic moment per impurity atom is realized in the system at low impurity concentrations. With increasing concentration, two metallization stages of the system have been found,[14] which correspond to the transitions: magnetic insulator $\rightarrow$ magnetic metal $\rightarrow$ paramagnetic metal. In these metallic states the Fermi level lies within the main peak of the localized states, but this peak lies within the impurity band of extended states.

In this letter we present a model of high-T_c superconductivity in the impurity bands. In the magnetic metal state the problem reduces to searching for superconductivity in a subsystem with low concentrations and kinetic energies of the electrons but with a high density of extended states at the Fermi level. Because of the spin dependence of the DOS in this state, only triplet pairing can be realized. Here we restrict ourselves to the BCS-type triplet pairing field caused by electron–phonon coupling. The hopping mechanism of superconductivity, which is also predicted by the model, will not be calculated numerically. We shall show that the superconducting gap in which single-electron extended states do not exist is overlapped by the distribution of the localized states. The latent superconducting gap must result in unusual properties of these superconductors.

The Hamiltonian of the system is

$$H = H_A + H_{el-ph}, \tag{1}$$

where H_{el-ph} describes the electron–phonon interaction, and H_A is the Anderson Hamiltonian describing the insulator in the single-band approximation (for definiteness, the valence band) with an ensemble of impurity atoms randomly distributed in the host lattice:

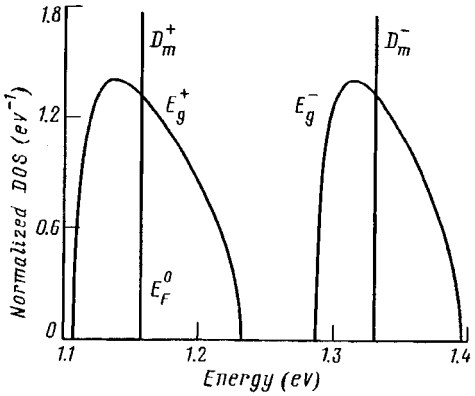

FIG. 1. The DOS per impurity atom for the magnetic metal state near the Fermi level $E_F^0=1.158$ eV. The energy is reckoned from the unperturbed valence band top. Parameter set: $N_t=0.2$ Å^{-3}, $D_b=1.5$ eV, $\varepsilon_0=D_b+0.5$ eV, $N_{im}=0.15N_t$, $V_{\mathbf{k}j}\,N_t^{1/2}=1.3$ eV, $U=0.5$ eV.

$$H_A=\sum_{\mathbf{k}\sigma}\ \varepsilon_{\mathbf{k}}a_{\mathbf{k}\sigma}^{+}a_{\mathbf{k}\sigma}+\sum_{j\sigma}\ \varepsilon_0 d_{j\sigma}^{+}d_{j\sigma}+\sum_{j}\ Un_{j\sigma}n_{j,-\sigma}+\sum_{j,\mathbf{k},\sigma}\{V_{\mathbf{k}j}a_{\mathbf{k}\sigma}^{+}d_{j\sigma}+\text{h.c.}\},\qquad(2)$$

where $a_{\mathbf{k}\sigma}$ and $d_{j\sigma}$ are the usual annihilation operators; σ is the spin index; $\mathbf{k}$ is the wave vector of an electron in the band state with the energy $\varepsilon_{\mathbf{k}}$; j is the number of the impurity atom; ε_0 is the bare impurity level located in the gap above the band top; $V_{\mathbf{k}j}$ is the matrix element of the hybridization; U is the on-site electron correlation for the impurity levels. Here $\Sigma_{\mathbf{k}\sigma}=N_t$ is the total number of band states; $\Sigma_j=N_{im}$ is the impurity concentration.

The Hamiltonian (2) has been solved in the Hartree–Fock approximation with self-consistent determination of the Fermi level (see Ref. 14 for details). To model the DOS modification, we chose the ''semi-elliptical'' model of a symmetrical, narrow valence band of width $2D_b$. At a certain impurity concentration the system goes to a metallic phase with a finite magnetic moment per impurity atom. The fraction of the σ-spin DOS per impurity atom near the Fermi level in the initial insulator gap at $N_{im}=0.15\ N_t$ is shown in Fig. 1. Here $\sigma=\pm$ denotes the spins. The δ-function peak of the localized states D_m^σ corresponds to a simple pole ξ_d^σ of the Green's function $G_{jj}^{(1)\sigma}$. This peak lies within the high-density band of extended states E_g^σ. That the position of this pole lies within the band E_g^σ is a common feature for the various parameter sets. The Fermi energy $E_F^0=\xi_d^+$ and, accordingly, the D_m^+ and E_g^+ bands are partially occupied. The total number of localized states per impurity atom (or, in other words, the pole amplitude) is $N_m^+=0.597$, and the occupation per impurity atom is $\eta_m^+=0.394$. The total number of extended states per impurity atom is $N_g^+=0.128$, and their occupation per impurity atom is $\eta_g^+=0.063$. The magnetic moment is $0.466\ \mu_B$; the bands with $\sigma=-$ are unoccupied.

Thus the problem reduces to one of searching for superconductivity in a subsystem with low concentrations and kinetic energies of the electrons but a high density of extended states at the Fermi level. From Fig. 1 one can estimate that the average DOS in the

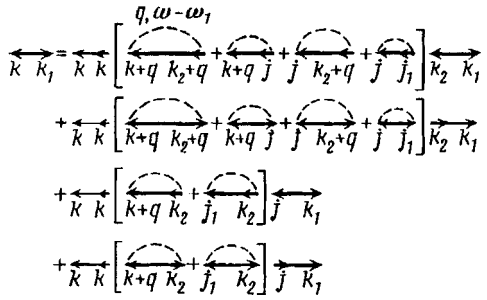

FIG. 2. The diagram equation for the anomalous Green's function $F^{+}_{-\mathbf{k}\mathbf{k}_1}(\omega)$. A line $\leftrightarrow$ represents the anomalous Green's function F^{+}, a line $\rightarrow\!\rightarrow$ represents the single-electron Green's function G, and a dashed line represents the unperturbed phonon Green's function $D(\mathbf{q},\omega-\omega_1)$.

narrow band E_g^+, which has a width of $\Delta = 0.124$ eV, is equal to $N_g^+ N_{im}/\Delta \simeq 0.3\times 10^{23}$ $\mathrm{cm}^{-3}\mathrm{eV}^{-1}$.

When the D_m^+ and E_g^+ bands are taken into account, the Hamiltonian (1) can be reduced to the form (the spin index is omitted):

$$H=\sum_{\mathbf{k}} \xi_{\mathbf{k}} c_{\mathbf{k}}^{+} c_{\mathbf{k}} + \sum_{l} \xi_d f_l^{+} f_l + H_{ph}^{0} + \sum_{l,\mathbf{k},\mathbf{q}} (\kappa_{l\mathbf{k}\mathbf{q}}\, f_l^{+} c_{\mathbf{k}} + \mathrm{h.c.})\,\phi_{\mathbf{q}}$$

$$+ \sum_{\mathbf{k},\mathbf{q}} \lambda_{\mathbf{q}} c_{\mathbf{k}}^{+} c_{\mathbf{k}-\mathbf{q}} \phi_{\mathbf{q}}, \tag{3}$$

where $c_{\mathbf{k}}$ is the annihilation operator of an electron in the E_g^+ band state with energy $\xi_{\mathbf{k}}$; f_l is the annihilation operator of an electron in the D_m^+ band state; $\kappa_{l\mathbf{k}\mathbf{q}}$ and $\lambda_{\mathbf{q}}$ are the matrix elements for electron–phonon scattering; $\phi_{\mathbf{q}} = b_{\mathbf{q}} + b_{-\mathbf{q}}^{+}$; $b_{\mathbf{q}}$ is the annihilation operator of a phonon with wave vector $\mathbf{q}$; H_{ph}^{0} describes the unperturbed phonons. Here $\Sigma_{\mathbf{k}} = N_g^+ N_{im}$ and $\Sigma_l = N_m^+ N_{im}$.

From Eq. (3) one can easily obtain a system of eight equations for the Green's functions in the superconducting state. In Fig. 2 we only show the diagram equation for the anomalous Green's function $F^{+}_{-\mathbf{k}\mathbf{k}_1}(\omega)$. These diagrams use the conventional notation. It is interesting to note here that for the mechanism of hopping superconductivity the diagrams including the anomalous Green's functions $F^{+}_{l_1 l_2}(\omega)$ and $F^{+}_{l\mathbf{k}}(\omega)$ are important. For this reason the most commonly used approximation in terms of the diagonal Green's functions cannot be applied. Here, since we are restricting ourselves to this approximation, hopping superconductivity will not be considered. Using the representation of a given number of electrons, the system of equations is reduced to the form (at least at zero temperature):

$$G_{ll}(\omega) = (\omega - \xi_d - \Sigma_{ll}(\omega))^{-1}, \tag{4}$$

where the self-energy

$$\Sigma_{ll}(\omega)=i\sum_{\mathbf{kq}}\int\frac{d\omega_1}{2\pi}|\kappa_{\mathbf{k}l\mathbf{q}}|^2D(\mathbf{q},\omega-\omega_1)G_{\mathbf{kk}}(\omega_1), \tag{5}$$

$$(\omega-\xi_{\mathbf{k}}-\Sigma^{\mathrm{loc}}_{\mathbf{kk}}(\omega)-\Sigma^{\mathrm{ext}}_{\mathbf{kk}}(\omega))G_{\mathbf{kk}}(\omega)=1+\Delta(\mathbf{k},\omega)F^{+}_{-\mathbf{kk}}(\omega), \tag{6}$$

where the self-energies

$$\Sigma^{\mathrm{loc}}_{\mathbf{k}\backslash\mathbf{k}}(\omega)=i\sum_{l,\mathbf{q}}\int\frac{d\omega_1}{2\pi}|\kappa_{\mathbf{k}l\mathbf{q}}|^2D(\mathbf{q},\omega-\omega_1)G_{ll}(\omega_1), \tag{7}$$

and

$$\Sigma^{\mathrm{ext}}_{\mathbf{kk}}(\omega)=i\sum_{\mathbf{q}}\int\frac{d\omega_1}{2\pi}|\lambda_{\mathbf{q}}|^2D(\mathbf{q},\omega-\omega_1)G_{\mathbf{k-q},\mathbf{k-q}}(\omega_1), \tag{8}$$

$$(\omega+\xi_{\mathbf{k}}-2E_F+\Sigma^{\mathrm{loc}}_{\mathbf{kk}}(-\omega)+\Sigma^{\mathrm{ext}}_{\mathbf{kk}}(-\omega))F^{+}_{-\mathbf{kk}}(\omega)=1+\Delta^{+}(\mathbf{k},\omega)G_{\mathbf{kk}}(\omega). \tag{9}$$

Here the superconducting gap function is given by

$$\Delta^{+}(\mathbf{k},\omega)=-i\sum_{\mathbf{q}}\int\frac{d\omega_1}{2\pi}|\lambda_{\mathbf{q}}|^2D(\mathbf{q},\omega-\omega_1)F^{+}_{\mathbf{-k+q},\mathbf{k-q}}(\omega_1). \tag{10}$$

The system (4)–(10) should be supplemented by the equation for determination of the Fermi level, which can be written in the form:

$$\eta_g^{+}+\eta_m^{+}=-\frac{1}{\pi N_{im}}\int_{-\infty}^{E_F}d\omega\ \mathrm{Im}\left(\sum_{l}\ G_{ll}(\omega)+\sum_{\mathbf{k}}\ G_{\mathbf{kk}}(\omega)\right). \tag{11}$$

The self-energy (8) has the same form as in the Eliashberg equations obtained for pure metals. This term is important in the strong-coupling case and its role is understood. A distinction of the present model is that both localized and extended states exist at E_F. Moreover the total number of the localized states and their occupation are much greater than those for the extended states, as was shown above. In order to determine how the localized states influence the pair condensate, we henceforth take into account the self-energy (7) only.

In the calculations $\kappa_{\mathbf{k}l\mathbf{q}}$ is taken to be independent of $\mathbf{k}$ and $\mathbf{q}$. Using the unperturbed Green's function for phonons, one obtains:

$$(2\pi)^{-1}\sum_{\mathbf{q}}\ |\kappa_{\mathbf{k}l\mathbf{q}}|^2D(\mathbf{q},\omega-\omega_1)=-\frac{2\kappa^2_{\mathbf{k}l\mathbf{q}}}{(\theta_D a_0)^3}T(\omega-\omega_1), \tag{12}$$

where

$$T(\omega)=\theta_D^2+\omega^2\log\frac{|\theta_D^2-\omega^2|}{\omega^2}+i\pi\omega^2\Theta(\theta_D-|\omega|). \tag{13}$$

Here θ_D is the Debye temperature and a_0 is the crystal lattice parameter. On introduction of the effective constant λ_{eff}, Eq. (10) can be reduced to a BCS-type equation for the superconducting gap Δ_0:

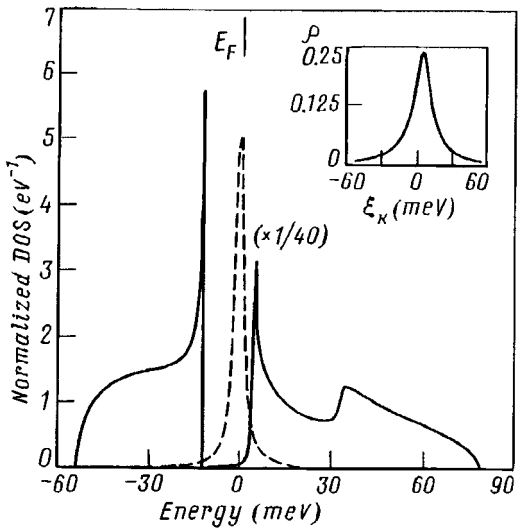

FIG. 3. The single-electron DOS for the superconducting state. The energy is reckoned from the E_F^0. The Fermi level $E_F=0.672$ meV. The solid curve is the impurity band E_g^+. The dashed curve is the impurity band D_m^+. The superconducting gap $\Delta_0=10$ meV. Inset: The energy distribution of the electron pairs. Parameter set: $\theta_D=33$ meV, $\lambda_{\text{eff}}=16.9$ eV Å^3, $\kappa_{\mathbf{kl}\mathbf{q}}^2 N_t/(\Theta_D^2 a_0^3)=0.47$.

$$\Delta^+ = -i\lambda_{\text{eff}} \sum_{\mathbf{k}} \int \frac{d\omega}{2\pi} F^+_{-\mathbf{k},\mathbf{k}}(\omega)\Theta(\theta_D - |\xi_{\mathbf{k}} - E_F|). \tag{14}$$

The self-consistency equations (4)–(7), (9), (11), and (14) for the superconducting state were solved by an iteration procedure.

The single-electron DOS per impurity atom for the superconducting state is shown in Fig. 3. Here $\Delta_0=10$ meV. In the superconducting gap region the density of single-electron extended states is equal to zero. The lower edge of the region is sharp, whereas the upper edge is smeared. The width of the region is about 14 meV, which is less than the $2\Delta_0$ corresponding to the ''big'' gap in the BCS model. Near the edges the DOS increases sharply, as expected.

The important result is that although single-electron extended states do not exist in the superconducting gap region, the peak of the localized states overlaps this region, as can be seen from Fig. 3. Thus the distribution of the localized states can obscure the superconducting gap in experimental observations. This can explain the observed qualitative distinction between the optical conductivity of $La_{1.85}Sr_{0.15}CuO_4$ and the conductivity of the classical BCS superconductor NbN.[15] A clear superconducting gap opens up in the conductivity of NbN at a photon energy $\leqslant 6$ meV. For $La_{1.85}Sr_{0.15}CuO_4$ the gap did not manifest itself up to a photon energy $\leqslant 3$ meV. In the present model, because the band D_m^+ of localized states is partially occupied and overlaps the superconducting gap, the optical conductivity at such low photon energies can be due to both hopping conductivity in the D_m^+ band and optical transitions from the localized states to the extended states above the upper edge of the E_g^+ band.

In conclusion we present data on the electron concentration in the superconducting state. The energy distribution of the electron pairs $\rho(\xi_{\mathbf{k}})$ is shown in the inset of Fig. 3. One can see that the distribution tends to 1/4 near E_F. We calculated the pair concentration $N_p = 2.3 \times 10^{20}$ cm^{-3}. From E_F and Eq. (11) we obtained the occupation number $\eta_m^+ = 0.396$ for the localized states $\eta_g^+ = 0.061$ for the extended states. The concentration of localized electrons $N_l = \eta_m^+ N_{im} = 1.188 \times 10^{22}$ cm^{-3}, and the electron concentration in the single-particle extended states $N_s = \eta_g^+ N_{im} - 2N_p = 1.38 \times 10^{21}$ cm^{-3}. Thus the relation $N_p \ll N_s \ll N_l$ shows the unusual character of the superconducting state.

[1] S. Uchida, T. Ido, H. Takagi *et al.*, Phys. Rev. B **43**, 7942 (1991).
[2] J. Orenstein, G. A. Thomas, A. J. Millis *et al.*, Phys. Rev. B **42**, 6342 (1990).
[3] G. A. Thomas, D. H. Rapkine, S. L. Cooper *et al.*, Phys. Rev. B **45**, 2474 (1992).
[4] S. L. Cooper, D. Reznik, A. Kotz *et al.*, Phys. Rev. B **47**, 8233 (1993).
[5] R. O. Anderson, R. Claessen, J. W. Allen *et al.*, Phys. Rev. Lett. **70**, 3163 (1993).
[6] E. Dagotto, Rev. Mod. Phys. **66**, 673 (1994).
[7] Y. Fukuzumi, K. Mizuhashi, K. Takenaka *et al.*, Phys. Rev. Lett. **76**, 684 (1996).
[8] P. Monthoux and D. Pines, Phys. Rev. Lett. **69**, 961 (1992).
[9] C. H. Pao and N. E. Bickers, Phys. Rev. Lett. **72**, 1870 (1994).
[10] P. Fulde and P. Horsch, Europhys. News **24**, 73 (1993).
[11] J. Hirsch, Physica B **199–200**, 366 (1994).
[12] D. Dessau, Z.-X. Shen, D. M. King *et al.*, Phys. Rev. Lett. **71**, 2781 (1993).
[13] A. I. Agafonov and E. A. Manykin, Phys. Rev. B **52**, 14571 (1995).
[14] A. I. Agafonov and E. A. Manykin, Zh. Eksp. Teor. Fiz. **109**, 1405 (1996) [JETP **82**, 758 (1996)].
[15] H. S. Somal, B. J. Feenstra, J. Schützmann *et al.*, Phys. Rev. Lett. **76**, 1525 (1996).

Published in English in the original Russian journal. Edited by Steve Torstveit.

Self-localized carrier states in disordered ferroelectrics

V. A. Stephanovich
Institute of Semiconductor Physics, Ukrainian National Academy of Sciences, 252028 Kiev, Ukraine

(Submitted 15 January 1997)
Pis'ma Zh. Éksp. Teor. Fiz. **65**, No. 5, 425–429 (10 March 1997)

A theory of self-localized states of free carriers near polarization fluctuations (fluctuons) in disordered ferroelectrics is developed. Calculations are carried out for the model disordered ferroelectric $K_{1-x}Li_xTaO_3$ ($x \ll 0.05$). The basic characteristics of the fluctuon — the energy and radius of the fluctuon state — are calculated as functions of the impurity dipole concentration and temperature. The theory predicts the appearence of stable fluctuon states in both the mixed ferroelectric–dipole-glass phase (a dipole glass is the electric analog of a spin glass) and the dipole-glass state of disordered ferroelectrics. The possible role of fluctuons in kinetic phenomena such as conductivity in these substances is discussed. © *1997 American Institute of Physics.* [S0021-3640(97)01305-4]

PACS numbers: 71.38.+i, 77.80.−e

Self-localized states of the charge carrier (electon, hole, or sometimes exciton), namely polarons[1] and fluctuons,[2] play an important role in the physics of insulators and semiconductors. While a great deal of scientific work has been devoted to investigations of polaron states (see, e.g., Refs. 1,4), the available information about fluctuon states is very limited. Since a fluctuon is known to be a carrier trapped near a polarization fluctuation,[2,3] the carrier can interact with fluctuations induced by both longitudinal and transverse phonons. The latter are especially important in ferroelectrics for which the spontaneous polarization is due to transverse phonons. A theory of fluctuon states in ordinary ferroelectrics was developed in Ref. 5, where the domain walls were considered as the main source of polarization fluctuations in the ferroelectric phase. However, the presence of short-range polar order in the dipole-glass state or a mixture of short- and long-range polar order in the mixed ferroglass phase is peculiar to disordered ferroelectrics (see, e.g., Ref. 6 and the references cited therein). In such a system polarization fluctuations are a basic characteristic of those phases. In view of the existence of a fundamental electric current in many disordered ferroelectrics,[7–9] the appearence of fluctuon states in these systems seems to be very probable. In the present work we propose a theory of self-localized (fluctuon) states of the charge carrier in disordered ferroelectrics with random electric dipoles which induce concentrational phase transitions of the dipole-glass–mixed-phase–ferroelectric type. The calculations are carried out for the model disordered ferroelectric $K_{1-x}Li_xTaO_3$ (KLT) ($x \ll 0.05$), the impurity Li^+ ions being electric dipoles with random site and orientation.

The disordered ferroelectric KLT is known to have an ordinary ferroelectric phase

transition for $x>0.05$ and dipole-glass–mixed-ferroglass phase transitions for $x\leqslant 0.05$ at low temperatures ($T\ll 50$ K).[10] The latter two phases correspond to $nr_c^3\leqslant 1$ ($n=x/a^3$, and x, r_c, and a are the dipole concentration and the host lattice correlation radius and lattice constant, respectively). It is known[10] that in this concentration interval the effects of disorder are quite strong (at large Li concentrations we simply have the case of the ordered ferroelectric $LiTaO_3$), so that spatial nonuniformity of the polarization should be taken into account.

The fluctuon energy functional, allowing for the interaction of the charge carrier with the polarization **P** in the effective mass approximation for strong coupling of the carrier to the polarization, can be written as in Ref. 1:

$$W=\frac{\hbar^2}{2m^*}\int |(\nabla\Psi)^2|d^3r-\int \mathbf{P}\cdot\mathbf{D}d^3r+\int f d^3r\,, \tag{1}$$

where f is the free-energy density of the disordered ferroelectric, m^* and $\Psi(r)$ and **D** are the effective mass and wave function of the carrier and the electric displacement produced by the carrier, respectively. The last is given by

$$\mathbf{D}(\mathbf{r})=-e\int |\Psi(\mathbf{r}_1)|^2\frac{(\mathbf{r}-\mathbf{r}_1)}{|\mathbf{r}-\mathbf{r}_1|^3}\,d^3\mathbf{r}_1\,. \tag{2}$$

The free energy f was calculated recently[11] for the case of 8-orientation dipoles and can be written in the form

$$f=-\frac{4\pi}{c}\left[\frac{1}{2}P^2+\frac{d^{*2}}{V_0^2\beta}\int_0^\infty\frac{(1-\cos(\rho P_1E_0(\rho)))\exp(F_1(\rho))d\rho}{\rho E_0(\rho)\sinh\left(\dfrac{\pi\rho}{2\beta}\right)}\right], \tag{3}$$

$$c=\frac{1}{\varepsilon_\infty}-\frac{1}{\varepsilon_0},$$

where $d^*=\gamma d\varepsilon_0/3$ is the effective dipole moment of the impurity, γ is the Lorentz factor, ε_0 and ε_∞ are the low- and high-frequency dielectric permittivities of the host lattice, $E_0(\rho)$ is the average electric field induced by the dipoles, $F_1(\rho)$ is the width of the distribution function of the random fields, calculated in Ref. 11, V_0 is the unit cell volume, and $\beta\equiv 1/kT$. Note that the factor c appears in (3) because only the inertial part of the polarization contributes to the energy of the self-localized carrier state.

Equation (1) in reference to (2) and (3) determines the properties of the fluctuon. Independent variation of (1) with respect to Ψ and P gives the following equations for the fluctuon structure:

$$-D[\Psi]+\frac{4\pi}{c}\left[P-\frac{d^*}{V_0\beta}\int_0^\infty\frac{\sin(\rho P_1E_0(\rho))\exp(F_1(\rho))d\rho}{\sinh\left(\dfrac{\pi\rho}{2\beta}\right)}\right]=0, \tag{4a}$$

$$-\frac{\hbar^2}{2m^*}\nabla^2\Psi-eP(\Psi)\int\Psi(\mathbf{r}_1)\frac{(z-z_1)}{|\mathbf{r}-\mathbf{r}_1|^3}d^3\mathbf{r}_1=0, \tag{4b}$$

$$P_1 \equiv \frac{PV_0}{d^*}.$$

System (4a), (4b) should be solved under the normalization condition

$$\int |\Psi|^2 d^3r = 1. \tag{4c}$$

Equation (4a) gives the relation between D and P. It therefore determines the dependence of the electric field of the carriers on the concentration of impurity dipoles, the characteristics of the host lattice, and the parameters of the distribution function of the random fields of the impurity dipoles (the latter were used in the calculation of the free energy 3; see Ref. 11). We must emphasize that in the case of a ferroelectric phase induced by electric dipoles ($nr_c^3 \gg 1$) the integral in Eq. (4a) can be calculated in the mean field approximation, which is valid at large impurity concentrations (see Refs. 10, 11), and turns out to equal βP_1. It is easy to see that the expression in the brackets in Eq. (4a) equals zero, so that $D=0$ and the fluctuon does not exist. This is because we did not take into account the domain walls, which have been shown[5] to be the main source of polarization fluctuations in ordinary ferroelectrics. Note that the system (4a), (4b) can also be applied to investigation of the influence of charge carriers on the polarization of disordered ferroelectrics. This influence has been shown to be important in many disordered ferroelectrics.[7–9] Since the system (4a), (4b) is rather complicated, we were not able to find its analytical solution. We shall therefore study the fluctuon properties by a direct variational method. To do this, we must substitute (4a) into (1) in reference to (2) and minimize the resulting expression subject to condition (4c) with some trial function Ψ.

To obtain the energy of fluctuon ground state we shall choose the one-parameter trial function which gives the lowest energy as compared to any other one-parameter trial function, in a form similar to Ref. 1:

$$\Psi = \frac{1}{\sqrt{7\pi} r_0^{3/2}} \left(1 + \frac{r}{r_0}\right) \exp\left(-\frac{r}{r_0}\right), \tag{5}$$

where r_0 is a variational parameter. Minimization of functional (1) in reference to relations (4a) and (2) and with the parameters values for KLT leads to the following form for the fluctuon energy:

$$W_\Psi = \frac{3\hbar^2}{14 m^* r_0} - \frac{0.428332 e^2 c}{6\Phi(\nu,\tau) r_0}, \tag{6}$$

$$\Phi(\nu,\tau) = \left(\frac{dP_1}{dD}\right)_{P_1 = P_0}, \tag{7}$$

where P_0 is the equilibrium homogeneous polarization ($D(P_0)=0$), $\nu \equiv nr_c^3$, and $\tau = T/T_{c\mathrm{mf}}$ ($T_{c\mathrm{mf}}$ is the ferroelectric phase transition temperature calculated in the mean field approximation).

A calculation of $\Phi(\nu,\tau)$ in reference to relation (4a) shows that the dependence of P_1 on D has a hysteretic character: on the $P_1(D)$ curve there are parts with

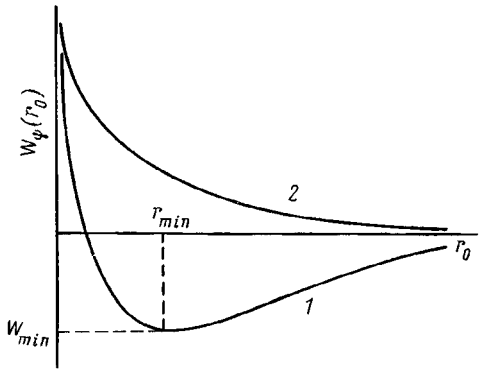

FIG. 1. Energy of fluctuon ground state as a function of the variational parameter r_0 for stable (1) and unstable (2) states of the fluctuon.

$dP_1/dD \ll 0$ and parts with $dP_1/dD > 0$. It follows from Eqs. (6) and (7) that the parts where $dP_1/dD \ll 0$ and the parts where $dP_1/dD > 0$ can lead to the maximum and minimum fluctuon energy, respectively. In the latter case the fluctuon is stable, and its energy and radius of localization are as follows:

$$r_{\min} = \frac{6\hbar^2 \Phi(\nu,\tau)}{m^* e^2 c}, \quad W_{\min} = -0.0054946 \frac{m^* e^4 c^2}{\hbar^2 \Phi^2(\nu,\tau)}. \tag{8}$$

These parameters are depicted in Fig. 1 along with the general form of the dependence of the fluctuon energy on r_0 as calculated on the basis of Eqs. (6) and (7) in reference to relation (4a). It is seen from relation (4a) that the dependence of the dimensionless radius of the fluctuon state on the dipole concentration and temperature is determined by $\Phi(\nu,\tau)$. The temperature dependence of $\Phi(\nu,\tau)$ is shown in Fig. 2 for parameters which correspond to the dipole glass ($\nu \ll \nu_{cr}$) and to the mixed phase ($1 \geqslant \nu > \nu_{cr}$) with coexistence of short- and long-range polar order, i.e., with the onset of spontaneous polarization. It is seen from Fig. 2 that in the latter case the localization radius has a temperature dependence similar to that of the spontaneous polarization. This is truly a manifestation of the fluctuon nature of the carrier localization in disordered ferroelectrics. Indeed, the increase of the spontaneous polarization with decreasing temperature means that its fluctuations are inhibited, which in turn decreases the fluctuon nucleation probability. This behavior also follows from Eq. (8) and Fig. 2, because $|W_{\min}| \sim 1/r_{\min}^2$, i.e., the localization radius growth decreases the depth of the fluctuon energy minimum. Points at which $\Phi(\nu,\tau) = 0$ correspond to the onset of spontaneous polarization, i.e., to the phase transition temperature.[11]

At these points $r_{\min} \to 0$ while $W_{\min} \to -\infty$. This means that the fluctuon collapses at phase transition points. At $T > T_c$ (paraelectric phase) $r_{\min} \neq 0$ and the localization radius is finite on account of polarization fluctuations induced by the random electric fields of the impurity dipoles. Fluctuons can also be stable in the dipole-glass state, where polar clusters of short-range order can induce strong polarization fluctuations (see Fig. 2).

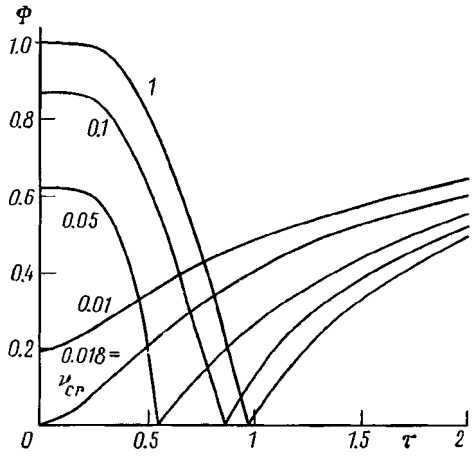

FIG. 2. Dimensionless localization radius $\Phi(\nu,\tau)$ versus the dimensionless temperature $\tau=T/T_{\mathrm{cmf}}$. The curves are labeled with the values of $\nu=nr_c^3$.

The calculations have shown that disordered ferroelectrics are suitable media for revealing and investigating self-localized fluctuon states of carriers. It can be supposed that the fluctuon contribution to the electric current (and photocurrent, which was observed recently in KLT)[9] might be substantial. This contribution depends on the position of the fluctuon local level in the ferroelectric band gap. To shed light on this question, let us make some numerical estimates of $r_{\min}$ and $W_{\min}$. We have from Eq. (8)

$$r_{\min}=3.18\,\frac{\Phi}{\alpha c}(\text{Å}),\quad W_{\min}=-0.16\,\frac{\alpha c^2}{\Phi^2}(\text{eV}), \tag{9}$$

where $\alpha=m^*/m_0$ (m_0 is the free electron mass). For validity of the effective mass approximation we must have $r_{\min}\geqslant(3\text{–}4)a$ ($a\simeq 4$ Å for $KTaO_3$). Putting $r_{\min}=3a$ in (9), we have $\Phi/\alpha c\simeq 3.8$, which gives

$$W_{\min}\simeq-\frac{0.01}{\alpha}(\text{eV}). \tag{10}$$

Therefore $|W_{\min}|\leqslant 0.01$ eV, i.e., fluctuons produce very shallow local levels in the lattice band gap near the valence band bottom for electrons. Note that the observed temperature anomalies of the photocurrent in KLT have been explained on the assumption that a very shallow local level exists near the valence band ceiling.[9] This level could be of a fluctuon nature. More-precise estimates of the fluctuon characteristics in disordered ferroelectrics and of their contribution to the conductivity and other kinetic phenomena require additional experimental and theoretical investigations.

[1] S. I. Pekar, *Collected Papers* [in Russian] (Kiev, Naukova Dumka, 1983).
[2] M. A. Krivoglaz, Usp. Fiz. Nauk **111**, 617 (1974) [Sov. Phys. Uspekhi **16**, 856 (1974)].
[3] M. I. Klinger, Usp. Fiz. Nauk **146**, 105 (1985) [Sov. Phys. Uspekhi **28**, 391 (1985)].
[4] Yu. A. Firsov (ed.), *Polarons* [in Russian], (Moscow, Nauka, 1975).

[5] B. V. Egorov, I. B. Egorova, M. A. Krivoglaz, Fiz. Tverd. Tela (Leningrad) **26**, 3112 (1984) [Sov. Phys. Solid State **26**, 1874 (1984)].
[6] M. D. Glinchuk, R. Farhi, J. Phys. Condens. Matter. **8**, 6985 (1996).
[7] A. I. Lebedev, I. A. Sluchinskaya, Fiz. Tverd. Tela (St. Petersburg) **35**, 629 (1993) [Sov. Phys. Solid State **35**, 321 (1993)].
[8] K. Woicik, J. Blaszczak, J. Handerek, Ferroelectrics **70**, 3946 (1986),
[9] R. S. Klein, G. E. Kugel, M. D. Glinchuk, R. O. Kuzian, I. V. Kondakova, Phys. Rev. B **50**, 9721 (1994).
[10] B. E. Vugmeister, M. D. Glinchuk, Rev. Mod. Phys. **82**, 993 (1990).
[11] V. A. Stephanovich, Ferroelectrics **80**, 4936 (1996).

Published in English in the original Russian journal. Edited by Steve Torstveit.

The possibility of a very large magnetoresistance in half-metallic oxide systems

A. M. Bratkovsky
Hewlett-Packard Laboratories, Palo Alto, California 94304-1392

(Submitted 22 January 1997)
Pis'ma Zh. Éksp. Teor. Fiz. **65**, No. 5, 430–435 (10 March 1997)

The tunnel magnetoresistance (TMR) is analyzed for ferromagnet–insulator–ferromagnet junctions, including novel half-metallic systems with 100% spin polarization. Direct tunneling is compared with the impurity-assisted and resonant TMR. Direct tunneling in iron-group systems leads to about a 20% change in resistance, as observed experimentally. Impurity-assisted tunneling decreases the TMR to 4% with Fe-based electrodes. A resonant tunnel diode structure would give a TMR of about 8%. The model applies qualitatively to half-metallics, where the change in resistance in the absence of spin flips may be arbitrarily large and even in the case of imperfect magnetic configurations the resistance change can be several thousand percent. Examples of half-metallic ferromagnetic systems are CrO_2/TiO_2 and CrO_2/RuO_2. A discussion of their properties is presented. © *1997 American Institute of Physics.* [S0021-3640(97)01405-9]

PACS numbers: 73.40.Gk, 73.61.−r, 75.70.Pa

Tunneling of spin-polarized electrons is of fundamental interest and is potentially applicable to magnetic sensors and memory devices.[1] In a search of systems with maximal performance it is important to consider the generic properties affecting the magnetoresistance and other characteristics. A standard model for spin tunneling has been formulated by Julliere[2] and further developed by Stearns[3] and Slonczewski.[4] This model is expected to work rather well for iron-, cobalt-, and nickel-based metals, according to Refs. 3 and 5. However, important aspects have not been taken into account there, such as an impurity scattering and a reduced effective mass of carriers inside the barrier. Both issues have important implications for magnetoresistance and will be considered here, along with proposed novel half-metallic systems which in principle should show the ultimate performance.

We shall describe electrons in ferromagnet–insulating-barrier–ferromagnet (f–b–f) systems by the Schrödinger equation[4] $(\mathcal{H}_0-\mathbf{h}\cdot\hat{\sigma})\psi=E\psi$, where $\mathcal{H}_0=-(\hbar^2/2m_\alpha)\nabla^2+U_\alpha$ is the single-particle Hamiltonian, with potential energy $U(\mathbf{r})$ and exchange energy $\mathbf{h}(\mathbf{r})$ ($=0$ inside the barrier), and $\hat{\sigma}$ stands for the Pauli matrices; the index $\alpha=1, 2, 3$ labels quantities pertaining to the left terminal, barrier, and right terminal, respectively. In a standard formalism the tunnel current is given by some integral of a transmission probability $T=\Sigma_{\sigma\sigma'}T_{\sigma\sigma'}$, which has a particularly simple form for a square barrier and

collinear [parallel (P) or antiparallel (AP)] moments on the electrodes.[6] Here σ (σ') stands for the spin index of the initial (final) state.

Taking into account the misalignment of the spin moments in ferromagnetic terminals (given by the angle θ between them), we obtain for the conductance of a square barrier the following corrected Slonczewski's formula[4] to leading order in $\exp(-\kappa w)$, assuming for the moment, that the electrodes are equivalent,

$$G = G_{\mathrm{fbf}}(1 + P_{\mathrm{fb}}^2 \cos(\theta)),$$

$$G_{\mathrm{fbf}} = \frac{e^2}{\pi\hbar}\,\frac{\kappa}{\pi w}\left[\frac{\kappa(k_\uparrow + k_\downarrow)(\kappa^2 + m_2^2 k_\uparrow k_\downarrow)}{(\kappa^2 + m_2^2 k_\uparrow^2)(\kappa^2 + m_2^2 k_\downarrow^2)}\right]^2 e^{-2\kappa w}, \tag{1}$$

$$P_{\mathrm{fb}} = \frac{k_\uparrow - k_\downarrow}{k_\uparrow + k_\downarrow}\,\frac{\kappa^2 - m_2^2 k_\uparrow k_\downarrow}{\kappa^2 + m_2^2 k_\uparrow k_\downarrow},$$

where G is the surface conductance per unit area, P_{fb} is the effective polarization of the electrode, $\kappa = [2m_2(U_0 - E)/\hbar^2]^{1/2}$, and U_0 is the top of the barrier.[a)] By taking a typical value of $G = 4$–5 S/cm^2 (Ref. 5), $k_\uparrow = 1.09$ Å^{-1}, $k_\downarrow = 0.42$ Å^{-1}, $m_1 \approx 1$ (for itinerant d electrons in Fe; Ref. 3) and a typical barrier height for Al_2O_3 (measured from the Fermi level μ) $\phi = U_0 - \mu = 3$ eV, at a thickness $w \approx 20$ Å, one arrives at the following estimate for the effective mass in the barrier: $m_2 \approx 0.4$.[b)] A reduced band mass for the oxide barrier is a natural consequence of the large width of the s–p bands in the insulator. These values give $P_{\mathrm{Fe}} = 0.28$, in fair agreement with the experimental value 0.4 (Refs. 1 and 5; $P_{\mathrm{Fe}} < 0$ if the mass correction is neglected). The existing formalism and parameters are sufficient for our present qualitative and even semi-quantitative analysis.

We define the magnetoresistance as the relative change in contact conductance upon a change of the mutual orientation of the spins from parallel P (G^{P} for $\theta = 0$) to antiparallel AP (G^{AP} for $\theta = 180°$), as

$$MR = (G^{\mathrm{P}} - G^{\mathrm{AP}})/G^{\mathrm{AP}} = 2PP'/(1 - PP'), \tag{2}$$

which differs from the standard definition[2,1] by the minus sign in the denominator.

The most striking feature of Eqs. (1) and (2) is that MR tends to infinity for vanishing $k_\downarrow$, i.e., when the electrodes are made of a 100% spin-polarized material ($P = P' = 1$) because of a gap in the density of states for minority carriers up to their conduction band minimum $E_{CB\downarrow}$. Although such half-metallic behavior is rare, some materials do possess this amazing property, most interestingly the oxides CrO_2 and Fe_3O_4 (Ref. 7). These oxides are most interesting for future applications in combination with matching materials, as we shall illustrate below.

A more accurate analysis of the I–V curve requires a numerical calculation for arbitrary biases and inclusion of image forces[6] (Fig. 1). The top panel in Fig. 1 shows I–V curves for an iron-based f–b–f junction with the parameters given above. The value of TMR is about 20% at low biases and steadily decreases with increased bias. In a half-metallic case ($k_\downarrow = 0$, Fig. 1, middle panel, where a threshold $eV_c = E_{CB\downarrow} - \mu = 0.3$ eV has been assumed) we obtain *zero* conductance G^{AP} in the AP configuration at biases lower than V_c. It is easy to see that above this threshold, $G^{\mathrm{AP}} \propto (V - V_c)^{5/2}$ at temperatures much smaller than eV_c. Thus, for $|V| < V_c$ in the AP geometry one has $MR = \infty$. In

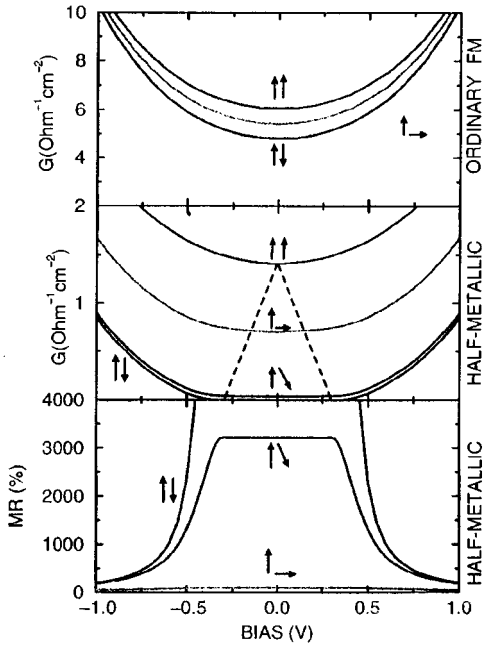

FIG. 1. Conductance and magnetoresistance of tunnel junctions versus bias at 300 K with multiple image potential and exact transmission coefficients. Top panel: conventional (Fe-based) tunnel junction (for parameters see text). Middle panel: half-metallic electrodes. Bottom panel: magnetoresistance for the half-metallic electrodes. The dashed line shows schematically a region where the transport is governed by a gap in the minority spin states. Imperfect antiparallel alignment ($\theta=160°$) is marked as $\uparrow\searrow$.

practice there are several effects that reduce this MR to some finite value, notably an imperfect AP alignment of moments in the electrodes. However, from Fig. 2 we see that even at a 20° deviation from the AP configuration the value of MR exceeds 3000% in the interval $|V|<V_c$, and this is indeed a very large value.

An important aspect of spin-tunneling is the effect of tunneling through defect states in the (amorphous) oxide barrier. Since the contacts under consideration are typically short, their I–V curve and MR should be very sensitive to defect resonant states in the barrier with energies close to the chemical potential, forming ''channels'' with nearly periodic positions of the impurities.[8] Generally, channels with one impurity (most likely to dominate in thin barriers) would result in monotonic behavior of the I–V curve, whereas channels with two or more impurities would produce intervals with negative differential conductance, as was shown by Larkin and Matveev.[9] We shall estimate the spin conductance in this model. Impurity-assisted spin tunneling at zero temperature [the general case would require integration with the Fermi factors] can be written in the form[9]

$$G_\sigma=\frac{2e^2}{\pi\hbar}\sum_i \frac{\Gamma_{l\sigma}\Gamma_{r\sigma}}{(E_i-\mu)^2+\Gamma^2}, \tag{3}$$

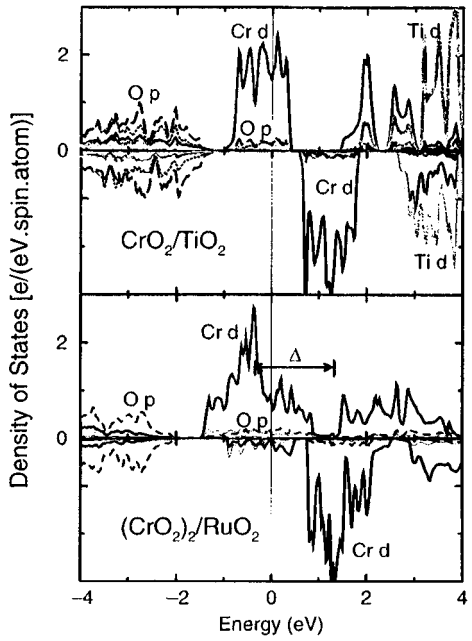

FIG. 2. Density of states of CrO_2/TiO_2 (top panel) and $(CrO_2)_2/RuO_2$ (bottom panel) half-metallic multilayers. Δ indicates a spin splitting of the Cr d band near E_F (schematic).

where $\Gamma_\sigma=\Gamma_{l\sigma}+\Gamma_{r\sigma}$ is the total width of a resonance given by a sum of the partial widths Γ_l (Γ_r) corresponding to electron tunneling from the impurity state at the energy E_i to the left (right) terminal. For a rectangular barrier we have

$$\Gamma_{l\sigma}=\epsilon_i \frac{2m_2 k_\sigma}{\kappa^2+m_2^2 k_\sigma^2} \frac{e^{-\kappa(w+2z_i)}}{\kappa(\frac{1}{2}w+z_i)}, \tag{4}$$

where z_i is the coordinate of the impurity with respect to the center of the barrier (Γ_r is obtained from the previous expression by substituting $z_i \rightarrow -z_i$ and taking the final spin state into account), and $\epsilon_i=\hbar^2\kappa^2/(2m_2)$. The conductance has a sharp maximum ($=e^2/(2\pi\hbar)$) when $\mu=E_i$ and $\Gamma_l=\Gamma_r$, i.e., for the symmetric position of the impurity in the barrier. Following Larkin and Matveev, we assume that we have ν defect levels per unit volume and unit energy interval in the barrier. Averaging over impurities, we obtain the following formula (which is similar to (1) and (2)) for impurity-assisted conductance to leading order in $\exp(-\kappa w)$:

$$MR_1=2\Pi_{\mathrm{fb}}\Pi_{\mathrm{f'b}}/(1-\Pi_{\mathrm{fb}}\Pi_{\mathrm{f'b}}), \tag{5}$$

where $\Pi_{\mathrm{fb}}=(r_\uparrow-r_\downarrow)/(r_\uparrow+r_\downarrow)$, with $r_\sigma=[m_2\kappa k_\sigma/(\kappa^2+m_2^2k_\sigma^2)]^{1/2}$. One may call Π_{fb} a ''polarization'' of the impurity channel. The impurity-assisted conductance per unit area is approximately $g_{\mathrm{fbf}}=e^2/(\pi\hbar)N_1$, where $N_1=\pi^2\nu\Gamma_1/\kappa$ is the effective number of one-impurity channels per unit area, and $\Gamma_1=\epsilon_i(r_\uparrow+r_\downarrow)^2\exp(-\kappa w)/(\kappa w)$.

Comparing the direct (3) and impurity-assisted contributions to the conductance, we see that the latter dominates when the impurity density of states

$\nu \sim (\kappa/\pi)^3 \epsilon_i^{-1} \exp(-\kappa w)$, and in our example a crossover takes place at $\nu \sim 10^{-7}$ $\text{Å}^{-3} \cdot \text{eV}^{-1}$. When resonant transmission dominates, the magnetoresistance will be just 4% in the case of Fe. With standard ferromagnetic electrodes, the conductance is enhanced but the magnetoresistance is reduced in comparison with the clean limit. With further increase of the defect density and/or the barrier width, the channels with two and more impurities will become more effective, as has been mentioned above.[9]

It is interesting to consider a resonant tunnel diode (RTD) type of structure with, for example, an ultrathin nonmagnetic layer placed between two oxide barrier layers, producing a resonant level at some energy E_r. The only difference from the previous discussion is the effectively 1D character of the transport in RTD in comparison with 3D impurity-assisted transport. However, all basic expressions remain practically the same, and the estimated magnetoresistance is:

$$MR_{\text{RTD}} = [(r_\uparrow^2 - r_\downarrow^2)/(2 r_\uparrow r_\downarrow)]^2, \tag{6}$$

which is 8% for Fe electrodes. We see that the presence of random impurity levels or a single resonant level reduces the value of the magnetoresistance as compared with direct tunneling.

It is very important that *in the case of half-metallics* one has $r_\downarrow = 0$, $\Pi_{\text{fb}} = 1$, and even with an imperfect barrier the magnetoresistance can, at least in principle, reach any value, limited only by spin-flip processes in the barrier/interface and/or misalignment of moments in the half-metallic ferromagnetic electrodes. This should combine a very large magnetoresistance with enhanced conductance in tunnel-MR junctions. Comparing with conventional systems (e.g., FeNi electrodes), we see that resonant tunneling significantly reduces the tunnel MR by itself, so that the possibility of improving the conductance and still having a very large magnetoresistance resides primarily with half-metallics.

We shall finish with a couple of examples of novel systems with half-metallic behavior, CrO_2/TiO_2 and CrO_2/RuO_2 (Fig. 2). They are based on half-metallic CrO_2 and all species have the rutile structure type with almost perfect lattice matching, which should yield a good interface and should help in keeping the system at the desired stoichiometry. TiO_2 and RuO_2 are used as the barrier/spacer oxides. The half-metallic behavior of the corresponding multilayer systems is demonstrated by the band structures calculated within the linear muffin-tin orbitals method (LMTO) in a supercell geometry with [001] growth direction and periodic boundary conditions. The present conclusions should also apply to single f–b–f junctions. The calculations show that CrO_2/TiO_2 is a perfect half-metallic, whereas $(CrO_2)_2/RuO_2$ is a weak half-metallic, since there is some small minority DOS around E_F (Fig. 2). In comparison, there are only states in the majority spin band at the Fermi level in CrO_2/TiO_2 (hence an exact *integer* value of the magnetic moment in the unit cell ($=2\mu_B$/Cr in CrO_2/TiO_2).

The electronic structure of CrO_2/TiO_2 shows a half-metallic gap which is 2.6 eV wide and extends on both sides of the Fermi level, where there is a gap either in the minority *or* majority spin band. Thus, a huge magnetoresistance should in principle be seen not only for electrons at the Fermi level biased up to 0.5 eV, but also for *hot* electrons. We note that states at the Fermi level are a mixture of Cr(d) and O($2p$) states, so that the p–d interaction within the first coordination shell produces a strong hybrid-

ization gap, and the Stoner spin splitting moves the Fermi level right into the gap for minority carriers (Fig. 2).

An important difference between the two spacer oxides is that TiO_2 is an insulator whereas RuO_2 is a good metallic conductor. Thus, the former system can be used in a tunnel junction, whereas the latter will form a metallic multilayer. In the latter case the physics of conduction is different from tunneling, but the effect of vanishing phase volume for transmitted states still works when current is passed through such a system *perpendicular to planes*. For the P orientation of the moments on the electrodes, CrO_2/RuO_2 would have normal metallic conduction, whereas in the AP orientation we expect it to have a semiconducting type of transport, with a crossover between the two regimes. One interesting possibility is to make a spin-valve transistor[10] and check the effect in a hot-electron region. CrO_2/TiO_2 seems to a be a natural candidate to check the present predictions about half-metallic behavior and for a possible record tunnel magnetoresistance. An important advantage of these systems is an almost perfect lattice match at the oxide interfaces. The absence of such a match of the conventional Al_2O_3 barrier with Heusler half-metallics (NiMnSb and PtMnSb) may have been among other reasons for their unimpressive performance in that case.[11]

By using all-oxide half-metallic systems, as the present examples show, one may bypass many materials issues. Then the main concerns for achieving a very large magnetoresistance will be spin-flip centers, magnon-assisted events, and imperfect alignment of moments. As to conventional tunnel junctions, the present results show that the presence of defect states in the barrier, or a resonant state like that in a resonant tunnel diode type of structure, reduces their magnetoresistance by severalfold but may dramatically increase the current through the structure.

I am grateful to R. S. Williams, G. S. Lee, C. Morehouse, J. Brug, T. Anthony, and J. Nickel for many valuable discussions.

[a)]For unlike electrodes G_{fbf} must be replaced by $G_{\mathrm{fbf}'}$ and $P_{\mathrm{fb}}^2 \to P_{\mathrm{fb}}P_{\mathrm{f}'\mathrm{b}}$ by substitutions $k_\uparrow \to k'_\uparrow$ and $k_\downarrow \to k'_\downarrow$. For the case of different masses $k_\sigma \to k_\sigma/m_\sigma$.

[b)]An even smaller value $m_2 = 0.2$ has been used by Q. Q. Shu and W. G. Ma for Al–Al_2O_3–metal junctions [Appl. Phys. Lett. **61**, 2542 (1992)].

[1] R. Meservey and P. M. Tedrow, Phys. Rep. **238**, 173 (1994).
[2] M. Julliere, Phys. Lett. A **54**, 225 (1975).
[3] M. B. Stearns, J. Magn. Magn. Mater. **5**, 167 (1977).
[4] J. C. Slonczewksi, Phys. Rev. B **39**, 6995 (1989).
[5] J. S. Moodera *et al.*, Phys. Rev. Lett. **74**, 3273 (1995); J. Appl. Phys. **79**, 4724 (1996); T. Miyazaki and N. Tezuka, J. Appl. Phys. **79**, 6262 (1996).
[6] C. B. Duke, *Tunneling in Solids* (Academic Press, New York, 1969); W. A. Harrison, Phys. Rev. **123**, 85 (1961).
[7] V. Y. Irkhin and M. I. Katsnelson, Usp. Fiz. Nauk **164**, 705 (1994) [Phys. Uspekhi **37**, 659 (1994)].
[8] I. M. Lifshitz and V. Ya. Kirpichenkov, Zh. Éksp. Teor. Fiz. **77**, 989 (1979) [Sov. Phys. JETP **50**, 499 (1979)].
[9] A. I. Larkin and K. A. Matveev, Zh. Éksp. Teor. Fiz. **93**, 1030 (1987) [Sov. Phys. JETP **66**, 580 (1987)].
[10] D. J. Monsma *et al.*, Phys. Rev. Lett. **74**, 5260 (1995).
[11] C. T. Tanaka and J. S. Moodera, J. Appl. Phys. **79**, 6265 (1996).

Published in English in the original Russian journal. Edited by Steve Torstveit.

Production of coherent states of excitons in semiconductors by means of the recombination of free carriers

A. N. Oraevskiĭ[a)]
P. N. Lebedev Physics Institute, 117924 Moscow, Russia

(Submitted 5 February 1997)
Pis'ma Zh. Éksp. Teor. Fiz. **65**, No. 5, 436–440 (10 March 1997)

It is shown that the modern experimental techniques make it possible to produce a coherent Bose condensate of excitons in semiconductors by the direct recombination of electrons from the conduction band and holes from the valence band. © *1997 American Institute of Physics.* [S0021-3640(97)01505-3]

PACS numbers: 71.35.Lk, 05.30.Jp

The generation of coherent states of an electromagnetic field is a well-mastered process in laser technology. A more exotic process is the production of coherent states of Bose particles with nonzero rest mass. The precipitation of particles into a Bose condensate is not sufficient to obtain a coherent state. For example, in an ''underexcited'' laser photons can accumulate in one cavity mode on account of *spontaneous* transitions, but such a state of the electromagnetic field will not be coherent. A coherent state of the electromagnetic field in a laser is produced on account of *stimulated* transitions with the self-excitation condition being satisfied. Analogous conditions must also be produced in order to obtain a coherent state of any Bose particles. In Ref. 1 it is shown that for a superconductor at temperatures below the critical temperature the condition for induced production of Cooper pairs is automatically satisfied, so that the superconducting Bose condensate is coherent. Another example of the production of a coherent Bose state could be the induced generation of excitons in semiconductors.

An experiment on induced generation of excitons in Cu_2O was performed in Ref. 2. An excitonic orthostate was excited with a dye laser, producing a population inversion with respect to the parastate, whose energy is lower. The coherent amplification of an excitonic parapacket as a result of transitions from the orthostate, which were induced by the excitonic parapacket, was observed experimentally.

It is of interest to obtain coherent excitonic states by means of the direct recombination of an electron from the conduction band and a hole from the valence band. In this case it is natural to use any excitation method applicable for pumping semiconductor lasers. Specifically, it is possible to produce a generator of coherent excitons on the basis of $p-n$ junctions in different modifications: homojunctions, heterojunctions, quantum wells, quantum wires, and even quantum dots. There is hope of producing a device in which laser generation and generation of coherent excitonic states are competing or successive processes.

The clarification of the possibility of realizing a mechanism for producing a coherent

condensate of excitons by direct recombination of free carriers is the subject of the analysis in this letter.

If a reaction channel leads to the formation of a different particle, then the newly produced particle can decay via the inverse channel. The condition that particle production via a definite channel exceeds the rate of decay of the particles via the inverse channel is a necessary condition for induced generation of particles and is called the *inversion condition.*

Let us examine the process whereby an electron with momentum p from the conduction band and a hole with momentum p' from the valence band recombine to form an exciton with momentum P. The spontaneous recombination of a pair of carriers with opposite charge into an exciton occurs with the emission or absorption of an acoustic phonon.[3,4] Its participation in the recombination process ensures conservation of momentum. But an acoustic phonon takes away a very small fraction of the energy. For this reason, energy conservation is ensured by a conversion of a large fraction of the energy into translational energy of the exciton formed.[3,4] However, if we are concerned with the induced production of a Bose condensate of excitons in a state with a definite value of the momentum, then the participation of only an acoustic phonon in this process cannot ensure the exact satisfaction of the law of conservation of energy. However, exact conservation of energy in the process of induced recombination is not required on account of the finite lifetime of the free carriers in a state with a specific energy (momentum). The inversion condition can be written as follows:

$$W(p,p';P;N_P)n_p^e n_{p'}^h - W(N_P;P;p,p')(1-n_p^e)(1-n_{p'}^h)>0, \tag{1}$$

where $W(p,p';P;N_P)$ and $W(N_P;P;p,p')$ are the kinetic coefficients of the recombination reaction of carriers into an exciton and of the inverse reaction, respectively, and N_P is the density of excitons in a state with momentum P.

Let us assume that each type of free carrier has a quasiequilibrium distribution in its band and is in temperature equilibrium with the lattice. Then

$$n_p^e=[\exp(\epsilon_p-\mu_e)+1]^{-1}, \quad n_{p'}^h=[\exp(\epsilon_{p'}-\mu_h)+1]^{-1}, \tag{2}$$

where $\mu_{e,h}$ are the chemical potentials of the carriers in the conduction and valence bands, respectively. The kinetic coefficients of the forward and inverse processes are related with one another by the well-known relation[5]

$$\frac{W(p,p';P;N_P)}{W(N_P;P;p,p')}=\exp\left(\frac{\Delta E}{kT}\right), \tag{3}$$

where $\Delta E=\epsilon_p+\epsilon_{p'}-(E_g-\epsilon_{ex}+\epsilon_P+\epsilon_q)$ is the energy difference between the initial and final states, E_g is the band gap, ϵ_P is the kinetic energy of the exciton formed, ϵ_{ex} is the binding energy of the pair in an exciton, and ϵ_q is the energy of the acoustic phonon. Substituting Eqs. (2) and (3), the condition (1) becomes

$$\mu_e+\mu_h>E_g-\epsilon_{ex}+\epsilon_P+\epsilon_q\,. \tag{4}$$

The relation (4) is of the same form as the inversion condition for a semiconductor laser.[6] In a semiconductor laser the energy difference on the right-hand side of the inequality (4) equals the energy of the photons generated by the laser. In the case at hand this difference

equals the sum of the energies of the exciton formed $E_P = E_g - \epsilon_{ex} + \epsilon_P$ and the energy ϵ_q of the phonon emitted in the process. One can see that the condition (4) holds best for an exciton at rest. We underscore the fact that it presupposes a temperature equilibrium inside the subsystem of free carriers and between free carriers and the lattice. If such an equilibrium does not exist, then the inversion condition depends strongly on the mechanism of induced production of excitons.

The inversion condition (4) certainly holds if the states of the electrons and holes are statistically degenerate. In this case their chemical potentials extend deep into the corresponding bands. But a degenerate state is unfavorable for exciton production because of Debye screening. A necessary condition for the existence of excitons is

$$r_D(n,T) > r_{ex}, \tag{5}$$

where r_D is the Debye screening radius (which depends on the carrier density and temperature), n is the electron density, and r_{ex} is the Bohr radius of the exciton.

In the general case the relation (5) cannot be written in an analytical form, and even a numerical investigation of the relation is a very unwieldy problem since the carrier density is a two-parameter function. To circumvent this difficulty we shall examine a special case. Let us assume that a carrier density corresponding to $\mu_e = E_g$ is maintained in the sample. In this case it can be assumed that the state of the carriers is statistically nondegenerate and the well-known formula[7]

$$r_D(n,T) = \left(\frac{kT}{4\pi} \frac{\chi}{e^2} \frac{1}{n} \right)^{1/2}, \tag{6}$$

where χ is the permittivity of the sample, can be used to calculate the Debye screening radius. For a prescribed chemical potential, the carrier density is determined by the relation

$$n(T) = \frac{4\pi}{(2\pi\hbar)^3} \int_0^\infty \frac{p^2 dp}{\exp(p^2/2m_e kT) + 1} = n_0 \int_0^\infty \frac{\sqrt{x}dx}{e^x + 1} \left(\frac{kT}{\epsilon_{ex}} \right)^{3/2}, \tag{7}$$

where

$$n_0 = \frac{4\sqrt{2}\pi (m_e \epsilon_{ex})^{3/2}}{(2\pi\hbar)^3}, \quad \int_0^\infty \frac{\sqrt{x}dx}{e^x + 1} = 0.678. \tag{8}$$

Since $r_{ex} = \chi\hbar^2/e^2 m_r$ (m_r is the reduced mass of the exciton), a limit on the temperature follows from the relations (5)–(7):

$$\frac{kT}{\epsilon_{ex}} < 5.4 \frac{m_r^3}{m_e^3}. \tag{9}$$

In many materials the hole mass is much greater than the electron mass in the conduction band. For this reason, the reduced mass ratio of the exciton is close to the electron mass so that the temperature of the sample can be approximately five times higher than the binding energy of the exciton.

Just as in the excitation of lasing in a laser, the inversion condition (4) is only necessary. A sufficient condition for coherent excitation of excitons is that the difference

of the rates of induced recombination of carriers into excitons and the inverse process exceeds the rate of decay of the coherence state of the excitons via other channels:

$$\sum_{p,p'} [W(p,p';P;N_P)n_p^e n_{p'}^h - W(N_P;P;p,p')(1-n_p^e)(1-n_{p'}^h)] > \frac{N_P}{\tau_{ex}}. \tag{10}$$

According to the rules of quantum mechanics, the rate of induced production of excitons can be expressed in terms of the cross section for spontaneous recombination of carriers into an exciton:

$$\sum_{p,p'} W(p,p';P;N_P)n_p^e n_{p'}^h = \sigma n^2 \frac{S_P}{\rho} N_P, \tag{11}$$

where

$$S_P = \left(\frac{m_h}{m_e}\right)^{3/2} \left\langle \frac{u}{\pi} \frac{\Gamma}{(\epsilon_e+\epsilon_h+\epsilon_{ex}-\epsilon_q)^2+\Gamma^2} \right\rangle \tag{12}$$

is the form factor for stimulated transitions averaged over the distribution of electrons and holes, Γ is the width of the resonance determined by the time for establishing a quasiequilibrium carrier distribution, u is the relative velocity of the electron and hole,

$$\rho = 4\pi\sqrt{2}\left(\frac{\sqrt{m_{ex}}}{2\pi\hbar}\right)^3 \left\langle \sqrt{\epsilon_e+\epsilon_h+\epsilon_{ex}-\epsilon_q} \right\rangle \tag{13}$$

is density of energy states, averaged over the electron and hole distributions, of spontaneously produced excitons per unit volume of the semiconductor sample, m_{ex} is the electron mass, and τ_{ex} is the lifetime of the coherent state of the excitons. In calculating (12) and (13) the energy of the acoustic phonon can be dropped because of its smallness compared with other terms.[3,4]

Now the relation (10) can be represented in the form

$$\sigma n^2 \frac{S_P}{\rho}\left[1-\exp\left(-\frac{\mu_e+\mu_h-E_P}{kT}\right)\right] > \frac{1}{\tau_{ex}}. \tag{14}$$

One can see that the condition for the production of a coherent state of excitons holds all the better, the lower the temperature and the lower the kinetic energy of an exciton are. We shall calculate the left-hand side of the relation (14) for $\mu_e = E_g$ and $P=0$. Direct numerical integration shows that in this case the relation

$$\frac{\mu_h}{kT} = \ln\left(\frac{m_e}{m_h}\right)^{3/2} \tag{15}$$

describes quite well (to within 10%) the chemical potential of the holes. Substituting expressions (7), (12), and (13) into the inequality (14) gives

$$\sigma n_0 \sqrt{\frac{2\epsilon_{ex}}{m_e}}\left(\frac{m_h}{m_{ex}}\right)^{3/2}\left\{\frac{S(\alpha)}{\rho(\alpha)}\frac{1}{\alpha}\left[1-\left(\frac{m_h}{m_e}\right)^{3/2} e^{-\alpha}\right]\right\} > \frac{1}{\tau_{ex}}, \tag{16}$$

where

$$S(\alpha)=\int_0^\infty \frac{x\sqrt{y}\,dx\,dy}{[(x+y+\alpha)^2+\beta^2\alpha^2](e^x+1)[(m_h/m_e)^{3/2}e^y+1]},$$

$$\rho(\alpha)=\int_0^\infty \frac{\sqrt{(x+y+\alpha)xy}\,dx\,dy}{(e^x+1)[(m_h/m_e)^{3/2}e^y+1]}, \quad \alpha=\frac{\epsilon_{ex}}{kT}, \quad \beta=\frac{\Gamma}{\epsilon_{ex}}.$$

For estimates, we take the typical values of the parameters: $\Gamma\approx 10^{13}$ s^{-1}, $\epsilon_{ex}\approx 10$ meV, $m_h\approx m_{ex}\approx 0.5m_0$, and $m_{ex}\approx 0.1m_0$. The factor on the right-hand of Eq. (17) has a maximum as a function of the parameter α, equal to $1.1\cdot 10^{-3}$ at $\alpha\approx 3.5$. The width of this maximum is such that in the interval $2.5<\alpha<6$ the values of the function $\geqslant 0.3\cdot 10^{-3}$. The choice of the parameter α in this interval is in complete agreement with the inequality (9). The cross section σ for spontaneous recombination is calculated in Refs. 3 and 4. It is virtually independent of the density and temperature and equals $10^{-11}-10^{-12}$ cm^2. Finally, the right-hand side of the inequality (16) is of the order of $2\cdot 10^8$ s^{-1}. The condition for the production of a coherent state of excitons will hold if the lifetime of the state exceeds $5\cdot 10^{-9}$ s. Excitons with even longer spontaneous decay times exist in nature. For example, the lifetimes of orthoexcitons in Cu_2O exceed 10^{-8} s, and paraexcitons last even longer — up to 10^{-5} s.[2,8] Incidentally, estimates for Cu_2O are more optimistic than the those made above, since electrons and holes in this material have the same masses and the binding energy of a pair in an exciton is 15 times greater than that used in our estimates.[3] According to Eq. (16), both facts facilitate the production of an inverted state. According to Eq. (7), the required free-carrier densities lie in the range $10^{16}-10^{18}$ cm^{-3}, depending on the effective mass of the carriers. There is no fundamental problem in obtaining the pumping intensities required to produce such free-carrier densities. Semiconductor lasers are an example.

In summary, the production of coherent states of excitons by the direct recombination of free carriers is easily achievable with modern experiment methods.

The new apparatus requires a suitable name. In Ref. 2 the authors propose the term ''Excitoner.'' This name is sonorous but it does not reflect the essence of the operation of the device. I venture the name ''Stemeks.'' This is a Russian transcription of the abbreviation Stemecs — Stimulated Emission of an Exciton Coherent State.

This work was supported by the Russian Fund for Fundamental Research (Grant 96-02-18051).

[a)]e-mail: oraevsky@sci.fian.msk.su

[1] A. N. Oraevskiĭ, Kvantovaya Elektron. (Moscow) **11**, 1763 (1984) [Sov. J. Quantum Electron. **14**, 1182 (1984)]; Zh. Éksp. Teor. Fiz. **89**, 608 (1985) [Sov. Phys. JETP **62**, 349 (1985)].
[2] A. Mysyrowicz, E. Benson, and E. Fortin, Phys. Rev. Lett. **77**, 896 (1996).
[3] A. A. Liphik, Fiz. Tverd. Tela (Leningrad) **3**, 2323 (1961) [Sov. Phys. Solid State **3**, 1683 (1961)].
[4] A. A. Lipnik, Fiz. Tverd. Tela (Leningrad) **6**, 1068 (1964) [Sov. Phys. Solid State **6**, 823 (1964)].
[5] E. M. Lifshitz and L. P. Pitaevskiĭ, *Physical Kinetics*, Pergamon Press, New York, 1981 [Russian original, Nauka, Moscow, 1979].
[6] N. G. Basov, O. N. Krokhin, and Yu. M. Popov, Zh. Éksp. Teor. Fiz. **40**, 1879 (1961) [Sov. Phys. JETP **13**, 1320 (1961)].

[7] L. D. Landau and E. M. Lifshitz, *Statistical Physics*, Pergamon Press, New York, 1980 [Russian oiginal, Nauka, Moscow, 1964].
[8] A. Mysyrovicz, D. Hulin, and A. Antonetti, Phys. Rev. Lett. **43**, 1123 (1979).

Translated by M. E. Alferieff